INAUGURAL – DISSERTATION

zur
Erlangung der Doktorwürde
der
Naturwissenschaftlich-Mathematischen Gesamtfakultät
der Ruprecht-Karls-Universität
Heidelberg

vorgelegt von
Hélio Roque

Tag der mündlichen Prüfung:

DISSERTATION

Submitted to the
Combined Faculties for the Natural Sciences and for Mathematics
of the Ruperto-Carola University of Heidelberg, Germany
for the degree of
Doctor of Natural Sciences

presented by
Hélio Roque

Date of oral examination:

A closer look at *Schizosaccharomyces pombe* interphase microtubule arrays

Referees: Damian Brunner
David Robinson

Summary

Determination of cell shape is an essential mechanism for cells like neurons, epithelial and fungal. In general, these cells are able to control their shape by positioning mechanisms that regulate cell growth and cell polarity. One key element for such a process is the microtubule cytoskeleton, which is organized into higher order assemblies in polarized cells. Therefore, an important question is to understand how these assemblies are established and maintained during interphase.

We addressed this question by making use of mutants of the fission yeast *Schizosaccharomyces pombe* to study the organization of Interphase Microtubule Assemblies in high ultra-structural detail, using a new emerging technology – electron tomography. Mto1p, Ase1p and Klp2p are key Microtubule Associated Proteins required for the organization of microtubules into interphase microtubule arrays (IMAs). We reconstructed high resolution 3D volumes of *mto*1, *ase*1 and *klp*2 deletion strains (and all double mutants) in order to study the formation and organization of IMAs.

We show that all mutants lacking *ase*1 maintain microtubule overlap regions but with altered inter-microtubule spacing. In addition, in *ase*1Δ *klp*2Δ cells the microtubules appear to have lost their connection to the spindle pole body. Interphase microtubule arrays in *klp*2Δ cells are mostly composed of only two microtubules instead of 2 to 9 in *wild type*. A similar phenotype is found in cells lacking Mto1p protein and cells lacking Mto1p and Klp2p proteins. Cells lacking Ase1p and Mto1p proteins form an interphase microtubule arrays composed of three microtubules, which extend the whole cell length. Both *mto*1Δ and *mto*1Δ *ase*1Δ cells present intra-nuclear microtubules but with a different organization. Finally, we show that impaired interphase microtubule arrays affect the mitochondria network structure in these deletion strains.

The electron tomography analysis of the Ase1p deletion strains suggest the existence of other putative proteins involved in the microtubule bundling process. We show that most microtubules ends in *mto*1Δ cells have open end structures allowing microtubules to show treadmilling behavior. Furthermore, cells lacking Mto1p and/or Klp2 show IMAs with only two MTs, suggesting a role of Klp2p in microtubule nucleation. We propose a mechanistic model to tentatively explain the formation of stable IMAs. Finally we discussed the effects of defective IMAs at the cellular level by showing how the mitochondria network is affected in the deletion mutants compared with *wild type* cells.

Zusammenfassung

Die Bestimmung der Zellform ist ein entscheidender Mechanismus für viele Zellen wie zum Beispiel Neurone, Epithel und Pilzzellen. Im Allgemeinen sind diese Zellen in der Lage, ihre Form zu kontrollieren, indem sie die Position der Mechanismen von Zellwachstum und Zellpolarität steuern. Hierbei spielt das Microtubuli Zytoskelett eine wichtige Rolle. Dieses ist in polarisierten Zellen in Zusammenschlüsse höherer Ordung organisiert. Es ist deshalb von zentraler Bedeutung zu verstehen, wie diese Zusammenschlüsse während der Interphase gebildet und aufrechterhalten werden. Wir haben uns mit dieser Frage befasst, indem wir die "Interphase Mikrotubuli Zusammenschlüsse" (IMAs) in verschiedenen Mutanten der Spalt-Hefe, *Schizosaccharomyces pombe* genauer untersuchten. Hierbei verwendeten wir eine der modernsten Technologien für die Darstellung ultrastruktureller Details, die Elektronentomographie. Mto1p, Ase1p und Klp2p sind wichtige "Microtubuli Assoziierte Proteine" (MAPs) welche für den Zusammenschluss von Microtubuli in IMAs benötigt werden. Wir rekonstruierten hoch auflösende 3D Volumina von Hefezellen welche kein Mto1p, Ase1p oder Klp2p Protein besitzen, sowie alle möglichen Variationen dieser Doppelmutanten.

Wir zeigen, dass Zellen welche kein Ase1p besitzen zwar noch überlappende microtubuli Regionen haben, jedoch einen veränderten inter-microtubuli Abstand aufweisen. Des Weiteren scheinen die microtubuli von Zellen, welche weder Ase1p noch Klp2p besitzen ihre Verbindung zum Spindelpolkörper (SPB) verloren zu haben. Die IMAs von Zellen ohne Klp2p bestehen meistens nur aus zwei- anstelle von zwei bis neun microtubuli im Wildtypen. Ein ähnlicher Phänotyp zeigte sich auch in *mto1* mutierten Zellen und in der *mto1, klp2* Doppelmutante. Die *mto1, ase1* Doppelmutante bildete IMAs welche aus drei microtubuli bestanden, die sich interessanter Weise über die gesamte Zell-Länge erstreckten. Sowohl *mto1*- als auch *mto1, ase1* mutierte Zellen besitzen intra-nukleare microtubuli welche eine besondere Organisation besitzen. Des Weiteren zeigen wir, dass die von wild typischen Zellen abweichenden IMA Strukturen in den oben genannten Mutanten das Mitochondriennetzwerk beeinflussen.

Die elektronentomographische Analyse der *ase1* mutierten Zellen zeigt, dass die IMAs immer noch überlappende microtubuli Regionen besitzen, jedoch einen veränderten inter-microtubuli Abstand aufweisen. Diese Beobachtungen weisen auf die Existenz weiterer Proteine hin, die für den Bündelungsprozess von microtubuli mitverantwortlich sind. Wir zeigen, dass die meisten microtubuli in *mto1* mutierten Zellen offene Endstrukturen besitzen. Diese offenen Endstrukturen können zum sogenannten "Treadmilling" von microtubuli führen, bei welchem hinten Tubulin ab- und vorne angebaut wird. Ausserdem weist die Tatsache, dass die IMAs von Zellen ohne Mto1p und/oder Klp2p nur zwei microtubuli besitzen darauf hin, dass Klp2 am Bildungsprozess neuer microtubuli beteiligt ist. Wir präsentieren ein Modell in dem wir versuchen die Bildung stabiler IMAs zu erklären. Abschließend wird der Effekt der vom Wildtypen abweichenden IMA Strukturen auf das Mitochondriennetzwerk diskutiert.

Acknowledgments

First of all I would like to thank Claude Antony, my supervisor, for giving me the opportunity to carry out my thesis work in his lab. Thank you for all your support and advice, whenever I needed it or asked for it. Furthermore, thank you for giving me the freedom to develop my own ideas, allowing me to grow scientifically.

I also want to thank all my lab collegues, past and present in no particular order: Thi Bach Nga, Charlotta, Sabine, Zsofia, Wandrille, Xavier, Catarina, for the good working atmosphere. Special thanks to Johanna Höög for introducing me to electron tomography and fission yeast and to Uta Haselmann for patience in answering all my questions and for always being ready to help me.

Thank you also to my “second” lab, the Brunner lab. Thanks to Damian for the discussions and allowing me to use and abuse his lab. To all the collegues that I worked with there, especially Lindsay Murrells for all the discussions, both scientific and non-scientific, and help with the fission yeast.

To the Boulder lab collegues, Cindi Schwartz, Eileen O’Toole and Mary Morphew, for helping me with all my problems whenever I passed by, and all the friendship that I always felt when visiting them. Special thanks to David Mastronarde for all the patience to my questions (some of them were quite…) and for always solving my problems with his software.

À comunidade portuguesa: Raquel e André, companheiros e amigos de “guerra" desde o primeiro dia aqui na EMBL (André não me esqueco dos risos e chuveirinhos!), Andreia e Catarina, que facilitaram, e muito, a passagem para o ambiente da EMBL e da levedura, Paulo, pelas guitarradas, Pedro pelas noitadas e Silvia pelas conversas e jantares de última hora! ☺ Mas especialmente, a todos pela amizade e companheirismo!

Aos meus pais e mana! Para quem o mais importante é sempre a minha felicidade. Pelo amor e apoio incondicional! A única maneira de agradecer é retribuir-vos! Um beijo muito especial para a mais pequena (por enquanto) da familia, Tânia, a menina dos meus olhos (e de toda a família! ☺)! Este trabalho é também vosso!

Groβer Dank und einen groβen Kuss an meine Janina, für all die Unterstützung und die Motivation weiter zu machen. Für das Anhören meiner Beschwerden mit einem Lächeln und das Aushalten meiner Reizbarkeit! Ohne dich waere es viel haerter gewesen!

Table of Contents

1 Introduction 1
1.1 Cell Polarity 4
1.2 Cytoskeleton Evolution 4
1.3 Actin: an overview 6
1.4 Intermediate filaments: an overview 7
1.5 Microtubules: an introduction 9
  1.5.1 Dynamic behavior and treadmilling 11
  1.5.2 Microtubule nucleation 12
  1.5.3 Microtubule organizing center 13
  1.5.4 Centrosomal *vs.* non-centrosomal microtubule arrays 14
1.6 Microtubule Associated Proteins 15
  1.6.1 Microtubule stabilizers 15
    1.6.1.1 Dis1/XMAP215 family 16
    1.6.1.2 +TIPs 16
      1.6.1.2.1 CLIP170 family 17
      1.6.1.2.2 EB1 family 17
      1.6.1.2.3 CLASP family 18
  1.6.2 Microtubule destabilizers 18
    1.6.2.1 Stathmin family 19
    1.6.2.2 Katanin and Spastin family 19
    1.6.2.3 Kinesin 13 family 19
  1.6.3 Motors 19
    1.6.3.1 Kinesins 20
    1.6.3.2 Dynein 21
  1.6.4 Microtubule bundlers: Map65/Ase1/PRC1 family 21
1.7 Cytoskeleton: dynamics to disease 23
1.8 Schizosaccharomyces pombe 24
  1.8.1 A model organism 24
  1.8.2 The fission yeast cell cycle 24
  1.8.3 The fission yeast actin cytoskeleton 25
  1.8.4 Fission yeast microtubule cytoskeleton 27
  1.8.5 IMAs generation: a three step model 28
    1.8.5.1 Microtubule nucleation 28
      1.8.5.1.1 Mto1p and Mto2p 29
    1.8.5.2 Formation of antiparallel microtubule overlap regions. 30
      1.8.5.2.1 Ase1p 31
      1.8.5.2.2 Klp2 32
    1.8.5.3 Regulation of microtubule catastrophe. 32
      1.8.5.3.1 Peg1p/Cls1p 32
1.9 Electron Tomography 39
  1.9.1 Automated electron tomography 39
  1.9.2 Sample preparation 40
  1.9.3 Electron tomography in the study of the microtubule cytoskeleton 41

1.9.4 Problems in electron tomography 42
1.10 Motivation 44
1.10.1 The questions behind this study 44

2 Results 47
2.1 Cells lacking Ase1p contain microtubule overlap regions 49
2.2 *klp*2Δ cells predominantly display IMAs with only two MTs 53
2.3 IMAs in *mto*1Δ also have only two MTs 57
2.4 *klp*2Δ cells and *mto*1Δ cells have similar or higher MT pairing length to *wild type* cells but show less MT overlap length 61
2.5 *ase*1Δ *klp*2Δ cells have MT overlap regions 63
2.6 *mto*1Δ *klp*2Δ cells are similar to *mto*1Δ cells 68
2.7 *mto*1Δ *ase*1Δ cells form a hyper IMA 71
2.8 *mto*1Δ cells and *mto*1Δ *ase*1Δ cells have different intra-nuclear MT assemblies 74
2.9 Disorganized IMAs affect the mitochondrial network 78

3 Discussion 81
3.1 MT overlap regions remain in *ase*1Δ, *ase*1Δ *klp*2Δ and *ase*1Δ *mto*1Δ cells 83
3.2 Parallel MT pairs are only observed in *ase*1Δ *klp*2Δ cells 85
3.3 Nucleation regions in the cell 86
3.4 *mto*1Δ cells and *klp*2Δ cells have two to three MTs per IMA 89
3.5 Less polymerized tubulin is found in all the analyzed mutants 90
3.6 Ase1p is essential for MT spacing 92
3.7 The origin of MTs in *mto*1Δ cells 93
3.8 A remaining question: how are IMAs formed and maintained in *mto*1Δ *ase*1Δ cells? 95
3.9 A unified model 96
3.10 The mitochondria network is affected by altered IMAs 98
3.11 Future directions 99

4 Materials and Methods 101
4.1 *S. pombe* cell culture techniques. 103
4.1.1 Strains under control of the *nmt*1 promoter 104
4.1.2 Construction of strains by crossing 104
4.1.3 Construction of strains by homologous recombination 104
4.1.3.1 Generation of PCR fragments for transformation 104
4.1.3.2 Transformation protocol for *S. pombe* cells 105
4.1.4 Screening transformants by colony PCR 106
4.2 Live cell imaging 107
4.2.1 Cell preparation 107
4.2.2 Microscopes used for imaging 107
4.2.3 Image analysis 108
4.3 Electron microscopy 108
4.3.1 High pressure freezing 108

4.3.2 Fixation and freeze substitution 109
4.3.3 Serial sectioning 109
4.3.4 Tomogram acquisition and calculation 110
4.3.5 Tomogram modeling and analysis 110

5 Annexes 113

6 References 123

Table of Figures

Introduction

Figure 1.1. Examples of actin networks. 6
Figure 1.2. Examples of intermediate filaments networks. 8
Figure 1.3. MT structure and dynamics. 10
Figure 1.4. Cells with non-centrosomal MT arrays 14
Figure 1.5. *S. pombe* cytoskeleton organization during cell cycle. 26
Figure 1.6. Latest model of IMA organization. 30
Figure 1.7. Principle of electron tomography and the missing wedge effect. 40
Figure 1.8. Microtubule end structures classes and color scheme used in models. 42

Results

Figure 2.1. Overlap MT regions are present in *ase*1Δ cells. 50
Figure 2.2. Neighbor density analysis showing MT – MT distances and a gallery of electron-dense bridges in *ase*1Δ cells. 52
Figure 2.3. IMAs with two MTs prevail in *klp*2Δ cells. 55
Figure 2.4. Neighbor density analysis showing MT – MT distances and a gallery of electron-dense bridges in *klp*2Δ cells. 56
Figure 2.5. *mto*1Δ cells have fewer IMAs. 58
Figure 2.6. Neighbor density analysis showing MT – MT distances and a gallery of electron-dense bridges in *mto*1Δ cells. 60
Figure 2.7. MT pairing length and IMA MT overlap region length, and MT pairing length does not correlate with MT length. 62
Figure 2.8. The *ase*1Δ *klp*2Δ mutant has MT overlap regions. 65
Figure 2.9. Neighbor density analysis showing MT – MT distances and a gallery of electron-dense bridges in *ase*1Δ *klp*2Δ cells. 67
Figure 2.10. *ase*1Δ *klp*2Δ mutants have lost the connection between SPB and MTs. 68
Figure 2.11. *mto*1Δ *klp*2Δ cells show different IMA organizations. 70
Figure 2.12. *mto*1Δ *ase*1Δ cells show hyper-IMAs. 72
Figure 2.13. *mto*1Δ cells have an intra-nuclear IMA that forms protrusions in the nuclear envelope. 75
Figure 2.14. Intra-nuclear MTs in *mto*1Δ *ase*1Δ cells do not form an IMA like structure. 77
Figure 2.15. Curvature of the mitochondrial network. 80

Discussion

Figure 3.1. A unified model for IMA formation in *S. pombe*. 97

Table of Tables

Introduction

Table 1.1. Members of the MAP65/Ase1/PRC1 family. 22
Table 1.2. Examples of diseases associated with the cytoskeleton or interacting proteins. 23
Table 1.3. Characteristics of the proteins involved in the generation and .... maintenance of IMAs.. 35

Results

Table 2.1. MT lengths, polymerized tubulin and electron-dense bridges .... angles of *wild type* and ase1Δ cells.. 49
Table 2.2. MT lengths, polymerized tubulin and electron-dense bridges .... angles of *wild type*, *ase*1Δ and *klp*2Δ cells. 54
Table 2.3. MT lengths, polymerized tubulin and electron-dense bridges...................... angles of *wild type*, *ase*1Δ, *klp*2Δ and *mto*1Δ cells................................ 59
Table 2.4. MT pairing and IMA MT overlap region in *wild type*, ... and all the analyzed mutants. 61
Table 2.5. MT lengths, polymerized tubulin and electron-dense bridges .... angles of *wild type*, *ase*1Δ, *klp*2Δ, *mto*1Δ and *ase*1Δ *klp*2Δ cells............. 64
Table 2.6. MT lengths, polymerized tubulin and electron-dense bridges .... angles of *wild type*, *ase*1Δ, *klp*2Δ, *mto*1Δ, *ase*1Δ *klp*2Δ and .... *mto*1Δ *klp*2Δ cells. 69
Table 2.7. MT lengths, polymerized tubulin and electron-dense bridges .... angles of *wild type*, and all the mutants analyzed.................................... 73
Table 2.8. Volume, number and ratio of volume to surface area for .... mitochondrial network in *wild type* and all analyzed mutants................. 79

Abbreviations

A	Absorvance
AAA	ATPases associated with various cellular activities
ADP	Adenosine diphosphate
APC	Adenomatous Polyposis Coli
ATP	Adenosine priphosphate
ATPase	Adenosine triphosphate hydrolase
CAP-Gly	Cytoskeletal associated protein-glycine rich
CDK	Cyclin depend kinase
CLIP	Cytoplasmic linker protein
EB1	End Binding protein 1
EBH	End binding homology domain
DHC	Dynein heavy chain
DLC	Dynein light chain
DMSO	Dimethylsulphoxide
dNTPs	De-oxynucleotide triphosphase
dsRed	*Discosoma sp*. red fluorescent protein
EMM2	Edinburgh minimal medium 2
EMMG	Edinburgh minimal medium glutamate
F-actin	Filamentous actin
FS	freeze-substitution
G-actin	Globular actin
GDP	Guanosine diphosphate
GFP	Green fluorescent protein
GMPCPP	Guanosine-5’-(α, β]-Methyleno)-triphosphate
GTP	Guanosine triphosphate
GTPase	Guanosine triphosphate hydrolase
HPF	High-pressure freezing
iMTOC	Interphase microtubule organising centre
IMA	Interphase Microtubule array
kDa	Kilo Dalton
M	Molar
MAP	Microtubule-associated protein
MDa	Mega Dalton
MPAK	Major sperm protein polymerization-activating kinase
MT	Microtubule
MTOC	Microtubule organising centre
mM	mili Molar
nm	Nanometre
nM	Nanomolar
µm	Micrometre
µM	Micromolar
OD	Optical density
PAA	Post-anaphase array
PCR	Polymerase chain reaction

PPB	Pre-prophase band
SPB	Spindle pole body
Tris	Tris-(hydroxymethyl)-aminomethane
YE5’S	Yeast extract medium containing 5 supplements
+TIP	Microtubule plus end associated protein
γ-TURC	Gamma-Tubulin ring complex

1 INTRODUCTION

The cytoskeleton is a major component of the cell. It allows chromosome segregation and cell division. It helps to determine cell polarity, which is essential for cell morphology. It acts as a structural support and provides mechanical strength. It is involved in the transport of molecules and molecular complexes. Cell organelles are able to anchor and/or move along it. It is responsible for cell motility, and plays a role in sensory functions and in transport processes across membranes.

The eukaryotic cytoskeleton is composed of **m**icro**t**ubules (MTs), actin and intermediate filaments. I first introduce some short general evolutionary concepts about the cytoskeleton. I subsequently describe MTs in more detail, including their organization into assemblies and proteins regulating their dynamics. Finally, I introduce the questions that guided this study, the model organism chosen, and the ultra-molecular complex that our study infringed upon.

1.1 Cell Polarity

Cell polarity is a fundamental feature of cells from unicellular to multicellular organisms. It is essential in most basic cellular processes, such as growth, development and migration. Cell polarity can refer to overall cell shape, or the non-symmetrical arrangement of cellular components. Both can be established with the use of positional values that cells acquire and interpret in terms of a genetically determined programme (Wolpert 1996).

Positional values can originate from external cues or from internal signals. Although establishment and maintenance of cell polarity are inherently complex processes, they can be depicted in a simple hierarchical pathway of events. First a specific site provides a positional value which is transmitted to the cell cytoskeleton and to the vesicle transport machinery. As a consequence determined physiological activities are directed to that site leading to pattern emergence. Later on, feedback loops involving the cytoskeleton and associated proteins, as well as membrane components allow for the maintenance of polarization (Nelson 2003; Harris 2006).

1.2 Cytoskeleton Evolution

Until the 1990's, the cytoskeleton was believed to have evolved only the eukaryotes. In 1992, several studies discovered a bacterial tubulin homolog, FtsZ, that like tubulin, hydrolyzes **g**uanoside **t**ri**p**hosphate (GTP) and has a seven amino-acid sequence, GGGTGTG, virtually identical to the "tubulin signature sequence" (de Boer *et al.* 1992; RayChaudhuri and Park 1992; Mukherjee *et al.* 1993). In the same year, a study using a sophisticated structure-based alignment (Bork *et al.* 1992) found three bacterial proteins possibly related to actin – FtsA, MreB and ParM. This early study was only followed up nine years later, when it was shown that MreB assembles into actin-like filaments (Jones *et al.* 2001; van den Ent *et al.* 2001). Bacterial intermediate filaments like genes (crescentin) are only known in a single bacterial species, *C. crescentus*. However, this gene was acquired by a recent horizontal transfer (Ausmees *et al.* 2003), making it more likely that intermediate filaments originated only in eukaryotes.

The evolution of bacterial and eukaryotic cytoskeleletons is a true enigma. On one hand, the divergence between bacterial and eukaryotic tubulins is so great that they are practically unrecognizable. On the other hand, the FtsZ sequence is poorly conserved across bacterial and archaea species (40% to 50% identical sequences), while eukaryotic tubulins are some of the most conserved proteins known (Doolittle 1995). Interestingly, the only amino acids that are conserved between FtsZ and tubulin are those involved in GTP binding and hydrolysis (Erickson 1998; Nogales *et al.* 1998). The same is true for MreB and actin. While MreB is moderately conserved across diverse species (~40% identical sequence), the sequence identity with actin is less than 15 % (Doolittle and York 2002).

It is believed that FtsZ is a very ancient protein, evolving as a functional protein even before the emergence of the genetic code as we know it (Davis 2002). This is supported by the very early necessity of a cell division mechanism that FtsZ provided, and still does today. As such, it is believed that FtsZ was present in a common ancestor and was passed to bacteria and euryarchaea. One explanation for the large divergence between FtsZ and tubulin, might be the evolution of an actin based machine for cytokinesis, allowing FtsZ to undergo large evolutionary changes, evolving into tubulin and the totally new function of building MTs (Doolittle 1995; Doolittle and York 2002).

Likewise, MreB probably evolved from a common ancestor of bacteria and eukaryotes, providing the cell with a mechanism to determine its shape and in some species the segregation of chromosomes (Kruse *et al.* 2006; Dye and Shapiro 2007). It is though that during evolution of eukaryotes MreB lost its function and evolved into a protein capable of forming machineries responsible for cell division, motile functions and phagocytosis (Erickson 2007).

1.3 Actin: an overview

The core constituent of actin cytoskeleton is monomeric **g**lobular (G) – actin associated with an **a**denosine **t**ri**p**hosphate hydrol**ase** (ATPase) that can self-assemble into a ~ 6 **n**ano**m**eters (nm) right-handed helical **f**ilament (F)-actin of two intertwined strands (Steinmetz *et al.* 1997a). G-actin is a polar molecule which determines the polarity of the filament with a highly dynamic plus end (barbed) where G-actin is added up to 12 times faster to the F-actin than at the less dynamic minus end (pointed; Kabsch and Vandekerckhove 1992).

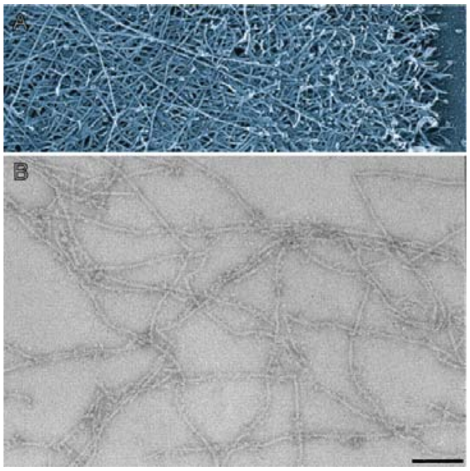

Figure 1.1. Examples of actin networks.
(A) Transmission electron micrograph of a keratocyte prepared by Triton fixation. Adapted from Pollard and Borisy (2003) (B) Negatively stained ragged and branched F-actin filaments imaged in transmission electron microscope. Bar, 100 nm. Adapted from Steinmetz *et al*. (1997a).

The polymerization of actin is tightly linked with **a**denosine **t**ri**p**hosphate (ATP) hydrolysis. When an actin molecule is incorporated into a filament the ATP associated with it is hydrolyzed to **a**denosine **d**i**p**hosphate (ADP). Since the release of the phosphate is slower than the formation of the filament, actin filaments have an ATP cap at their barbed end, while monomers containing ADP transiently accumulate in the remaining filament. Such a process leads to a phenomenon of treadmilling (Kabsch and Vandekerckhove 1992; Steinmetz *et al.* 1997b).

In cells, actin filaments function as force-generating polymer motors, structural scaffolds and tracks for motor proteins (Figure 1.1). In muscle cells, actin is the main component of sarcomeres, where together with the motor protein myosin, is responsible for muscle contraction (Squire 1997). In migrating cells, actin is essential for the formation of protrusions at the leading edge that determine the movement direction. Finally several examples of actin based intracellular movement are also known (Pollard and Borisy 2003).

In *S. pombe* actin performs essential functions in the regulation of cell growth and polarity (Feierbach and Chang 2001; Pelham and Chang 2001; Bretscher 2005; Chang *et al.* 2005; see section 1.8.3).

1.4 Intermediate filaments: an overview

Intermediate filaments are flexible, rod-shape fibers with ~ 10nm in diameter, a size ‘intermediate’ between the thin and thick filaments of chicken muscle cells (Ishikawa *et al.* 1968) which exist only in eukaryotes. Intermediate filaments form extensive networks that appear to connect the cell surface with the nucleus. The fact that intermediate filaments interact with desmosomes, hemidesmosomes, focal adhesions and the extracellular matrix, suggest that it forms a continuous link between the exterior and the nucleus surface through which signals can be transmitted (Goldman *et al.* 2008).

A well know example of intermediate filaments are the nuclear laminas. These form a fibrous network beneath the inner nuclear envelope membrane, which provides support to the interphase nuclear envelope and provides anchoring sites for the chromatin (Parnaik 2008). Other examples of intermediate filaments are vimentin and keratin (Figure 1.2). Vimentin is present in smooth muscle cells, endothelial cells and neurons. In this latter, vimentin was reported has being essential for signal transduction after sciatic nerve crush injury (Goldman *et al.* 2008). Keratins are the major constituent of nails and hair, and are also found in axons and neurons.

Intermediate filaments form a large protein family whose members are composed by a conserved central α-helical rod domain flanked by a non- α-helical N-(head) and C-terminal (tail) domains. The head and tail domains are variable in size and sequence, which contributes to the diversity of this super family (Parry *et al.* 2007). Intermediate filaments polymerize by self-association of monomers into dimers, which then associate in a parallel fashion to form the filaments. These filaments do not posses an intrinsic polarity. Nonetheless they can be highly dynamic with phosphorylation playing a major role (Helfand *et al.* 2004).

No intermediate filament protein is known in *S. pombe*.

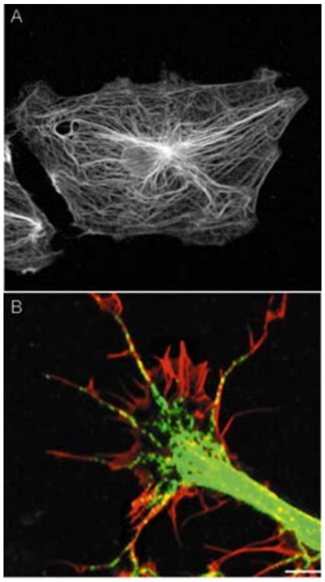

Figure 1.2. Examples of intermediate filaments networks.

(A) Keratin filament network of a rat kangaroo kidney epithelial cell (PtK2). Adapted from Goldman *et al*. (2008). (B) Differentiated PC12 cells fixed and stained from actin (red) and peripherin (green), a neuronal intermediate filament. Adapted from Helfand *et al*. (2004).

1.5 Microtubules: an introduction

MTs are mainly composed of three types of tubulins: *α, β* and γ-tubulin. Both *α* and *β*-tubulin are monomers of about 450 amino acids, have a mass of ~50 **k**ilo (k) **Da**ltons (Da), and share ~50% identical sequence at the amino acid level (Valiron *et al.* 2001). Both *α* and *β*-tubulin form a heterodimer with two binding sites for GTP, one exchangeable and the other not (Mitchison and Kirschner 1984).

A MT is a hollow left-handed helical tube of approximately 25 nm diameter with walls made of tubulin heterodimers (*αβ*-tubulin) stacked head-to-tail to form protofilaments that run lengthwise along the wall of the tube (Wade 2007). This polarity of the tubulin dimers dictates the polarity of the MT, which is essential for their dynamic behavior (see section 1.5.1). As a consequence MTs are characterized by having a ‘plus’ more dynamic end and a ‘minus’ less dynamic one (Mitchison and Kirschner 1984).

The MT *in vivo* has a total of 13 protofilaments with a predominant B-lattice, where each tubulin homodimer from the neighbouring protofilament forms lateral contacts. Due to the fact that each protofilament is shifted slightly lengthwise by ~0.9 nm with respect to its neighbour, when the first and thirteen protofilaments close the tube there is a mismatch in the B-lattice and *α* and *β*-tubulin interact laterally forming a A-lattice (Nogales *et al.* 1999; Figure 1.3A – B).

In addition to the α-tubulin and β-tubulin monomers, the third most predominant tubulin is γ-tubulin which shares ~30% similarity with α and β-tubulin (Oakley and Oakley 1989). γ-tubulin belongs to a different subfamily of tubulin and appears to exist in all eukaryotes being involved in MT nucleation and stabilization (Dutcher 2003).

.

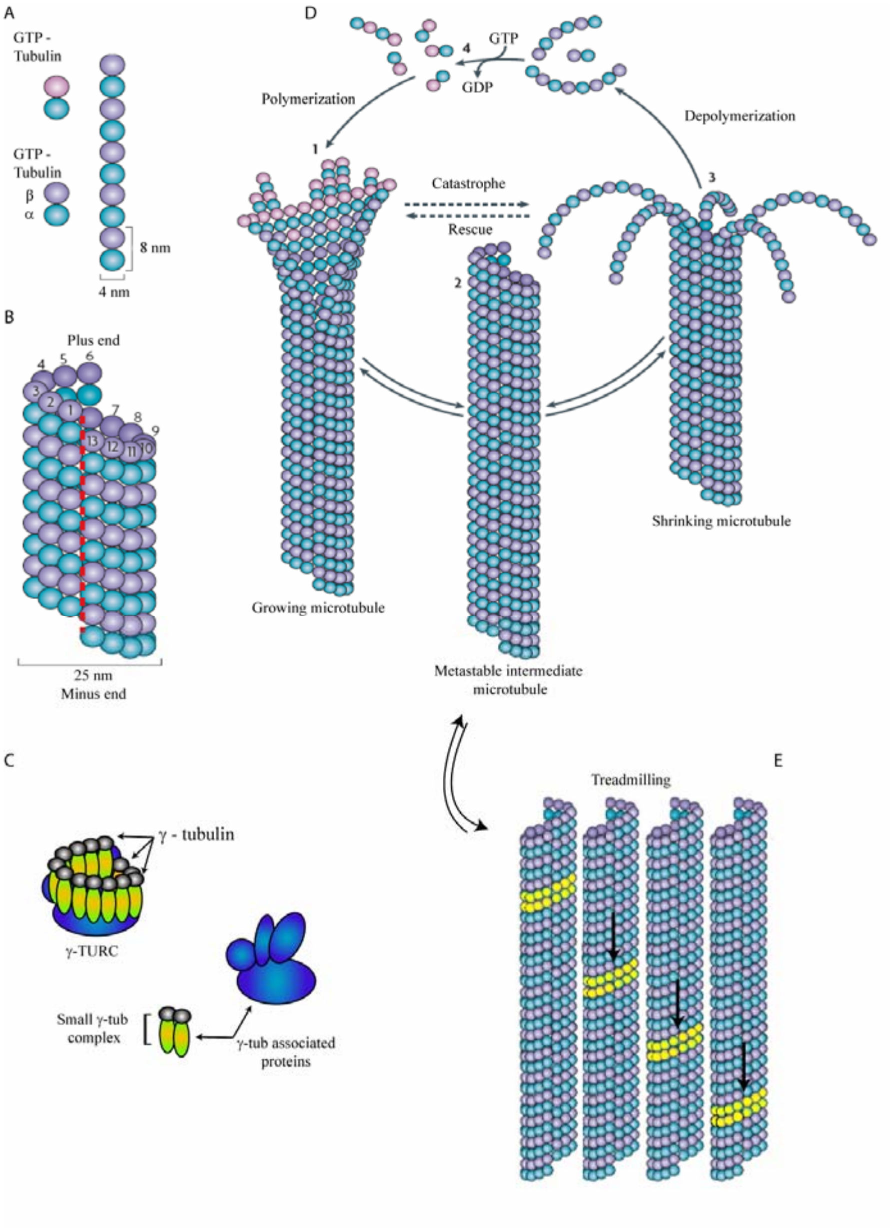
A
GTP - Tubulin
GTP - Tubulin
β
α
8 nm
4 nm
B
Plus end
4 5 6
3 2 1
7 8 9
13 12 11 10
25 nm
Minus end
C
γ - tubulin
γ-TURC
Small γ-tub complex
γ-tub associated proteins
D
4
GTP
GDP
Polymerization
Depolymerization
1
Catastrophe
Rescue
3
2
Growing microtubule
Metastable intermediate microtubule
Shrinking microtubule
E
Treadmilling

Figure 1.3. MT structure and dynamics.

MTs are composed of α/β-tubulin dimers stack head-to-tail forming a protofilament. Each dimer has 4 nm of width and 8 nm of height (A). An *in vivo* MT is typically a cylindrical and helical structure composed of 13 protofilaments. The helical pitch of 12 nm in combination with the 8 nm dimer height generates a lattice seam (red dashed line) (B). MT nucleation is believed to occur in the γ-TuRC complex which acts as a template for the MT. Some species do not possess the full γ-TuRC but a small version comprising only three proteins called γ-tubulin small complex - γ-TUSC (C). A growing MT is characterized by a fountain-like array of protofilaments structures (D). MTs can reach a steady state in which polymerization at the plus ends is negatively compensated by depolymerization at the minus end (E). See text for more details. A, B and D adapted from Akhmanova and Steinmetz (2008).

In all cell types so far examined, γ-tubulin associates with one or more proteins which are also highly conserved, forming the **γ**-**tu**bulin **r**ing **c**omplex (γ-TuRC; Figure1.3C; Dictenberg *et al.* 1998), a oligomer of more than 2 **m**ega (M) Da in higher eukaryotes (Moritz *et al.* 2000). The γ-TuRC is believed to be essential for MT nucleation *in vivo* by providing a template where *αβ* heterodimers are added.

Other tubulins recently identified (δ, ε, ζ and η-tubulin) all seem to localize to the centrosomes and basal bodies (Ruiz *et al.* 1987; Dutcher and Trabuco 1998; Chang and Stearns 2000; Ruiz *et al.* 2000; Vaughan *et al.* 2000)

1.5.1 Dynamic behavior and treadmilling

The large spectrum of functions that MTs are able to perform is largely dependent of their dynamic properties.

The term dynamic instability was first used to describe the process of growth and shrinkage of MTs by Mitchison and Kirchner (1984). Dynamic instability comprises all MT stages: growth or polymerization; catastrophe or depolymerization; pause and rescue (Figure 1.3D; Walker *et al.* 1988). This behavior allows MTs to respond to external cues modifying their network as to better perform their function.

In vivo, MTs grow by addition of αβ-tubulin dimers to the γ-TuRC, forming protofilaments that interact with each other laterally. As previously mention, both α and β-tubulin bind GTP, but while GTP is attached permanently to α-tubulin, the β-tubulin is a **GTP** hydrol**ase** (GTPase), hydrolyzing the GTP into **g**uanosine **d**i**p**hosphate (GDP) at the moment the next αβ-tubulin docks to the protofilament (Nogales *et al.* 1999). This causes MTs to be composed mostly β-tubulin – GDP except at its growing end where it is believed that MTs possess a 'GTP-cap', which stabilizes the MT growth (Mitchison and Kirschner 1984; Carlier *et al.* 1988). The hydrolysis of GTP is necessary only for the disassembly of MTs, since MTs still grow in the presence of non-hydrolysable GTP analogue, **g**uanosine-5'-([α,β]-**m**ethyleno)-tri**p**hosphate (GMPCPP; Muller-Reichert *et al.* 1998).

While β-tubulin – GTP as a straight configuration, the GDP form is curved. Nonetheless this latter form is constrained to be straight within the MT wall. This provides a large amount of potential energy to disassembly the MT (Wade 2007).

The transition from growth to shrinkage is a stochastic event called catastrophe, where it is believed that the GTP hydrolysis rate overcomes the αβ-tubulin incorporation at the plus end rate. This leads to the loss of the GTP-cap, which destabilizes the MT leading to shrinkage. (Mitchison and Kirschner 1984; Desai and Mitchison 1997; Amos and Schlieper 2005). The passage from shrinkage to growth is termed rescue and is still an event not well understood. Finally MTs can also pause, a state where no growth or shrinkage occurs (Mitchison and Kirschner 1984)

Besides dynamic instability, MTs also exhibit another behavior know as treadmilling (Figure 1.3E). This behavior was first discovered *in vitro* by the continuous uptake of GTP by a polymer population at steady state (Margolis and Wilson 1978). Treadmilling is possible due to the different behavior of both MT ends at steady state. On the plus ends new tubulin dimers are continuously incorporated, while the minus end continuously looses them (Valiron *et al.* 2001). Even though it was believed that treadmilling would only occur *in vitro* it was later shown that treadmilling is present *in vivo*, for example, in the *Xenopus leavis* were it is responsible for chromosome migration (Margolis and Wilson 1998).

1.5.2 Microtubule nucleation

In vitro MTs can spontaneously polymerize without γ-tubulin due to the high concentrations of purified α and β- tubulin. *In vivo*, the concentration of these is smaller and γ-tubulin is needed to overcome the kinetic barrier of MT nucleation (Oakley and Oakley 1989).

γ-tubulin normally associates with several other proteins, known as Dgrips in *Drosophila*, to form the γ –TURC (Figure 1.3C and for a list γ–TURC complexes in the various species please view Annex I). It is believed that γ-tubulin controls the MT nucleation by providing a 13 protofilament basal template. This model is supported by the observation that γ–TURCs form a capped structure of ~ 25 nm rings diameter in centrosomes (Moritz *et al.* 2000). Furthermore *in vitro* studies showed that γ–TURCs form a cap structure at the minus end of MTs (Zheng *et al.* 1995; Moritz *et al.* 2000), and latter *in vivo* studies supported this observation (O'Toole *et al.* 2003b). Several proteins are known to interact with γ–TURCs targeting them to specific locations inside the cell like the centrosome or the cortex in plants (Gunawardane *et al.* 2000; Wiese and Zheng 2006).

1.5.3 Microtubule organizing center

MT nucleation is generally localized to specific structures in cells called **m**icrotubule **o**rganizing **c**enters (MTOCs). Their shape, size and occurrence vary greatly between species and even within a cell at different stages of cell cycle (Schiebel 2000). The most intensively studied MTOC is the centrosome of vertebrate cells. The centrosome consists of a pair of centrioles, cylinders assembled from nine MT triples, and pericentriolar material that contains the γ –TURC. Other proteins function to target and tethering the γ –TURC to the centrosome. MTs are then nucleated and anchored to the centrosomes forming the MT array (Dictenberg *et al.* 1998; Megraw *et al.* 1999; Moritz *et al.* 2000; Bartolini and Gundersen 2006)}. Two types of arrays are normally present during the cell cycle. An interphase radial array where all the MTs derive from duplicated and tethered centrosomes, and a mitotic one where two anti-parallel MT arrays derive from the two separated centrosomes, which are now at each pole of the spindle (Hyman and Karsenti 1998; Andersen 1999; Bettencourt-Dias and Glover 2007).

Centrioles are not essential for the existence of centrosomes. Indeed both budding and fission yeasts and have no centrioles but still possess the **s**pindle **p**ole **b**ody (SPB; centrosome equivalent) where the MTs are nucleated from.

1.5.4 Centrosomal *vs.* non-centrosomal microtubule arrays

The existence of centrosomes is not a requirement for the existence of organized MT arrays. Indeed, differentiated animal cell types, including muscle, epithelia and neuronal cells, as well as most fungi and vascular plants, possess non-centrosomal arrays that are non-radial (Figure 1.4). Two unifying characteristics of these cell types are that they are all axially polarized and non migratory (Bartolini and Gundersen 2006).

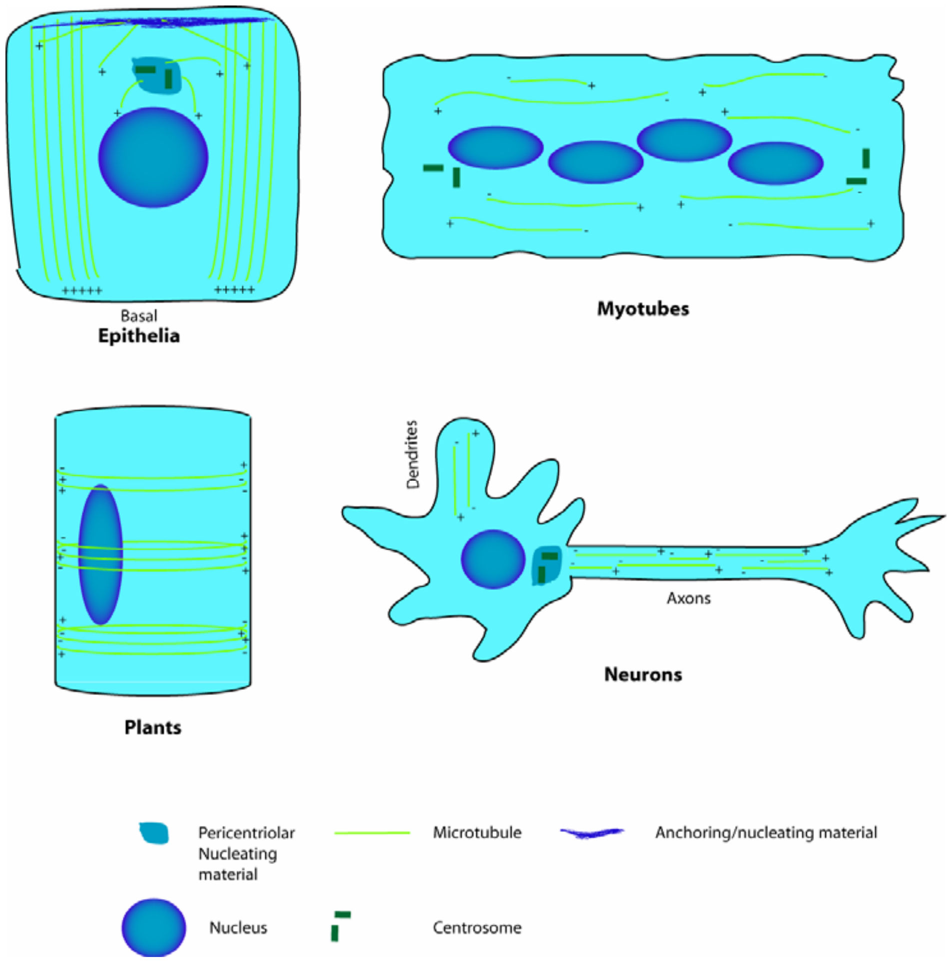
Basal
Epithelia
Myotubes
Plants
Dendrites
Axons
Neurons
Pericentriolar Nucleating material
Microtubule
Anchoring/nucleating material
Nucleus
Centrosome

Figure 1.4. Cells with non-centrosomal MT arrays.

Most polarized epithelial cells mainly have a non-centrosomal MT array aligned along the apical-basal axis of the cell, while in myotubes the non-centrosomal MT arrays are arranged along the cell long axis. Somatic plant cells lack an MTOC and normally present MT bundles of mixed polarity aligned perpendicular to the cell growth axis. Finally, fully differentiated neurons present both centrosomal arrays and non-centrosomal arrays. Dendrites have MT bundles of mixed polarity while axons have MT bundles of uniform polarity. Adapted from Bartolini and Gundersen (2006).

These non-radial MT arrays are less well understood. There are two major differences in these arrays compared to centrosomal arrays: 1) usually linear; 2) and in differentiated cells many MTs become stabilized (Gundersen and Bulinski 1986; Gundersen *et al.* 1989; Chapin *et al.* 1991). A model for generating such non-centrosomal arrays has been proposed by Bartolini and Gundersen (2006) and comprises three steps: 1) generation of non-centrosomal MTs; 2) movement of non-centrosomal MTs to the sites of assembly and; 3) assembly of non-centrosomal MTs into higher order arrays. Later, the *Schizosaccharomyces pombe* MT cytoskeleton and the formation of both centrosomal and non-centrosomal arrays in interphase cells will be described in greater detail.

1.6 Microtubule Associated Proteins

In cells the dynamics of MTs are normally modulated by a number of proteins that interact with the MTs. They are called **m**icrotubule **a**ssociated **p**roteins (MAPs). Indeed, MAPs influence the cell MT dynamics in all their stages. MAPs are known to be essential for MT nucleation (see section 1.5.2) and to promote MT assembly rates and stability of MT plus ends in specific contexts. Furthermore, MAPs are also known to promote MT catastrophe, rescue, treadmilling and even MT severing (Amos and Schlieper 2005)

MAPs can be generally divided into four main classes: stabilizers, destabilizers, motors and bundlers.

1.6.1 Microtubule stabilizers

The group of MT stabilizing MAPs is composed by several protein families, namely, the Dis1/XMAP215 family, the EB1 family and the CLIP170 family and several others. All these families have been grouped according to prominent structural elements that are conserved throughout their members (Akhmanova and Steinmetz 2008).

1.6.1.1 Dis1/XMAP215 family

The Dis1/XMAP215 family is characterized by the existence of repeating units of ~200 amino acids at their N-terminal, known as **T**umor **O**verexpressed **G**ene (TOG) domains which bind to tubulin and MTs (Gard and Kirschner 1987). Each of these TOG-like domains comprises several HEAT repeats, a module containing 37 to 47 amino acids. Arrays of HEAT repeats form a rod-like helical structure that participates in protein-protein interactions (Slep and Vale 2007).

The main functions of Dis1/XMAP215 family proteins are MT stabilization, promotion of MT growth and MT-cortex interaction. Interestingly *S. pombe* is so far the only organism in which two members of the Dis1/XMAP215 exist: Alp14p and Dis1p (Nabeshima *et al.* 1995; Garcia *et al.* 2001).

1.6.1.2 +TIPs

Since the discovery of the first +TIP – **C**ytoplasmic **Li**nker **P**rotein of 170 kDa (CLIP170; Diamantopoulos *et al.* 1999; Perez *et al.* 1999) – several families of +TIPs have been identified, namely, the **e**nd **b**inding proteins (EB1) family, the **a**denomatous **p**olyposis **c**oli (APC) and **kar**yogamy protein 9 (Kar9) family (Groden *et al.* 1991; Miller and Rose 1998), the CLASP family (see section 1.6.1.2.3), and several others (see Annex II for a complete listing of +TIPs proteins). Despite structurally unrelated, these proteins share a common localization and several similar activities. Furthermore +TIPs seem to be constituted by a limited set of evolutionary conserved modular binding domains, repeat sequences and linear motifs (Akhmanova and Steinmetz 2008).

1.6.1.2.1 CLIP170 family

CLIP170 was identified as a linker between endocytic vesicles and MTs. They are characterized by a **c**ytoskeleton-**a**ssociated **p**rotein **Gly**cine-rich (CAP-Gly) domain at their N-terminal. These are responsible for the interaction with MTs and EB proteins Furthermore, CLIPs contain a coiled-coil domain that allows the formation of parallel dimers, and a cargo-binding domain at their C-terminal, characterized by two tandemly repeated metal-binding motifs and a C-terminal EEY/F motif (Pierre *et al.* 1994).

Besides linking vesicles to MTs, CLIP proteins also promote MT rescue and stability. They target dynein to MT ends and promote MT interaction with the cell cortex and kinetochores (Pierre *et al.* 1992; Akhmanova *et al.* 2001).

The protein Tip1p is the member of this family in *S. pombe* (Brunner and Nurse 2000). It is transported along MTs by the kinesin motor Tea2 and its accumulation at the cell tips depends of the EB1 homologue Mal3 (Busch and Brunner 2004; Busch *et al.* 2004; Bieling *et al.* 2007).Tip1 is important for the spatial regulation of interphase MTs, stabilizing MTs that contact the cell cortex, allowing them to reach the cell poles where they deposit the polarity factors (Brunner and Nurse 2000).

1.6.1.2.2 EB1 family

The EB1 protein family is conserved from yeast to mammals. It is characterized by highly conserved N and C-terminal domains that are separated by a less conserved linker sequence. The N-terminal domain is necessary and sufficient for MT binding (Hayashi and Ikura 2003). It is a globular domain characteristic of the **c**alponin **h**omology (CH) domain, normally found in actin-binding and signaling proteins (Gimona *et al.* 2002). The C-terminal part contains a coiled-coil domain which allows for homo-dimerization of EB1. This coiled-coil domain partially overlaps with the **e**nd-**b**inding **h**omology domain (EBH) which is unique to this family (Slep *et al.* 2005).

This family of proteins acts mainly in promoting MT growth and dynamicity, has an anti- MT catastrophe activity and targets several others +TIPs to the MT plus end.

In *S. pombe*, the EB1 homologue is Mal3p. Its deletion leads to shorter MTs that do not reach the cell ends (Busch and Brunner 2004). Furthermore it was shown *in vitro* that Mal3p binds the MT lattice, likely contributing to its stabilization (Sandblad *et al.* 2006). More recently it was shown also *in vitro* that Mal3p promotes the formation of 13 protofilament MTs with A-lattice (des Georges *et al.* 2008), reviving the discussion of the MT structure *in vivo*.

1.6.1.2.3 CLASP family

CLIP-**as**sociated **p**roteins (CLASPs; Akhmanova *et al.* 2001) are characterized by the presence of TOG-like domains and domains enriched in basic and Ser residues. CLASPs also show MT plus tip localization, but this localization is normally restricted to the leading edge in a migratory cell. Furthermore they also localize to the Golgi apparatus where they may be involved in the nucleation of MTs (Efimov *et al.* 2007).

In *S. pombe* Peg1p/Cls1p is the member of the CLASP family (Grallert *et al.* 2006; Bratman and Chang 2007). Since is protein is involved in this study it will be discussed later (see section 1.8.5.3.1).

1.6.2 Microtubule destabilizers

The existence of MT destabilizers is very important since it allows a quick response from the MT network to external signals. Protein families of this class of MAPs include the Stathmin or **O**nco**p**rotein 18 (Op18), the Katanin and Spastin family and the Kinesin 13 family.

1.6.2.1 Stathmin family

Stathmin or **O**nco**p**rotein 18 (Op18) was initially identified as a protein phosphorylated in response to several extracellular signals and associated with several forms of cancer. Its function as a MT destabilizing agent was determined later on (Belmont and Mitchison 1996).

This protein family is characterized by a highly conserved N-terminal polyproline II helix domain. The rest of the N-terminal is unstructured with most of the protein having a predicted α-helical structure. Stathmin destabilizes MTs by either sequestering tubulin dimers or by stimulating plus end catastrophes (Howell *et al.* 1999a; Howell *et al.* 1999b).

1.6.2.2 Katanin and Spastin family

This family is a member of the **A**TPases **a**ssociated with various cellular **a**ctivities (AAA) family. They are characterized by a **m**icrotubule **i**nteracting and an endosomal **t**rafficking (MIT) domain at the N-terminus and the AAA domain at the C-terminus (Salinas *et al.* 2007).

These proteins destabilize MTs by severing them creating a new MT minus end without a γ-TuRC associated and therefore more prone to depolymerize. (Salinas *et al.* 2005).

1.6.2.3 Kinesin 13 family

Kinesin 13 (or Kin 1) family members use the hydrolysis of ATP to bind to MTs and peel the protofilaments apart (Moores *et al.* 2006; Moores and Milligan 2006; 2008). This family of proteins is characterized by a motor domain, which contains the MT and ATP-binding sites, in the middle of the amino acid sequence (Moores and Milligan 2006).

1.6.3 Motors

All the families of MT motors (with the exception of Kinesin I family) use the hydrolysis of ATP to move along MTs. The cellular functions of motors range from vesicular transport, to chromosome oscillation by spatial regulation of MT dynamics (Gardner *et al.* 2008).

Three types of motors exist: kinesins and dyneins which move along MTs, and myosins which move along actin filaments.

1.6.3.1 Kinesins

Kinesins are characterized by a ~360-residue globular motor domain that contains both the catalytic pocket for the hydrolysis of the ATP and the binding sites for MTs. This motor domain is normally followed by a flexible region and a coiled-coil domain which allows the oligomerization. According to sequence alignments of the motor domain there are 14 families of kinesis (Goodson *et al.* 1994).

Kinesins 'walk' along MTs in different ways. Some kinesins are processive, which means they give several steps before dissociating (Song *et al.* 2001; Marx *et al.* 2008), while others are non-processive, giving one to two steps before dissociating (Yildiz and Selvin 2005).

In *S. pombe* eight kinesins are known to exist according to sequence alignments and experimental data: Klp2p, Klp6p, Cut7p, Tea2p, Klp8p, Klp5p, Klp3p, Pkl1p and an uncharacterized member. Klp2p is a major subject on this thesis and will be discussed later.

Klp6p forms a complex with Klp5p (both are from Kinesin 8 family) and are responsible for coordinate bipolar chromosome attachment (Sanchez-Perez *et al.* 2005). *cut*7 (Kinesin 5 family) is an essential gene that localizes to the SPB. Its absence blocks spindle formation (Hagan and Yanagida 1992). Tea2p forms a complex with Tip1 which it transports to the MT plus tips and is essential to generate polarized growth in fission yeast (Browning *et al.* 2000). The association and loading of the complex to the MT lattice is dependent on Mal3p (see section 1.6.1.2.2; Bieling *et al.* 2007). Klp8p and Klp3p (Kinesin 1 family) are still largely uncharacterized but the latter when overexpressed leads to mitotic growth inhibition (Jeong *et al.* 2002). Finally, Pkl1p (kinesin 14 family) is localized only in the nucleus of *S. pombe* where it is involved in the organization of the spindle (Pidoux *et al.* 1996; Troxell *et al.* 2001).

1.6.3.2 Dynein

Dyneins like the Katanin and Spastin family are members of the AAA ATPase. They are minus-end directed motors characterized by the **d**ynein **h**eavy **c**hain (DHC) which contains a large motor domain composed of 6 AAA^+ ATPase-like domains. From here a coiled-coil domain extends links to a small globular domain that mediates the attachment to MTs (Vale 2003).

Dynein functions in higher eukaryotes range from vesicular transport and nuclear positioning to mitotic chromosome movement and spindle positioning (Bloom 2001).

In *S. pombe* the loss of dynein function (by deleting the **d**ynein **h**eavy **c**hain, dhc 1, or the **l**ight **c**hain, dlc1) leads to altered chromosome segregation (Courtheoux *et al.* 2007; Grishchuk *et al.* 2007).

1.6.4 Microtubule bundlers: Map65/Ase1/PRC1 family

The organization of MT arrays as well as the proper function of such arrays depend not only on proteins that altered MT dynamics but also on proteins that allow MTs to be ‘loosely fixed’ in between each other, keeping an regular spacing and orientation in relation to each other.

The main responsibles for this function are the members of the family Map65/Ase1/PRC1 (Table 1.1). These proteins are ‘professional’ MT bundlers. First discovered in *Saccharomyces cerevisiae* (Pellman *et al.* 1995), these proteins are conserved through out the eukaryotes. They are characterized by a MT binding domain that occupies most of the protein sequence.

As this subject is a major theme in this thesis, it will be discussed in more detail later on.

Table 1.1. Members of the MAP65/Ase1/PRC1 family.

Protein	Species	Molecular characteristics (*in vitro*)	Sub-cellular localization	Putative function (*in vivo*)	References
NtMAP65-1a	Tobacco	MT binding MT bundling MT polymerization, phosphorylation by MPAK and CDKs	Cortical MTs, PPBs, mitotic spindles and phragmoplast expansion	Stabilization of MT-based structures, phragmoplast expansion	(Chang-Jie and Sonobe 1993; Smertenko *et al.* 2000; Sasabe *et al.* 2006)
NtMAP65-1b	Tobacco	MT binding MT bundling, phosphorylation by MPAK	Not analyzed	Stabilization of MT-based structures	(Wicker-Planquart *et al.* 2004)
MAP65	Carrot	MT binding MT bundling	Cortical MTs, PPBs, mitotic spindles, phragmoplast	Stabilization of MT-based structures	(Chan *et al.* 1996; Chan *et al.* 1999)
AtMAP65-1	*Arabidopsis*	MT binding MT bundling, phosphorylation by MPAK	Cortical MTs,PPBs, mitotic spindles, phragmoplast	Stabilization of MT-based structures	(Ubersax *et al.* 2003; Smertenko *et al.* 2004; Van Damme *et al.* 2004a; Van Damme *et al.* 2004b; Mao *et al.* 2005)
AtMAP65-3 /PLE	*Arabidopsis*	MT binding MT bundling	Cortical MTs, PPBs, phragmoplast midzone	Stabilization of phragmoplast midzone	(Muller *et al.* 2004; Van Damme *et al.* 2004a)
AtMAP65-4	Arabidopsis	Not analyzed	Nucleus MTs, spindle pole, mitotic spindles	Spindle dynamics	(Van Damme *et al.* 2004b)
AtMAP65-5	*Arabidopsis*	Not analyzed	Cortical MTs, early phragmoplasts, cell plates	Formation of plasmodesmate	(Van Damme *et al.* 2004a; Van Damme *et al.* 2004b)
AtMAP65-6	*Arabidopsis*	MT binding MT bundling	Mitochondria	Organelle positioning	(Mao *et al.* 2005)
AtMAP65-8	*Arabidopsis*	Not analyzed	Cortical MTs, spindle pole, mitotic spindles, phragmoplast MT minus-ends	MT dynamics at minus-ends	(Van Damme *et al.* 2004a)
PRC1	Mammals	MT binding MT bundling phosphorylation by CDK	Nucleus, mitotic spindle, central spindle midzone	Stabilization of central spindle midzone	(Jiang *et al.* 1998; Mollinari *et al.* 2002; Zhu and Jiang 2005; Zhu *et al.* 2006)
SPD1	*C. elegans*	Not analyzed	Nucleus around centrosomes, central spindle midzone	Stabilization of central spindle midzone	(Verbrugghe and White 2004)
Feo	*Drosophila*	Not analyzed	Central spindle midzone	Stabilization of central spindle midzone	(Verni *et al.* 2004)
Ase1	*S. cerevisiae*	MT binding MT bundling phosphorylation by CDK	Mitotic spindles, anaphase spindle midzone	Stabilization of anaphase spindle midzone	(Pellman *et al.* 1995; Juang *et al.* 1997; Schuyler *et al.* 2003)
Ase1p	*S. pombe*	MT binding MT bundling	Cytoplasmic MTs, mitotic spindles, spindle pole bodies, anaphase spindle midzone	Stabilization of anaphase spindle midzone, nuclear positioning	(Loiodice *et al.* 2005; Yamashita *et al.* 2005; Janson *et al.* 2007)

Adapted from Sasabe and Machida (2006).

1.7 Cytoskeleton: dynamics to disease

The important roles that the cytoskeleton plays in mitosis, cell signaling, motility and mechanical integrity are highlighted by a growing list of diseases whose occurrence are directly associated with MTs, actin or intermediate filaments (Table 1.2).

The large majority of diseases in which MTs and actin are involved are the ones caused by molecules that interact directly with either the MT or the actin cytoskeleton. As such, both MTs and actin are targets for a growing number of drugs, specifically anti-cancer drugs. In this field, the use of the drugs that suppress MT dynamics leading to arrest of cell proliferation by apoptosis, have been in medical use since the 1960's (Zelnak 2007). While MT-targeting drugs are routinely used in cancer therapy, very few actin-targeting drugs have so far been characterized and none are used in the clinic. Nonetheless, several compounds that affect the dynamics of the actin cytoskeleton with high therapeutic value have been identified and efforts to evaluate its clinical potential are underway (Giganti and Friederich 2003).

Table 1.2. Examples of diseases associated with the cytoskeleton or interacting proteins.

Microtubules[1]	**Actin**[2]	**Intermediate Filaments**[3]
Alzheimer's disease	Actin myopathy	Epidermolysis bullosa simplex
Down's syndrome	Nemaline myopathy	Amyotrophic disease
Multiple system atrophy	Intra-nuclear rod myopathy	Parkinson disease
Pick's disease	Rod-core disease	Neuronal IF inclusion disease
Extraskeletal myxoid chondrosarcoma	Congenital fiber type disproportion	Amyotrophic lateral sclerosis

[1] Source: (Hisaoka *et al.* 2003; Robert and Mathuranath 2007)
[2] Source: (Laing and Nowak 2005)
[3] Source: (Godsel *et al.* 2008)

1.8 Schizosaccharomyces pombe

1.8.1 A model organism

In 1893, P. Lindner was the first to describe fission yeast *Schizosaccharomyces pombe* (Leupold 1950). He isolated the yeast from East African beer, and chose as its epithet the Swahili word for beer, 'pombe'. His isolate was a homothallic strain containing cells of both the h+ and h- mating type, which can mate pair-wise and form asci containing four ascospores (Wixon 2002). *S. pombe*, being a distant relative from the baker's yeast *S. cerevisiae*, did benefit from the classical genetic biochemical and molecular biology methods developed for *S. cerevisiae* (Glick 1996), as well as with the sequence and annotation of its genome (Wood *et al.* 2002). Furthermore, in some aspects *S. pombe* resembles mammalian cells more closely than does *S. cerevisiae*, and if a process is similar in *S. pombe* and *S. cerevisiae*, it is likely to be conserved throughout eukaryotes (Moreno *et al.* 1991).

Most of the research work in *S. pombe* aimed at understanding the cell cycle (Nurse 2000) and its regulation (Moser and Russell 2000). It also provided greater understanding in diverse areas of research as MT arrays formation (Hagan and Petersen 2000), meiotic differentiation (Yamashita *et al.* 1997), cellular morphogenesis (Brunner and Nurse 2000) and cell polarity (Bahler and Peter 2000). In these latter fields, genetic studies have enabled the study and characterization of several genes that control cell morphogenesis and polarity (Snell and Nurse 1994; Verde *et al.* 1995).

1.8.2 The fission yeast cell cycle

Fission yeast is a rod shape organism, with a rigid cell wall (Figure 1.5A). It grows in a polarized manner by extension at its ends and divides by medial fission to generate two equal sized daughter cells (Hayles and Nurse 2001). Initially, the new cells only grow at the old end which existed before division. Later in the cell cycle, they initiate growth at the new end, derived from the septation, becoming bipolar. This process is known as **n**ew-**e**nd-**t**ake-**o**ff or (NETO; Mitchison and Nurse 1985). The position of the two growth sites at opposite ends of *S. pombe* determines the long cell axis, and likewise its shape.

1.8.3 The fission yeast actin cytoskeleton

Actin in fission yeast is encoded by a single gene (*act*1) and exists in two states: G-actin, a minority form, and polymerized or F-actin. Actin patches, cables and the contractile ring are comprised of F-actin (Marks *et al.* 1986; Arai *et al.* 1998; Arai and Mabuchi 2002). Actin patches are the primary sites of actin nucleation. The maintenance of both actin patches and cables requires continuous actin polymerization. Normally actin patches concentrate at the cell tips or at the septum, exhibiting non-directed movement or moving away from those sites (Figure 1.5A; Pelham and Chang 2001).

Actin cables have their barbed end facing the cell tips, and extend to the interior of the cell along its long axis (Kamasaki *et al.* 2005). This orientation is essential to maintain the polarized cell growth, since it allows the transport of actin patches, secretory vesicles and polarity factors to the growth sites. (Arai *et al.* 1998; Feierbach and Chang 2001; Pelham and Chang 2001).

At the onset of mitosis, the actin cables re-orient such that the barbed ends face the mid-region of the cell. This allows the transport of the required materials to the formation site of the contractile ring and septum (Kamasaki *et al.* 2005). Later on, the actin cables accumulate in the middle of the cell and together with myosin form the contractile ring (Arai and Mabuchi 2002).

After septation, actin patches concentrate at the old end and only at NETO are they visible at both cell ends (Figure 1.5A; Marks *et al.* 1986).

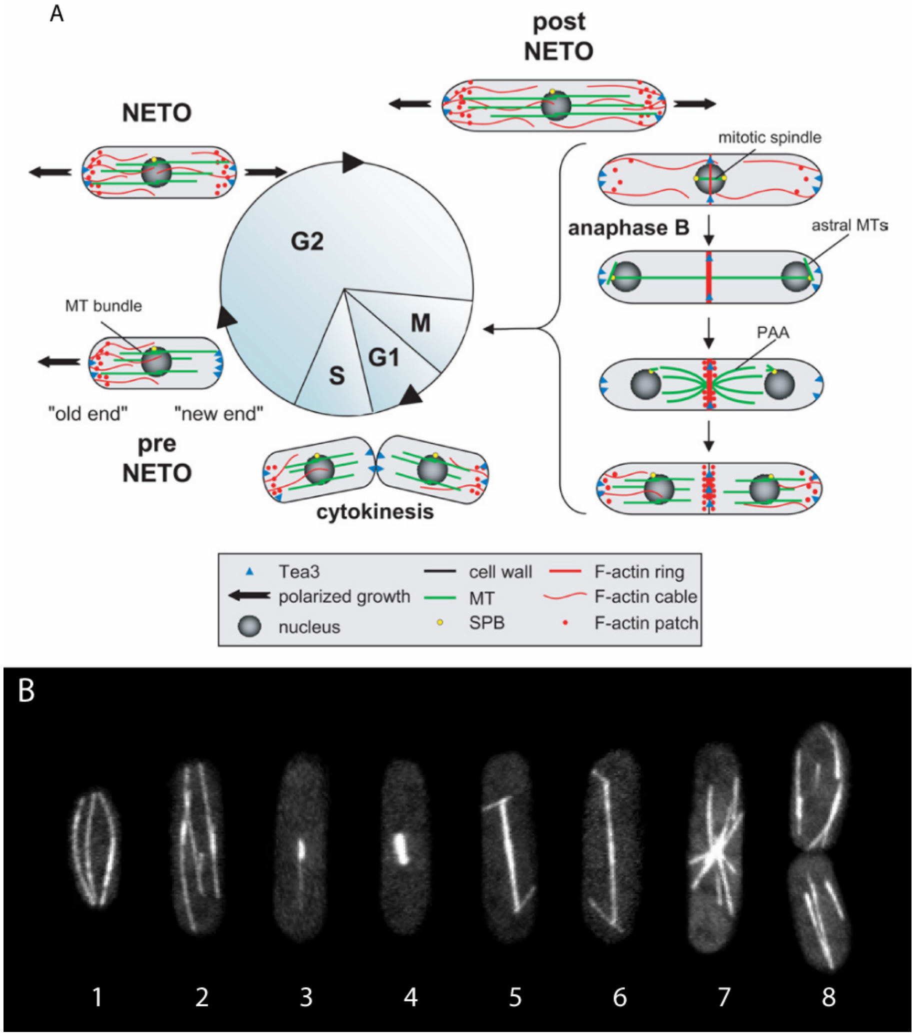
A
post
NETO
NETO
mitotic spindle
anaphase B
astral MTs
G2
MT bundle
M
G1
S
PAA
"old end"
"new end"
pre
NETO
cytokinesis
Tea3
polarized growth
nucleus
cell wall
MT
SPB
F-actin ring
F-actin cable
F-actin patch
B
1
2
3
4
5
6
7
8

Figure 1.5. *S. pombe* cytoskeleton organization during cell cycle.

(A) In this case polarized localization of Tea3p is shown as an example of proteins that influence polarized growth in *S. pombe*. Also note the very short G1 and S phase of *S. pombe*, having a longer G2 phase. See text for more details of A. Adapted from (La Carbona *et al.* 2004).

(B) This panel shows the MT cytoskeleton of *S. pombe* expressing an integrated allele of GFP-α-tubulin (the native gene is still present) during cell cycle. 1, Pre-NETO; 2, Pos-NETO; 3, beginning of Mitosis; 4, Metaphase; 5, Early anaphase; 6, Late anaphase; 7, Post-anaphase array; 8, Cytokinesis.

1.8.4 Fission yeast microtubule cytoskeleton

Interphase cells are characterized by having 3 to 6 **i**nterphase **m**icrotubule **a**rrays (IMAs; Figure 1.5A and B; Hagan 1998; Drummond and Cross 2000). These are MT bundles composed of 2 to 9 MTs (Hoog *et al.* 2007) that extend from the cell center to the cell tips. At the cell tips, they deposit polarity markers, namely Tea1p, responsible for the correct positioning of the growth zones (Mata and Nurse 1997).

IMAs are characterized by a stable medial MT overlap region, (also called **i**nterphase **m**icro**t**ubule **o**rganizing **c**enter – [iMTOC]), where the MT minus ends are localized, and a distal part, where the MT plus ends undergo repeated cycles of MT growth and shrinkage. Two different types of iMTOCs exist in *S. pombe*. The SPB-associated iMTOC, which is in direct contact with the SPB, and the non SPB iMTOCs which do not contact the SPB but the nuclear envelope (Tran *et al.* 1999; Brunner and Nurse 2000; Drummond and Cross 2000).

The SPB iMTOC is connected to the nuclear envelope by a network of membrane proteins, which link the SPB to the heterochromatin (King *et al.* 2008). Among this network of proteins is Sad1p, a SUN domain protein (Miki *et al.* 2004) which is embedded in the inner nuclear membrane and links the inner nucleus with the cytoplasm via Kms1p and Kms2p KASH domain proteins (Miki *et al.* 2004). Although poorly characterized, Sad1p is present also at the non-SPB iMTOCs (Tran *et al.* 2001) raising the possibility that all iMTOCs that are in contact with the nuclear envelope are connected to the heterochromatin. How the MTs are connected to the KASH proteins remains to be elucidated.

As cells enter mitosis, the IMAs that are not connected to the SPB are progressively depolymerized. Only the IMA that is connected to the already duplicated SPBs undergoes additional cycles of growth and shrinkage (Sagolla *et al.* 2003). At this point, a fenestra in the nuclear envelope membrane appears underneath the SPBs through were the SPBs are progressively embedded in the nuclear membrane (Ding *et al.* 1997). Concomitantly, an intra-nuclear mitotic spindle forms (Hagan 1998; Sagolla *et al.* 2003). Before the SPBs separate and the mitotic spindle is formed, short highly dynamic intra-nuclear MTs are visible extending from the SPB intra-nuclear region into the center of the nucleus. These MTs are no longer observed as the SPBs separate and move to opposite sites of the nucleus with the mitotic spindle assembled between them.

As mitosis progresses with the spindle elongation, new cytoplasmic MTs called ‘astral’ MTs appear at the onset of anaphase A. These originate from the cytoplasmic face of the SPB (Sagolla *et al.* 2003). At the end of anaphase B, both nuclei have reached the opposite ends of the cell and the mitotic spindle breaks down. Cytokinesis occurs and two identical daughter cells are formed. At this point the MTs are nucleated from the SPB and from the **e**quatorial **m**icro**t**ubule **o**rganizing **c**enter (eMTOC), which localizes at the septation site and forms the MT **p**ost-**a**naphase-**a**rray (PAA). At the end of septation, the eMTOC disappears and the IMAs are reestablished (Sagolla *et al.* 2003).

1.8.5 IMAs generation: a three step model

The generation and maintenance of IMAs is achieved by three main events: localization of MT nucleation, formation of antiparallel MT overlap regions and regulation of MT catastrophe (Figure 1.6).

1.8.5.1 Microtubule nucleation

The MAPs Mto1p (Table 1.3; also known as Mbo1p or Mod20p; Sawin *et al.* 2004; Venkatram *et al.* 2004; Zimmerman and Chang 2005) and Mto2p (Table 1.3; Janson *et al.* 2005; Samejima *et al.* 2005; Venkatram *et al.* 2005) have been implicated in MT nucleation and its localization during interphase.

By associating with the γ-TuRC, the Mto1p/Mto2p complex form what we subsequently refer to as a nucleation seed. This nucleation seed allows MT nucleation to be targeted to the SPB, the nuclear surface, the lattice of other MTs and occasionally to the cytoplasm (Sawin *et al.* 2004; Janson *et al.* 2005). This greatly facilitates the formation and maintenance of IMAs (Figure 1.6: number 1).

1.8.5.1.1 Mto1p and Mto2p

While Mto2p shows no similarity with other proteins, Mto1p has significant similarity with *S. pombe* Pcp1p (Flory *et al.* 2002), a protein homologous to *S. cerevisiae* Scp110, and with *S. cerevisiae* Scp110 itself, which interacts with and anchors the γ-TuRC to the nuclear face of the *S. cerevisiae* SPB (Knop and Schiebel 1998; Vinh *et al.* 2002). Furthermore, Mto1p also shows a similarity with proteins in the fungus *Neurospora crassa* and the protein apsB from *Aspergillus nidulans*. Finally, the N-terminal of Mto1p has a small region of sequence similarity shared in higher eukaryotes including the *Drosophila melanogaster* centrosomin (Sawin *et al.* 2004) which plays a role in MT nucleation and recruitment of γ-TuRC to the centrosome (Megraw *et al.* 1999; Vaizel-Ohayon and Schejter 1999; Terada *et al.* 2003).

Cells in which *mto*1 or *mto*2 are deleted show severe defects in cytoplasmic MT nucleation. In the case of *mto*1Δ cells, cytoplasmic nucleation is completely absent and these cells lack both eMTOC and iMTOCs (Sawin *et al.* 2004; Venkatram *et al.* 2004; Zimmerman and Chang 2005). In fact, cytoplasmic MTs normally originate from the MTs of the spindle midzone which fail to disassemble at late anaphase and are broken by cell fission leading to the release of MTs into the cytoplasm. In addition, in some cases the spindle does not disassemble even after fission and cytoplasmic MTs originate by intra-nuclear MTs that grow and pierce the nuclear envelope escaping into to the cytoplasm (Zimmerman and Chang 2005).

In *mto*2Δ cells the phenotype is less severe. These cells have an eMTOC, albeit less focused than in the *wild type*, and present one IMA, presumably originated from nucleation at the cytoplasmic face of the SPB (Janson *et al.* 2005; Samejima *et al.* 2005; Venkatram *et al.* 2005).

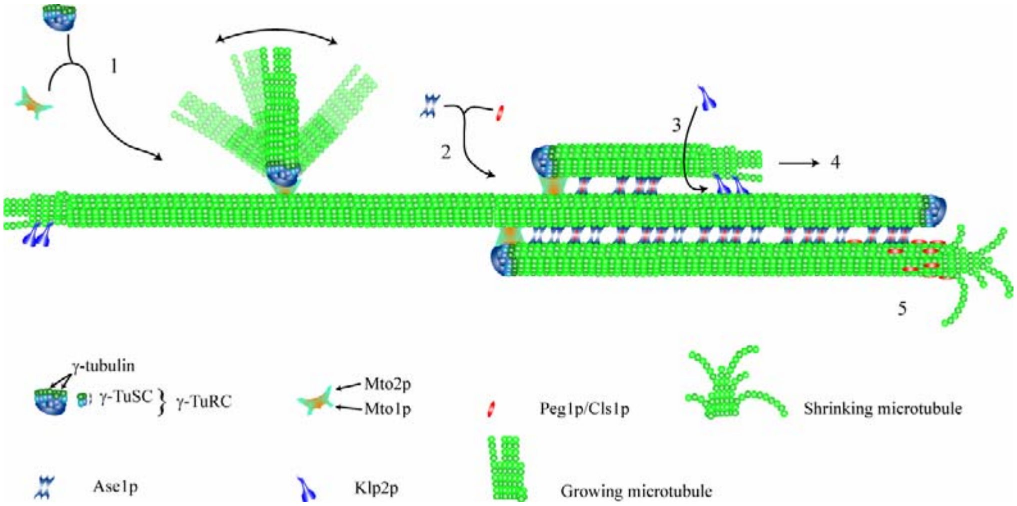

Figure 1.6. Latest model of IMA organization.

The formation of an IMA in *S. pombe* and its maintenance involves several steps and numerous proteins. 1 – Targeting of nucleation to the MT lattice. 2 – Determination of antiparallel orientation between adjacent MTs by MT selective bundling and targeting of stabilizing agent. 3 and 4 – Focusing of MT overlap region by MT sliding. 5 – MT overlaps maintenance by stabilization of depolymerizing MT and subsequent growth rescue. See text for more details.

1.8.5.2 Formation of antiparallel microtubule overlap regions.

Upon new nucleation of MTs, antiparallel MT overlap regions are believed to be formed mainly by the action of two MAPs: Ase1p and Klp2p (Table 1.3).

During interphase, Ase1p localizes to the MT overlap regions where it bundles adjacent MTs with an antiparallel orientation (Loiodice *et al.* 2005). *In vitro* work showed that Ase1p favors by ~9 fold the bundling of antiparallel MTs. Due to this, it is believed that the bundling action of Ase1p is responsible for determining the antiparallel orientation of a MT newly nucleated along the lattice of a preexisting one (Figure 1.6: number 2).

Following, Klp2p, a member of the minus-end-directed Kinesin–14 family (Troxell *et al.* 2001), is believed to attach to the growing MT plus ends via its non-motor domain such that the motor domain is free to move along the lattice of another MT. Like this, Klp2p pulls a newly nucleated growing MT towards the minus end of an adjacent and antiparallel MT, stabilizing the MT overlap region (Janson *et al.* 2007; Figure 1.6: numbers 3 and 4).

1.8.5.2.1 Ase1p

Ase1p is a member of the MAP65/PRC1/ASE1 family of MT bundling proteins (Loiodice *et al.* 2005). In *S. cerevisiae* Ase1 stabilizes the spindle midzone, allowing anaphase spindle elongation (Schuyler *et al.* 2003). In *Caenorhabditis elegans*, SPD-1 has similar function in stabilizing the spindle midzone (Verbrugghe and White 2004) while in *D. melanogaster*, Feo organizes the central spindle which is essential for subsequent cytokinesis (Verni *et al.* 2004). Likewise, PRC1 in humans organizes the spindle midzone which is essential for the subsequent cytokinesis (Mollinari *et al.* 2002). In plants, MAP65 has several isoforms, some of which function during mitosis while others function during interphase in the organization of cortical arrays of MTs (Chan *et al.* 1999; Muller *et al.* 2004). In fact, it was shown *in vitro* that MAP65 in carrot forms electron-dense bridges in between MTs with average inter- MT spacing of 25nm to 30 nm (Chan *et al.* 1999). Interestingly, even though only one member of Ase1 family exists in *S. pombe*, it functions both in mitosis and interphase, unlike its plant homologs (Loiodice *et al.* 2005).

Cells lacking *ase*1 show severe defects in the organization of IMAs. These defects include an increased number of IMAs per cell, which are very unstable and were reported to lack a medial region of higher fluorescent intensity. This suggested that the observed IMAs in *ase*1Δ cells are in fact single MTs (Loiodice *et al.* 2005). As a consequence, *ase*1Δ cells grow more slowly and display aberrant cell shapes and have defects in nuclear positioning during interphase (Loiodice *et al.* 2005).

1.8.5.2.2 Klp2

S. pombe has a second member of the Kinesin-14 family, Pkl1p which localizes to the nucleus during interphase (Troxell *et al.* 2001). Other members of this family include the *S. cerevisiae* Kar3, protein that destabilizes MTs preferably at the minus ends and is also required for karyogamy (Endow *et al.* 1994; Maddox *et al.* 2003), and *D. melanogaster* Ncd that, together with a the bipolar kinesin motor Klp61F, is responsible for mitotic spindle integrity (Sharp *et al.* 1999).

Cells lacking Klp2p have IMAs with multiple and unstable MT overlap regions and aberrant polarities, i. e., an excess of MTs growing towards the nucleus region instead of away from it (Carazo-Salas *et al.* 2005). Moreover, computer simulations predicted that cells without Klp2p often possess IMAs with a wider overlap region, reduced to two antiparallel MTs (Janson *et al.* 2007). These simulations also suggested that the combined function of Ase1p and Klp2p is sufficient to generate stable bipolar bundles (Janson *et al.* 2007).

1.8.5.3 Regulation of microtubule catastrophe.

Finally, the maintenance of an IMA is achieved by controlling MT catastrophe at the overlap regions. It was recently shown that Ase1p targets the protein Peg1p/Cls1p (Table 1.3 and Figure 1.6: number 2) to the MT overlap regions where it stabilizes a subset of MTs by stopping their full depolymerization and allowing an overlap region to be maintained (Figure 1.6: number 5; Bratman and Chang 2007).

1.8.5.3.1 Peg1p/Cls1p

Peg1p/Cls1p belongs to the conserved CLASP protein family (see section 1.6.1.2.3). In vertebrates they are required for ordered cell migration and for the local modulation of MT dynamics (Mathe *et al.* 2003). In vertebrates, CLASPs are require for local modulation of MT dynamics, while in mammals CLASP stabilizes the association of MTs with the cell cortex (Lee *et al.* 2004).

It should be noted that the exact function of Peg1p/Cls1p in *S. pombe* interphase is still subject of debate. Two independent groups determined different cellular localizations and different functions for this protein. Grallert *et al* (2006) found that Peg1p/Cls1p localizes to the MT plus ends where it induces MT instability and slows polymerization at cell ends. Conversely, Bratman and Chang (2008) found that Peg1p/Cls1p localizes to the MT overlap regions where it stabilizes MTs and allows the rescue of a depolymerizing MT to a growing state. Additionally, a third group has found a new role for Peg1p/Cls1p in the organization of the interphase mitochondria network (Chiron *et al.* 2008).

Table 1.3. Characteristics of the proteins involved in the generation and maintenance of IMAs.

Mto1p / Mod20p / Mbo1p

Protein characteristics/domains[1]	Phenotype of deletion mutant in interphase and mitosis	Family/Homology[2]	Reference
128.4 kD 1115 amino acids 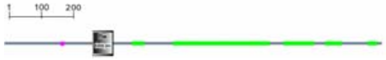	More curved cells; Fewer and ticker IMAs; Lack of astral MTs in mitosis; Mitotic spindle fails to breakdown after anaphase; Lack of eMTOC; MT bundles curve around cell tips and exhibit bent-and-break phenotype; IMAs do not connect the SPB; MTs exhibit treadmilling.	An apsB Sp pcp1 Dm centrosomin Hs myomegalin Hs_CDK5RAP2 Sc_Scp110p	(Sawin *et al.* 2004; Vanoosthuyse *et al.* 2004; Zimmerman and Chang 2005)
Acronym	**Localization in interphase**	**Protein interactions**	
Microtubule organizer 1 Morphology defective 20 Microtubule organizer 1	SPB; nuclear surface; satellites along IMAs; eMTOC	Mto2p	

Mto2p

Protein characteristics/domains[1]	Phenotype of deletion mutant in interphase and mitosis	Family/Homology[2]	Reference
44.0 kDa; 347 amino acids 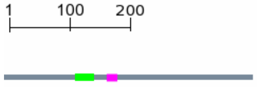	MT bundles curve around cell tips and exhibit bent and break phenotype; Mostly one IMA in interphase, possibly originated from the SPB; MTs exhibit treadmilling.	Non observed	(Janson *et al.* 2005; Samejima *et al.* 2005; Venkatram *et al.* 2005)
Acronym	**Localization in interphase**	**Protein interactions**	
Microtubule organizer 2	iMTOC eMTOC Actinmyosin ring	Mto1p Alp4p Alp6p	

(continues)

Ase1p

Protein characteristics/domains[1]	**Phenotype of deletion mutant in interphase and mitosis**	**Family/Homology[2]**	**Reference**
83.1 kDa; 731 amino acids 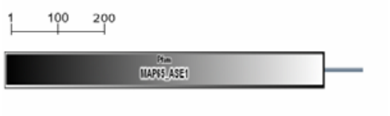	Higher number of IMAs; Loss of medial zone of higher fluorescence intensity in IMAs; Slower anaphase II; Nuclear and septum position defects; Spindle elongation defects and premature breakdown.	ASE1/PRC1/MAP65 family (see text)	(Loiodice *et al.* 2005; Yamashita *et al.* 2005)
Acronym	**Localization in interphase**	**Protein interactions**	
Anaphase spindle elongation 1	MT overlap regions	Peg1/Cls1p	

Klp2p

Protein characteristics/domains[1]	**Phenotype of deletion mutant in interphase and mitosis**	**Family/Homology[2]**	**Reference**
91.0 kDa; 817 amino acids; 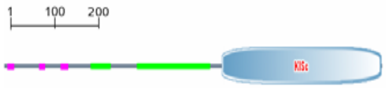	IMA decrease stability; Lack of fusion of MT overlap; Aberrant polarity of MTs; Lack of MT sliding in IMAs.	Kinesin 14 family (see text)	(Troxell *et al.* 2001; Carazo-Salas *et al.* 2005; Janson *et al.* 2007)
Acronym	**Localization in interphase**	**Protein interactions**	
Kinesin like protein	Along MT lattice and MT plus end	Tubulin	

Peg1p/Cls1p

Protein characteristics/domains[1]	**Phenotype of deletion mutant in interphase and mitosis**	**Family/Homology[2]**	**Reference**
164.0 kDa 1462 amino acids Heat repeats Basic serine-rich stretch	Mitosis terminal arrests at metaphase plate formation; Less and more stable IMAs; Altered MT dynamics; Unstable MT overlap regions; Mitochondria network collapse.	Clip170 Associated Proteins Family (see text)	(Grallert *et al.* 2006; Bratman and Chang 2007; Chiron *et al.* 2008)
Acronym	**Localization in interphase**	**Protein interactions**	
Unknown	MT plus tips or MT overlap regions	Tip1p or Ase1p	

[1] Source: *S. pombe*GB (http://www.genedb.org/genedb/pombe/) and SMART (http://smart.embl-heidelberg.de/).

[1] An, *Aspergillus nidulans*, Sp, *Schizosaccharomyces pombe*, Dm, *Drosophila melonogaster*, Hs, *Homo sapiens*, Sc, *Saccharomyces cerevisiae*

Legend of SMART domains:

🟪 Segments of low compositional complexity determined by the SEG program.

🟩 Coiled coil region determined by the Coils2 program.

Pfam [illegible] Pfam domain Microtubule-associated (PF07989).

Pfam MAP65_ASE1 Pfam domain Microtubule associated protein MAP65/ASE1 family (PF03999).

KISc Kinesin motor, catalytic domain, ATPase (SM00129).

1.9 Electron Tomography

Electron tomography is a method of generating 3D images from multiple 2D projection images of a 3D object, obtained over a wide range of viewing directions. For generating a 3D image, a set of 2D projection images are recorded while tilting the object incrementally round an axis (Figure 1.7A). Each 2D image is subsequently back-projected, with the appropriated weighting, to form a 3D density distribution of the original object (Figure 1.7B; Baumeister *et al.* 1999). Since macromolecules are slightly denser than the solvent in which they are prepared, they will interact more strongly than the solvent with the electrons in the beam path – a process known as ‘electron scattering’ (McIntosh *et al.* 2005).

The resulting reconstructions can be view in 2D image planes at selected values of the third dimension. Such electronic slices are only a few nanometers thick (2 to 4nm) allowing to determine the position of complex features relative to the other slices (McIntosh *et al.* 2005).

1.9.1 Automated electron tomography

With the computerization of transmission electron microscopes and the development of large-area **c**harge-coupled **c**amera **d**evices (CCD), complex image-acquisition schemes can be run fully automated (Koster *et al.* 1992). This makes recording of tomography data sets much less time consuming as well as allowing for new developments in the acquisition to be integrated. One of these developments was brought by the software SerialEM (Mastronarde 2005), which offers the possibility of recording a montage micrograph at each increment. Such a feature allows capturing two to nine adjacent overlapping images of an area. Furthermore, the possibility of joining tomograms from serial sections was also implemented in the software package IMOD (Kremer *et al.* 1996; Mastronarde 1997). Together these advances have enabled the reconstruction of large cell volumes (Hoog and Antony 2007).

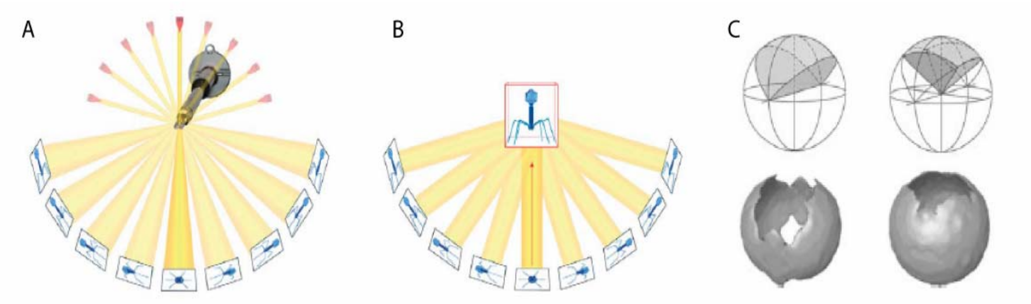

Figure 1.7. Principle of electron tomography and the missing wedge effect.

A biological specimen can be imaged from several orientations by tilting the holder in the microscope (A). Later by computed back-projection, each tilted view is used to contribute to the reconstruction of the original structure (B). Due to physical limitations the specimen cannot be tilted to 90º, creating the missing wedge effect (C). Both images represent a schematic of the missing Fourier domain in a single-axis tilting (left) – a missing wedge, and in a double-axis tilting (right) – a missing pyramid. Bellow are illustrated the real space information. Adapted from Lucic *et al.* 2005; McIntosh *et al.* (2005).

1.9.2 Sample preparation

The amount of detail that can be extracted from a tomogram has evolved along with the microscope developments as well as with the improvements in sample preparation. Indeed the first cellular samples visualized by electron tomography were prepared by chemical fixation, dehydration and embedding (McEwen *et al.* 1986; Belmont *et al.* 1987). Although such samples provided information at the cellular level, the ultra-structural details could not be interpreted due to fixation artifacts – a constant cause for concern in electron microscopy.

In recent years, major efforts in sample preparation techniques have allowed the development of several methods to prepare samples for electron tomography while preserving the native structure of the organism. These include ultra-rapid freezing and **h**igh-**p**ressure **f**reezing (HPF). In the first the specimen is plunged into liquid ethane to drop their temperature rapidly enough to preserve the native structure (McIntosh 2001). This method, albeit successful, only works on cells that are thin enough to be frozen without forming ice crystals. Unfortunately, most cells are too thick and can not be frozen using this method. HPF deals with this problem by using high hydrostatic pressure as a physical cryoprotectant. As water expands when it freezes, if the pressure is increased quickly followed by rapid freezing, the water in the sample will vitrify preserving the native structure and avoiding the formation of ice crystals (Giddings *et al.* 2001).

1.9.3 Electron tomography in the study of the microtubule cytoskeleton

Electron tomography has been a very useful tool in the study of the organization of the MT cytoskeleton in different organisms (O'Toole *et al.* 1999; O'Toole *et al.* 2003a; O'Toole *et al.* 2003b; Hoog *et al.* 2007). One of the major advantages of this technique is the ability to track MTs through a volume. Contrary to the classical technique of serial sectioning where the resolution is anisotropic and limited to the thickness of the section (normally > 40 nm; Ding *et al.* 1993), the ability to section a volume electronically in slices of ~ 2 nm, with isotropic resolution allows the visualization of the MT end structures from which one can infer the polarity of the MT. Indeed, a previous study (O'Toole *et al.* 2003b) showed that the MT ends at the mitotic centrosome of *C. elegans* have a distinct structure (in the form of a cap) to those found away from the centrosome. This capped structure was attributed to the presence of the γ-TuRC at the MT minus end (see section 1.5.2).

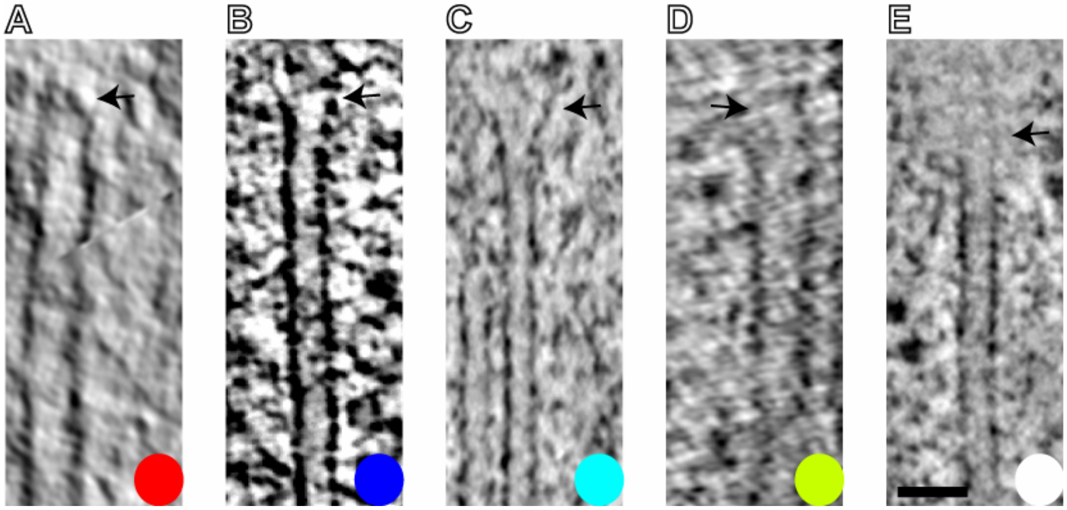

Figure 1.8. Microtubule end structures classes and color scheme used in models.

Arrows point to the MT ends.
(A) Example of a capped end structure. Marked with a red sphere in our models.
(B) Example of a blunt end structure. Marked with a blue sphere in our models.
(C) Example of a flared end structure. Marked with a cyan sphere in our models.
(D) Example of a sheet end structure. Marked with a green sphere in our models.
(B) Example of an ambiguous end structure. Marked with a white sphere in our models.

Based on previous studies (O'Toole *et al.* 2003b; Hoog *et al.* 2007) we classified our MT end structures in five classes in accordance to the scheme used in Hoog *et al*. (2007): capped, blunt, flared, sheet and ambiguous (Figure 1.8). To allow the reader to immediately know the MT end structure in the models we used colored spheres positioned at the end of MTs.

1.9.4 Problems in electron tomography

Like all techniques, electron tomography has some disadvantages. Most of these are related with the preparation of the sample and/or data acquisition.

In order to avoid fixation artifacts by post freezing treatments, cryo-electron tomography was developed, where the sample is kept at -160ºC after being frozen. This allows the imaging of cells close to native structure. Nonetheless such samples are very sensitive to the electron dose that they are subjected to under the microscope beam. This means that the sample is not always stable enough for large areas reconstructions (Steven and Aebi 2003).

To reconstruct large areas of a cell, HPF combined with freeze-substitution is normally used. This technique relies on HPF for keeping the native structure of the specimen, and substitution of the water in the sample by adequate plastics at very low temperatures (Giddings *et al.* 2001) – a method known as HPF/**f**reeze-**s**ubstitution (HPF/FS). With this method the biological samples are stained with heavy metals salts to increase the signal to noise ratio which raises some problems. First, since the sample is stained, what is visualized in the micrographs is not the actual cellular structures but the stain. Secondly, most of these heavy metals salts show aggregation events which limit the resolution to ~ 6nm (Lucic *et al.* 2005). Finally, even though such samples are much less sensitive to the electron dose applied, they still shrink perpendicularly to the axis of the beam path, which may cause artifacts in the reconstruction of tomogram (albeit software algorithms can already compensate in part of such artifacts [Mastronarde 1997]). Furthermore, due to the physical impossibility of tilting the specimen over a range of 180º, the reconstruction misses data – normally called the missing wedge data (Figure 1.7C). To tackle this latter problem, one can remove the sample and rotate it by 90 º. Subsequently, a new tilt-series at the same position is acquired and both tomograms can be combined without loss of resolution – refered as dual-axis tomography. This technique allows for reduce the loss of data due to the missing wedge effect and increases the contrast of structures that were orthogonal to the beam path in the first tilt-series acquired (Mastronarde 1997).

1.10 Motivation

1.10.1 The questions behind this study

MT assembly into IMAs has so far only been analyzed by careful visualization and quantification of a combination of biochemistry, molecular, genetic and fluorescent live imaging methods. Despite great advances in the understanding of IMA organization, several questions of great importance remain unanswered mostly due to the limitations in resolution of optical microscopes.

Electron tomography has been successfully applied to study the differences between a *wild type* organism and several mutant strains (O'Toole *et al.* 1999; O'Toole *et al.* 2003a), specifically to yeast cells (O'Toole *et al.* 2002). Indeed, the early reconstruction of the *wild type* spindle of *S. pombe* by classical serial sectioning technique showed that *S. pombe* is a very good organism for electron microscopy studies (Ding *et al.* 1993). Furthermore, the reconstruction of large cell volumes of *wild type S. pombe* by electron tomography has demonstrated the potential of this technique to answer questions related to the ultra-structural organization of IMAs (Hoog and Antony 2007). Indeed, only electron tomography can reveal exact numbers of MTs per IMA, their orientation in relation to other MTs, the relation between MTs and SPB and the relation between MTs and cell organelles (Hoog *et al.* 2007).

We decided to use electron tomography to investigate a number of open questions regarding the function of several proteins involved in the formation of IMAs. One of the first questions we addressed was if cells lacking Ase1p possessed MT overlap regions, and if these existed, what was their MT pairing orientation and their inter-MT distance. Secondly we wanted to assess the *in silico* predictions made for *klp*2Δ mutants, regarding the type of IMA and MT orientation (see section 1.8.5). Third, we asked if *mto*1Δ cells would possess IMAs or only single MTs. Finally we sough to explain how single MTs or IMAs would show a treadmilling behavior in *mto*1Δ cells.

2 RESULTS

2.1 Cells lacking Ase1p contain microtubule overlap regions

A recent study showed that the **m**icro**t**ubule (MT) overlap regions of fission yeast **i**nterphase **m**icrotubule **a**rrays (IMAs) are composed of MTs paired in both parallel and antiparallel directions (Hoog *et al.* 2007). Previous reports, based on fluorescence microscopy data, proposed that MT overlap regions are virtually absent in cells lacking Ase1p (Loiodice *et al.* 2005; Yamashita *et al.* 2005). Moreover, *in vitro* data showed that the probability that Ase1p bundles antiparallel MTs was 9.4 times higher than that of bundling parallel MTs (Janson *et al.* 2007). So far, these studies have been limited by the impossibility to resolve single MTs.

We generated tomograms and 3D models to describe the exact MT cytoskeleton in *ase*1Δ cells. The reconstructed partial volumes of *ase*1Δ cells (Figure 2.1; see Annex III for a complete list of volumes acquired) showed striking differences in the organization of the MT cytoskeleton compared to *wild type.* The observed number of IMAs per volume varied from 0 to 3 (1.89 ± 0.93 on average; n = 17 in 9 volumes; see Annex IV for a comparison of bundles per cell in *wt* and all the analysed mutants). Single MTs were observed, as proposed in previous reports (Loiodice *et al.* 2005), and varied from 1 to 6 per volume (3.1 ± 1.54 on average; n = 28). Several single MTs, likely to emanate from the nucleus surface, were observed while others were disconnected from the nucleus and dispersed in the cytoplasm (Figure 2.1A). The average length of MTs was very similar to the published wild type values (Table 2.1).

Table 2.1. MT lengths, polymerized tubulin and electron-dense bridges angles of *wild type* and ase1Δ cells.

	MT lengths (**m**icro**m**eters [µm])				Relative polymerized tubulin($\mu M\ \mu m^{-1}$)		Electron-dense bridges (degrees)		
	Average	SD	MAX	n	Average	SD	Average	SD	n
wt	1.64[1]	1.43[1]	6.0[1]	70[1]	0.22	0.15	73.94	8.08	11
*ase*1Δ	1.62	1.61	6.8	35	0.16	0.13	62.53	9.95	22

[1](Hoog *et al.* 2007); SD, standard deviation; MAX, maximum MT length found.

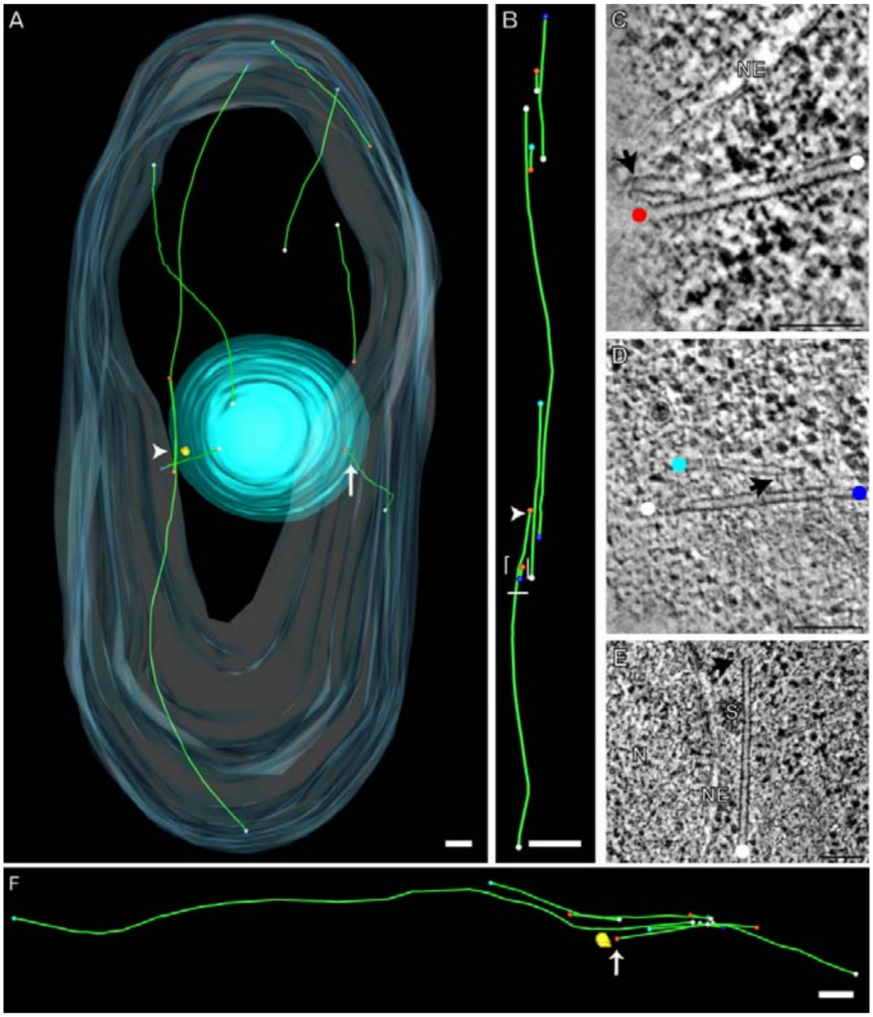

Figure 2.1. Overlap MT regions are present in *ase*1Δ cells.

(A) Reconstruction of a partial volume of *ase*1Δ mutant, where two IMAs crossing the SPB (yellow) in perpendicular orientations (arrowhead) are visible. Note that the MT perpendicular to the cell long axis seems to have emanated from the nuclear envelope surface (arrow).

(B) Non SPB-associated IMA with two small MT overlap regions. Arrowhead points to a MT spreading apart from the lattice of an adjacent MT. Note the capped end of the MT spreading apart next to the lattice of the adjacent MT.

(C) Tomographic slice of a close-up from the delineated area in B showing a small MT spreading apart from the MT lattice of the adjacent microtuble. Note the MT blunt end close to the adjacent MT lattice. Arrow points to the capped end. Colored circles indicate the end structure of the MT not visible in the image.

(D) Detail from a tomographic slice in which a capped end (minus) is visible in the vicinity of another MT lattice. An electron-dense bridge is visible linking the capped end and the MT lattice (arrow).

(E) Tomographic slice of the only MT lattice laterally attached to the SPB (S), with its capped end in the vicinity of the SPB (arrow).

(F) SPB-associated IMA with the overlap region shifted away from the SPB, and a MT that appears to have emanated from the SPB (arrow).

MT ends structures are represented by colored spheres: red (capped structure), blue (blunt structure), cyan (flared structure) and white (undetermined structure).Nucleus (N) and nuclear envelope (NE). SPB (S). White bars: 250 nm. Black bars: 100 nm.

Overlap MT regions were observed in most reconstructed volumes (Figure 2.1A, B, and F). We analyzed the orientation of overlapping MTs by determining their polarity according to the MT end structure. We characterized the MT end structures in four types: capped, blunt, flared and ambiguous (Figure 1.8).

We found 10 MTs spreading apart from the lattice of a neighbour MT (Figure 2.1B to D; MTs obliquely orientated to the MT lattices adjacent to it). For 8 such cases we could determine the polarity of the MT spreading apart. Of these, 6 had their capped (minus) end as the closest point to the lattice of the neighbor MT (Figure 2.1B and D) while 2 had their plus ends (Figure 2.1C).

To determine if the analyzed mutants had altered inter-MT spacing within the MT overlap regions, compared with the *wild type*, we performed neighbor density analysis (Ding *et al.* 1993). The major density peak for the global inter-MT distribution in *ase*1Δ mutants had a centroid (the center of mass of the peak) at 11.8 **n**ano**m**eters (nm; Figure 2.2A). This is significantly below the globally prefered inter_MT values of 25 to 30 nm in *wild type* (Hoog *et al.* 2007). We refined our analysis by measuring MT overlap regions only if we could determine the MT orientations (n = 4). This revealed a preferred inter-MT spacing between antiparallel MTs with a centroid at 12.7 nm (Figure 2.2B).

The presence of electron-dense bridges between MTs of an IMA has been documented for Ase1p homologs (Chan *et al.* 1999; Mollinari *et al.* 2002). More recently, electron-dense bridges were visualized *in vivo* in *wild type* fission yeast cells, but have so far not been attributed to a specific protein (Hoog *et al.* 2007). To search for such electron-dense bridges, we generated dual axis tomograms of *wild type* cells and *ase*1Δ mutant cells. Indeed, we could observe such electron-dense bridges not only in *wild type* but also in *ase*1Δ cells (Figure 2.2C and D). Since in the latter case the inter-MT spacing is significantly reduced compared to *wild type*, we measured the smallest angle of these bridges with respect to the MT walls. Interestingly, *ase*1Δ cells electron-dense bridges had an average angle smaller than *wild type* (Table 2.1). This suggests that the altered inter-MT spacing might influence the type of cross bridge formed in between MTs.

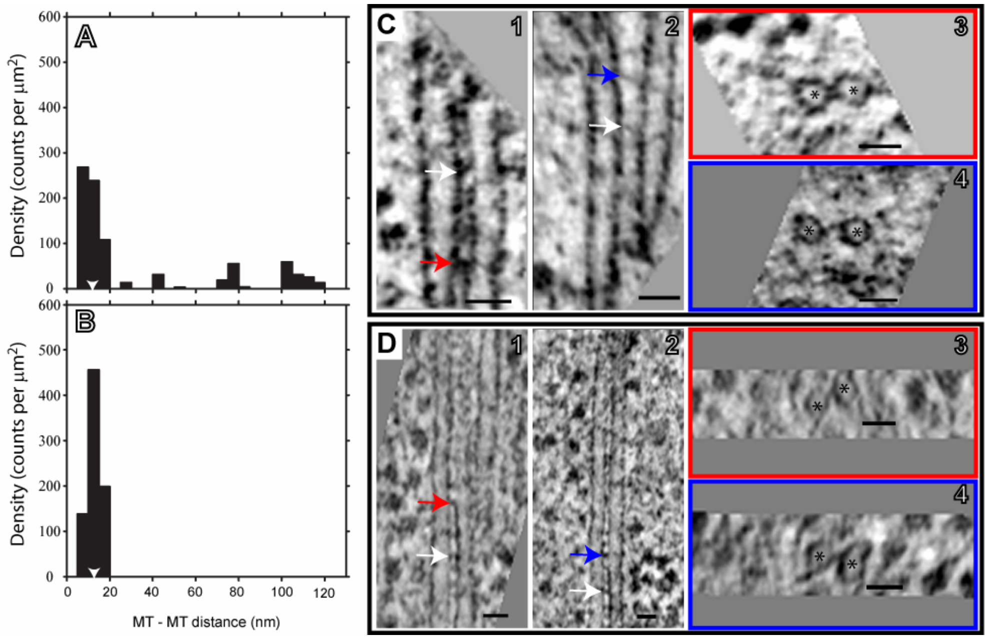

Figure 2.2. Neighbor density analysis showing MT – MT distances and a gallery of electron-dense bridges in *ase*1Δ cells.

(A and B) Global inter-MT distances and distances of antiparallel MTs in IMAs for *ase*1Δ cells, respectively. Triangles points to the centroid of each major density peak.
(C1 and C2) *wild type* selected longitudinal tomographic slices of two adjacent MTs showing electron-dense bridges (arrows). Volumes were rotated into the MT lattice plane. (C3 and C4) Cross slice of 1 and 2, respectively, in the plane of red and blue arrows. Note the two MT walls and lumen (asterisk) as well as the density connecting both MT walls.
(D) Similar to (C) for *ase*1Δ cells.
Bars: 25 nm.

To see if *ase*1Δ had an influence in the amount of polymerized tubulin, we estimated the amount of total polymerized tubulin relative to the total volume reconstructed (see Materials and Methods), for all the reconstructed *ase*1Δ mutant cell volumes and additional *wild type* volumes. We found a reduction of 26% in the relative amount of polymerized tubulin in *ase*1Δ mutant compared to *wild type* (Table 2.1).

We next wanted to see if there is a difference between **s**pindle **p**ole **b**ody (SPB)-associated and non SPB-associated IMAs, as observed in *wild type* (Hoog *et al.* 2007). In all reconstructed *ase*1Δ volumes, the SPB-associated IMAs had a higher number of MTs (4.86 ± 2.48 on average; n = 7) than the non-SPB-associated IMAs (3.4 ± 1.5 on average; n = 10). Two of the IMAs observed (one SPB-associated and one non-SPB-associated) as well as four single MTs were orientated perpendicular to the long cell axis (Figure 2.1A). We also observed, in three cases, IMAs and/or single MTs in the SPB region orientated perpendicular to each other (Figure 2.1A). Strikingly, in most cases there was no MT lattice laterally connected to the SPB, as observed in *wild type* cells (Hoog *et al.* 2007). Instead, MTs appeared to emanate from the SPBs with the closest MT end to the SPB being a capped end (Figure 2.1F, arrow). Only in one case of the seven SPB-associated IMAs, was a MT lattice connected to the SPB. However, the capped end of this MT was located very close to the contact point between the SPB and the MT lattice (Figure 2.1E).

These data clearly show that in the absence of Ase1p, antiparallel MT overlap regions are still present. *ase*1Δ cells have a reduced number of IMAs and a higher number of individual MTs, compared to *wild type* cells. *ase*1Δ IMAs have a significantly reduced inter-MT spacing compared to *wild type* values, which seems to affect the angles of the electron-dense bridges observed in *ase*1Δ cells. Furthermore, the electron tomography analysis of *ase*1Δ cells confirmed that MTs emanate from the SPB surface (Hoog *et al.* 2007), and also from other MT lattices. In both cases the capped end was located proximal to the SPB surface or to the lattice of the other MT.

2.2 *klp*2Δ cells predominantly display IMAs with only two MTs

Klp2p is believed to stabilize IMAs by focusing their MT overlap regions. It pulls a newly nucleated MT along another antiparallel MT towards its minus end (Carazo-Salas *et al.* 2005; Janson *et al.* 2007) IMAs in *klp*2Δ cells were reported to possess multiple MT overlap regions and to be less stable than in *wild type* cells (Carazo-Salas *et al.* 2005). Furthermore, *in silico* experiments predicted that without Klp2p, IMAs tend to form wide MT overlap regions reduced to two antiparallel MTs (Janson *et al.* 2007).

Similarly to *ase*1Δ cells, we generated tomograms and modeled large partial volumes in *klp*2Δ cells. The reconstructed volumes possess 1 to 5 IMAs (3.5 ± 1.4; n = 21 in 5 different cells; see Annex IV for a comparison of bundles per cell in *wt* and all the analysed mutants) and 1 to 3 single MTs (1.83 ± 0.98; n = 11). Most IMAs consisted of two MTs (53.1% of total number of IMAs; Figure 2.3A to D) with a maximum of 5 MTs in one IMA (single occurrence). The average MT length was slightly smaller than in *wild type* or *ase*1Δ cells (Table 2.2). The IMAs displayed overlapping regions where MTs were paired in antiparallel orientations (Figure 2.3D).

Only in one case did we observe MTs which were bundled with parallel orientations (Figure 2.3A and B). Single MTs with one end in close proximity to the nuclear envelope were also observed (Figure 2.3A).

In this mutant, the SPB-associated IMAs had on average more MTs (3.5 ± 1.73; Figure 2.3F) than the non SPB-associated IMAs (2.29 ± 0.85). Similarly to *ase*1Δ volumes, we observed MTs that seemed to emanate from the SPB with their capped end adjacent to the cytoplasmic surface of the SPB (Figure 2.3E).

Table 2.2. MT lengths, polymerized tubulin and electron-dense bridges angles of *wild type*, *ase*1Δ and *klp*2Δ cells.

	MT lengths (μm)				Relative polymerized tubulin(μM μm^{-1})		Electron-dense bridges (degrees)		
	Average	SD	MAX	n	Average	SD	Average	SD	n
wt	1.64[1]	1.43[1]	6.0[1]	70[1]	0.22	0.15	73.94	8.08	11
*ase*1Δ	1.62	1.61	6.8	35	0.16	0.13	62.53	9.95	22
***klp*2Δ**	**1.30**	**1.43**	**3.4**	**44**	**0.12**	**0.04**	**75.1**	**9.5**	**14**

[1] (Hoog *et al.* 2007); SD, standard deviation; MAX, maximum MT length found. Data relative to this section in bold.

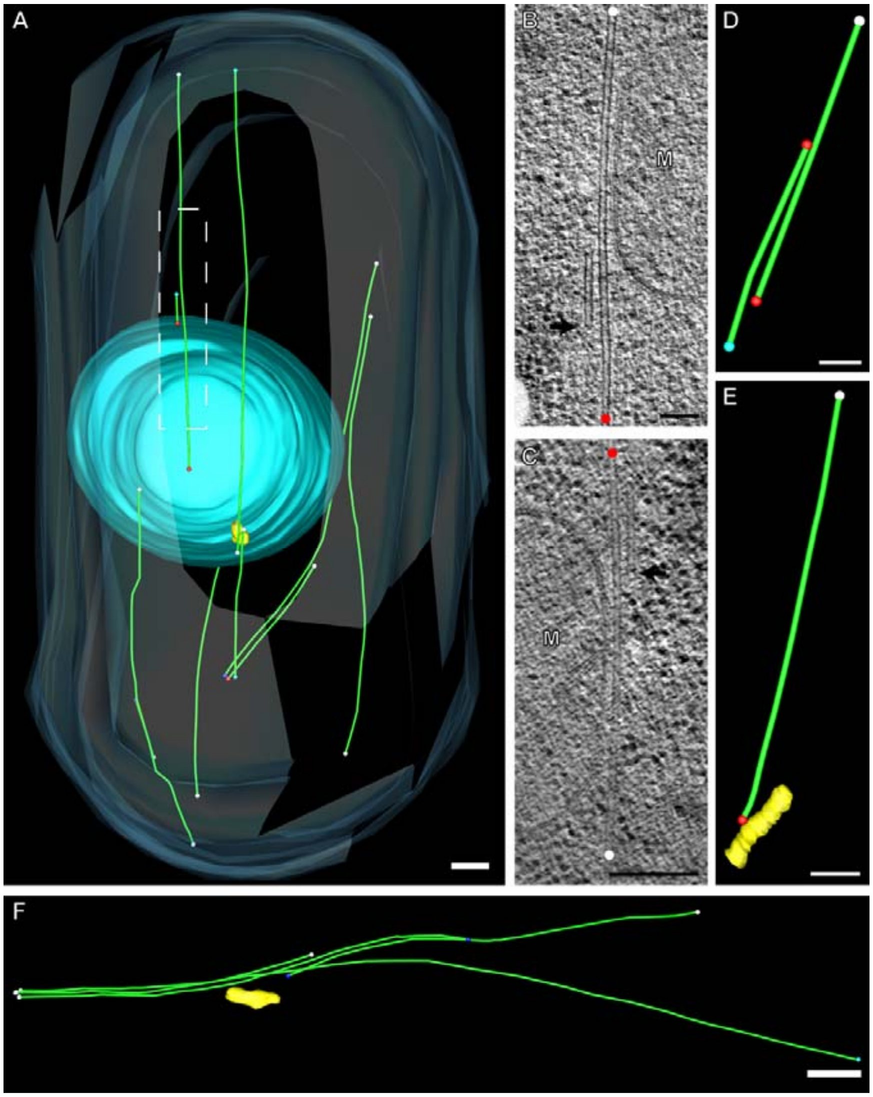

Figure 2.3. IMAs with two MTs prevail in *klp*2Δ cells.

(A) Reconstruction of a partial cell volume of a *klp*2Δ mutant with MT overlap regions consisting of only two MTs. MTs that appear to emanate from the nuclear surface and from the SPB are also visible.

(B) Tomographic slice of the non SPB-associated IMA from the delineated area in (A) showing the only parallel MT pair found in *klp*2Δ cells. Notice the lateral association of the MT with the mitochondria (M). Arrow points to the capped end of the small MT. Colored circles indicate the MT end structures which are not visible in the image.

(C) Tomographic slice showing a non SPB-associated IMA with only two antiparallel MTs. Once more, the lateral contact with the mitochondria can be seen. Arrow points to the capped end of smaller MT.

(D) Example of a non SPB-associated IMA with two antiparallel MTs.

(E) MT that appears to have emanated from the SPB.

(F) SPB-associated IMA with a large overlapping region.

MT ends structures are represented by colored spheres: red (capped structure), blue (blunt structure), cyan (flared structure) and white (undetermined structure). Mitochondria (M).

White bars: 250 nm. Black bars: 100 nm.

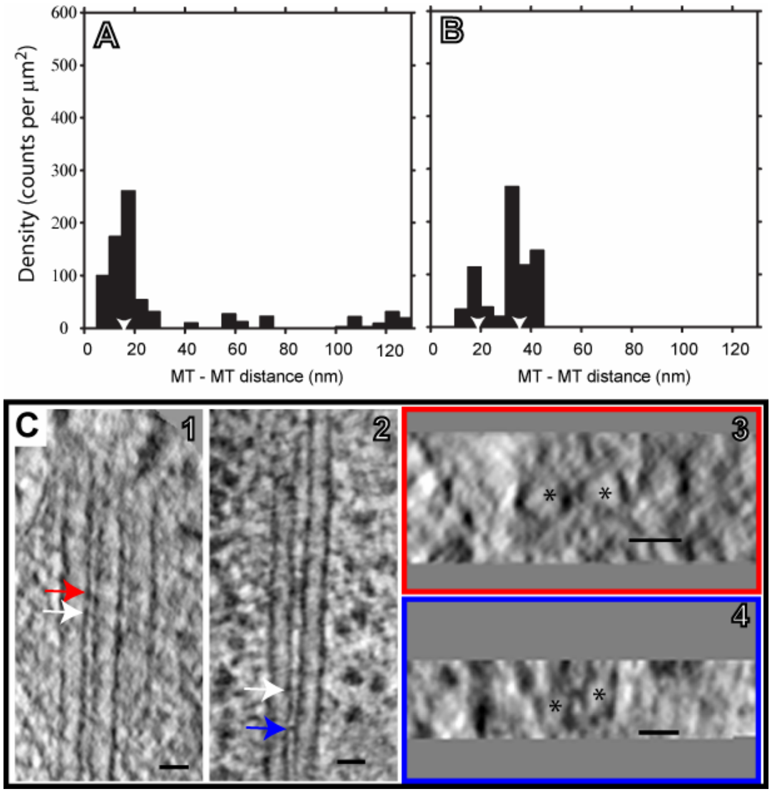

Figure 2.4. Neighbor density analysis showing MT – MT distances and a gallery of electron-dense bridges in *klp*2Δ cells.

(A and B) Global inter-MT distances and distances of antiparallel MTs, respectively, in IMAs for *klp*2Δ cells. Triangles points to the centroid of each major density peak.

(C1 and C2) *klp*2Δ selected longitudinal tomographic slices of two adjacent MTs showing electron-dense bridges (arrows). Volumes were rotated into the MT lattice plane. (C3 and C4) Cross slice of 1 and 2, respectively, in the plane of red and blue arrows.

Bar: 25 nm.

We wondered if *klp*2Δ would affect the inter-MT spacing of MT overlap regions, knowing that Ase1p was present in these cells. We performed neighbor density analysis on the MT overlap regions of *klp*2Δ cells and found a single peak for the global inter-MT spacing with a centroid at 16.8 nm (Figure 2.4A). Once more, we refined our neighbor density analysis by taking into consideration only MT overlaps were we could determine the MT orientation (n=7). The density distribution for antiparallel MT overlaps (n=6) showed two peaks, one with a centroid at 18.7 nm and the other with a centroid at 35.5 nm (Figure 2.4B). The only parallel MT pair had an inter-MT spacing of 35 to 40 nm.

In order to visualize inter-MT electron-dense bridges, we calculated dual axis tomograms. We could visualize such electron-dense bridges in *klp*2Δ cells (Figure 2.4C). These had an average angle similar to the value of *wild type* (Table 2.2), reinforcing the idea that these angles are dependent on the inter-MT spacing.

To see if *klp*2Δ affected the amount of polymerized tubulin, we estimated the relative total amount of polymerized tubulin for all the reconstructed volumes and found that the value obtained for *klp*2Δ cells was 36% lower than the *wild type* value (Table 2.2).

In agreement with the *in silico* data (Janson *et al.* 2007) we could clearly show that the IMAs and the MT overlap regions in *klp*2Δ cells are mostly limited to 2 MTs, but not exclusively, with MTs appearing as antiparallel pairs. Furthermore, the inter-MT spacing was sightly decreased compared to *wild type*, while the angles of the electron-dense bridges were similar to *wild type*.

2.3 IMAs in *mto*1Δ also have only two MTs

*mto*1Δ is known to severely affect MT nucleation (Sawin *et al.* 2004; Venkatram *et al.* 2004; Zimmerman and Chang 2005). Interphase MTs normally originate from the spindle midzone MTs which fail to disassemble at late anaphase and are broken by the cell fission leading to release of MTs into the cytoplasm. In addition, in some cases the spindle does not disassemble, even after fission, and cytoplasmic MTs originate by intra-nuclear MTs that grow and pierce the nuclear envelope escaping into to the cytoplasm (Zimmerman and Chang 2005). Once in the cytoplasm, no MT nucleation seems to occur (Sawin *et al.* 2004).

The fact that only a small MT piece seems to “escape” the nuclear envelope into the cytoplasm, made us wonder if *mto*1Δ IMAs, as visualized by fluorescence microscopy, were single MTs or indeed IMAs. In addition, if they were IMAs, could we visualize MTs spreading apart from the lattice of another MT? Furthermore, we asked if electron-dense bridges were visible between the capped end and the lattice of the adjacent MT, as observed in *ase*1Δ cells. To investigate this we applied the same procedure as previously to *mto*1Δ cells.

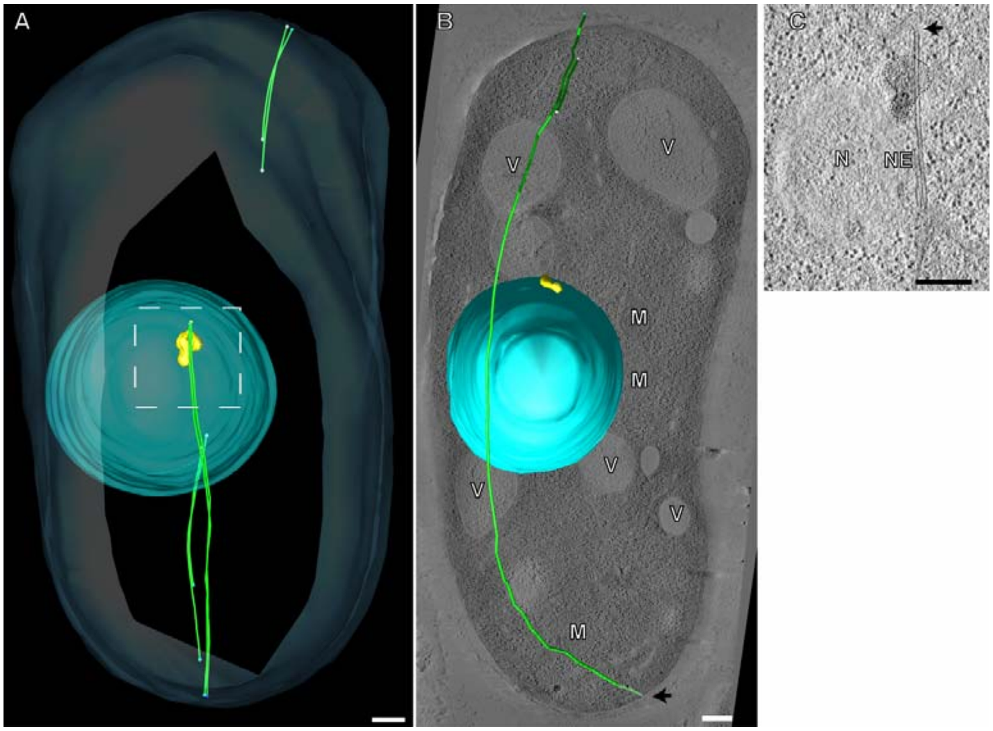

Figure 2.5. *mto*1Δ cells have fewer IMAs.

(A) Reconstruction of a partial cell volume of an *mto*1Δ mutant with only three IMAs. All the MT overlap regions consist of two MTs, as visualized in *klp*2Δ mutant volumes. This was the only volume where MTs appeared in contact with the SPB density (framed). Note that all the MT end structures identified are open structures.

(B) Partial volume of an *mto*1Δ mutant with a single IMA (model) curling around the cell end (tomographic slice). The cell bends at the tip where the MT is curling (arrow). Several vacuoles (V) and mitochondria (MT) are visible in the tomographic slice.

(C) Tomographic slice of the framed area in (A) showing the MT lattice in direct contact with the SPB density (dashed line). Also visible is the MT end sheet structure (arrow), the nucleolus (N) and the nuclear envelope (NE) with nuclear pore complexes.

MT ends structures are represented by colored spheres: red (capped structure), blue (blunt structure), cyan (flared structure) and white (undetermined structure). Vacuole (V), mitochondria (M), nucleus (N), nuclear envelope (NE). Bars, 250 nm.

We did not find any MTs spreading apart from a neighboring MT in *mto*1Δ cells. Instead, we observed distinct IMA organizations (Figure 2.5). As in *klp*2Δ volumes, all IMAs observed were composed of two MTs (n = 5; Figure 2.5A to C). In one case, the cell seemed to possess only one IMA and no single MTs (Figure 2.5B; see Annex IV for a comparison of bundles per cell in *wt* and all the analysed mutants). This IMA had a MT that spanned the whole cell length, curling at one of the poles. The curling was at the same pole where the cell was bent (Figure 2.5C). The other partial volumes had between 0 to 3 IMAs per volume (n = 4 partial volumes) while the number of single MTs also varied from 0 to 2 (n =4 partial volumes). Since Mto1p has a function in MT nucleation (Sawin *et al.* 2004; Venkatram *et al.* 2004; Zimmerman and Chang 2005) we estimated the relative amount of polymerized tubulin in our volumes. We found a drastic decrease of 68% in the relative amount of polymerized tubulin compared with *wild type* (Table 2.3).

Table 2.3. MT lengths, polymerized tubulin and electron-dense bridges angles of *wild type*, *ase*1Δ, *klp*2Δ and *mto*1Δ cells.

	MT lengths (μm)				Relative polymerized tubulin (μM μm^{-1})		Electron-dense bridges (degrees)		
	Average	SD	MAX	n	Average	SD	Average	SD	n
wt	1.64[1]	1.43[1]	6.0[1]	70[1]	0.22	0.15	73.94	8.08	11
*ase*1Δ	1.62	1.61	6.8	35	0.16	0.13	62.53	9.95	22
*klp*2Δ	1.30	1.43	3.4	44	0.12	0.04	75.1	9.5	14
***mto*1Δ**	**2.29**	**1.83**	**6.97**	**12**	**0.07**	**0.02**	**62.53**	**17.66**	**10**

[1](Hoog *et al.* 2007); SD, standard deviation; MAX, maximum MT length found. Data relative to this section in bold.

We measured the inter-MT distance in the IMAs and obtained a distribution with two peaks. The main peak had values between 0 nm and 35 nm with the centroid at 15.3 nm (Figure 2.6A). When we analyzed the MT end structures to determine the MT orientation in the bundles, we discovered that several MTs showed open (flared, blunt or sheet like) structures at both ends (Figure 2.5A). Only in one single MT could we visualize a capped end structure. Finally, we measured the angle of electron-dense bridges and obtained an average angle similar to that in *ase*1Δ cells (Table 2.3).

Only in one case of the four partial volumes calculated, we observed an IMA laterally associated with a density that we believed to be the SPB

(Figure 2.5C). This is consistent with 71% of SPBs previously observed that do not localize with an IMA (Zimmerman and Chang 2005). The SPB that we observed was different from previously observed SPBs by us and others (Ding *et al.* 1993; Ding *et al.* 1998; Zheng *et al.* 2006; Hoog *et al.* 2007; Toya *et al.* 2007). It appeared to be a duplicated SPB that continued to enlarge becoming deformed. Also this SPB was protruding from the nucleus surface, as if it was being pushed away from it.

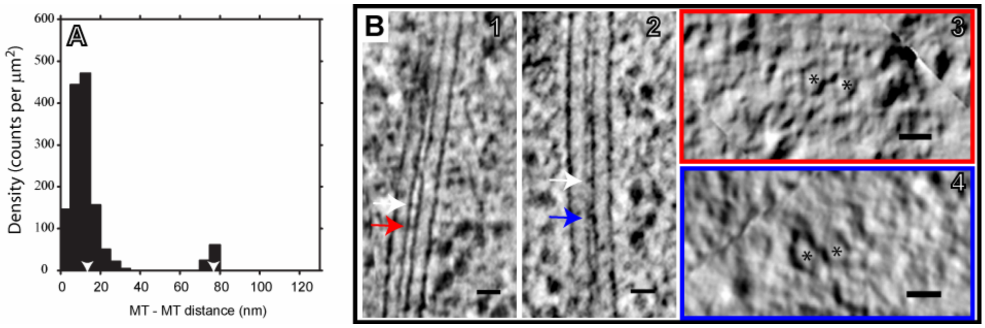

Figure 2.6. Neighbor density analysis showing MT – MT distances and a gallery of electron-dense bridges in *mto*1Δ cells.

(A) Global inter-MT distances in IMAs for *mto*1Δ cells. Triangles point the centroid of each major density peak.

(B1 and B2) *mto*1Δ selected longitudinal tomographic slices of two adjacent MTs showing electron-dense bridges (arrows). Volumes were rotated into the MT lattice plane. (B3 and B4) Cross slice of 1 and 2, respectively, in the plane of red and blue arrows.

Bar: 25 nm.

These results show that *mto*1Δ cells form IMAs with predominantly two MTs, even though single MTs are also present. The IMAs have a global preferred inter-MT distance of ~15 nm and the MTs pair with another MT along their entire length. MT pairing orientation was not possible to determine due to the fact that most MTs had open structures at both ends. In addition, in the only case where an IMA was associated with the SPB, this was larger and deformed compared to *wild type* SPBs.

2.4 *klp*2Δ cells and *mto*1Δ cells have similar or higher MT pairing length to *wild type* cells but show less MT overlap length

The restriction of two MTs *per* IMA observed in *klp*2Δ mutants prompted us to try and find out how this could correlate with the predicted widening of the MT overlap regions on *klp*2Δ cells (Janson *et al.* 2007).

We measured the length of MT pairs in IMAs for *wild type* and the analyzed mutants by estimating for each MT the summed absolute length over which MTs would be closer than 35nm to one another (Figure 2.7A).

We found that *wild type* cells showed an average MT pairing length of ~ 0.88 µm (Table 2.4), roughly half the average length of a MT. *ase*1Δ mutant volumes showed the most significant decrease in the MT pairing length, while *klp*2Δ mutants had similar values to *wild type*. In *mto*1Δ, we found this value to be higher than the one obtained for *wild type* and all the previous mutants. In fact, the length of the pairing was defined by the smallest MT in the IMA.

In order to rule out the possibility that the higher MT pairing lengths observed were due to higher individual MT lengths, we compared them and found no evidences for a correlation between the MT length and its MT pairing length in *ase*1 and/or *klp*2 mutants (Figure 2.7B to E). On the contrary, the *mto*1 mutants showed a slight correlation (Figure 2.7F and G).

Table 2.4. MT pairing and IMA MT overlap region in *wild type*, and all the analyzed mutants.

	MT pairs (µm)			*IMA overlap (µm)*		
	Average	*SD*	*MAX*	*Average*	*SD*	*MAX*
wt	0.88	0.8	3.3	2.00	1.50	4.98
*ase*1Δ	0.48	0.6	2.58	0.99	0.62	2.23
*klp*2Δ	0.74	0.92	3.98	1.00	0.95	3.52
*mto*1Δ	1.21	1.04	3.13	1.30	1.10	3.22
*ase*1Δ *klp*2Δ	0.59	0.59	2.25	1.00	1.00	3.8
*mto*1Δ *klp*2Δ	2.1	1.72	4.8	1.65	1.30	4.00
*mto*1Δ *ase*1Δ	8.43	3.19	11.24	6.50	0.55	6.88

SD, standard deviation; MAX, maximum length observed.

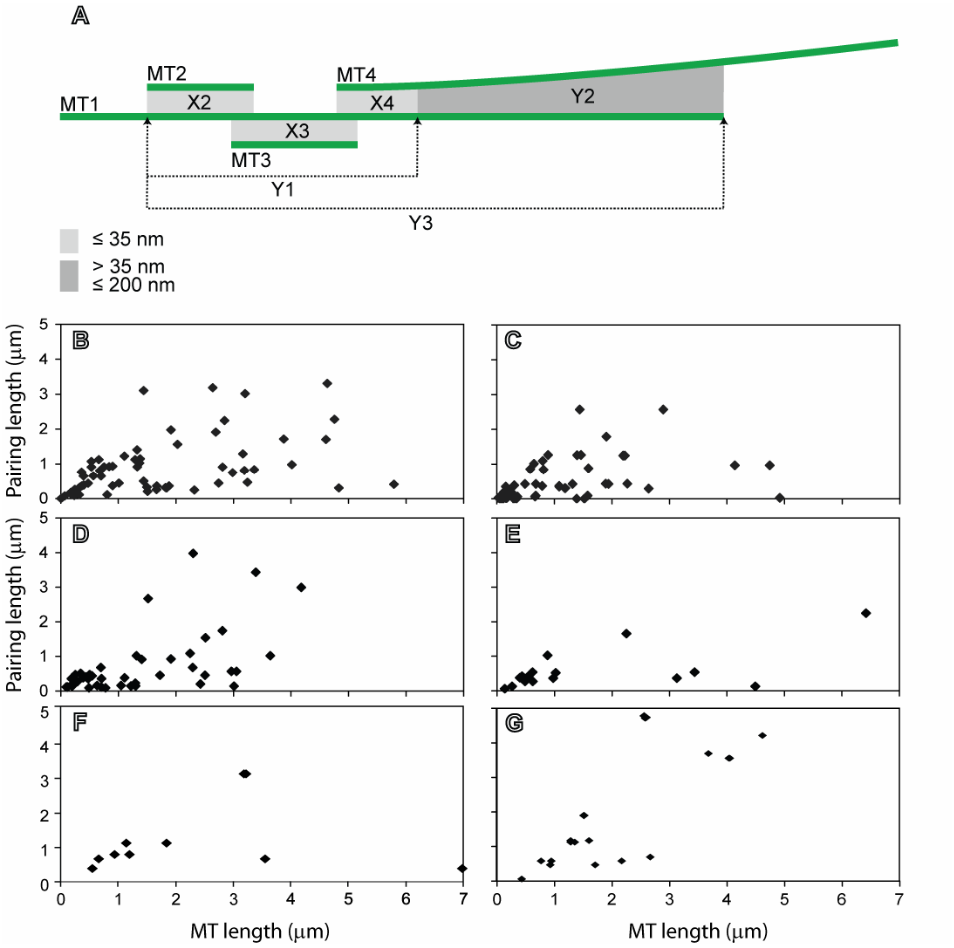

Figure 2.7. MT pairing length and IMA MT overlap region length, and MT pairing length does not correlate with MT length.

(A) Schematic to illustrate the difference between MT pairing length and IMA MT overlap region length. MT pairing length refers to single MTs, while IMA MT overlap region refers to IMAs.
In this example the MT pairing lengths for MT2 = X2, for MT3 = X3 and for MT4 = X4. Notice that the MT pairing length of MT1 is the sum of X2, X3 and X4 fractions, i.e., the summed absolute length of MT1 pairing. Also, the MT pairing length of MT4 equals only to X4 since the MT spreads apart of MT1 and in Y1 it is more than 35 nm apart of MT1. The IMA MT overlap region is determined by the overlap of 2 or more MTs closer than 200 nm. In this IMA the MT overlap region would be Y3 = Y1 + Y2.
(B to E) The length of a MT does not influence its pairing length in either *wild type* (B), ase1Δ (C), klp2Δ (D) or ase1Δ klp2Δ cells (E). No correlation is seen between the MT length increase and the MT pairing length increase. In *mto*1Δ (F) there is a slightly correlation between MT length and MT pairing length, which is more pronounced in *mto*1Δ *klp*2Δ (G). In the mutant *mto*1Δ *ase*1Δ a similar effect was observed (see text for details).

Having analyzed the MT pairing lengths, we estimated the MT overlap region lengths of the IMAs by measuring for each discrete IMA the distance over which two or more MTs would overlap, within 200nm of each other (Figure 2.7A). We found that the measured value for *wild type* (Table 2.4) correlated with the published value for the MT overlap regions of *wild type* cells (Daga *et al.* 2006), hence validating our measurements. In both *ase*1Δ and *klp*2Δ mutants, we observed a clear decrease in the average IMA MT overlap region lengths (Table 2.4). For *mto*1Δ cells, as expected, the MT overlap region lengths average was similar to the length of the MT pairing.

This value was higher than for *ase*1Δ and *klp*2Δ mutants, but still smaller than *wild type* (Table 2.4).

We show here that *ase*1Δ volumes display a significant decrease in the MT pairing length as well as in the length of IMA MT overlap regions. *klp*2Δ mutant volumes show similar MT pairing lengths to *wild type* values, while the IMA MT overlap region length is smaller. *mto*1Δ mutants have a higher MT pairing length than *wild type*, but a smaller IMA MT overlap region length.

2.5 *ase*1Δ *klp*2Δ cells have MT overlap regions

Several studies have suggested that the Klp2p homologs in *C. elegans* and *D. melanogaster* are not only involved in MT sliding, but also in MT bundling (Sharp *et al.* 1999; Segbert *et al.* 2003; Furuta and Toyoshima 2008). Having observed a decrease in the length of MT overlap regions in *klp*2Δ cells, we next asked if Klp2p could also contribute to MT bundling in *S. pombe* and could account for the MT overlap regions which we observed in the *ase*1Δ mutant cells.

We therefore analyzed tomograms and generated 3D models of *ase*1Δ *klp*2Δ cells (gift from P. Tran). We also observed MT overlap regions in the double mutant. For the first time, we observed a MT spanning the entire length of a cell which was part of an IMA with a significantly extended MT overlap region (Figure 2.8A, D). The number of IMAs per reconstructed volume varied from 0 to 2 (1.2 ± 1.1; n=6, in 5 partial volumes; see Annex IV for a comparison of bundles per cell in *wt* and all the analysed mutants), while the number of single MTs per volume varied from 1 to 7 (3.6 ± 2.4, n

= 18). The average MT length for this mutant was slightly increased compared to *wild type* (Table 2.5). The estimated relative amount of polymerized tubulin for all reconstructed volumes showed a similar decrease to the *ase*1Δ mutant in comparison with the *wild type* value (Table 2.5).

Confirming our previous results, *ase*1Δ *klp*2Δ cells displayed features similar to both single mutants, such as single MTs apparently originating from the nucleus surface (Figure 2.8A), IMAs with only two MTs and MTs perpendicular to the long cell axis (Figure 2.8B). Small MTs could also be observed spreading apart from a neighbor MT lattice with both minus and plus ends as the closest point to the adjacent MT lattice (Figure 2.8B).

Table 2.5. MT lengths, polymerized tubulin and electron-dense bridges angles of *wild type*, *ase*1Δ, *klp*2Δ, *mto*1Δ and *ase*1Δ *klp*2Δ cells.

	MT lengths (μm)				Relative Polymerized tubulin(μM μm^{-1})		Electron-dense bridges (degrees)		
	Average	SD	MAX	n	Average	SD	Average	SD	n
wt	1.64[1]	1.43[1]	6.0[1]	70[1]	0.22	0.15	73.94	8.08	11
*ase*1Δ	1.62	1.61	6.8	35	0.16	0.13	62.53	9.95	22
*klp*2Δ	1.30	1.43	3.4	44	0.12	0.04	75.1	9.5	14
*mto*1Δ	2.29	1.83	6.9	12	0.07	0.02	62.53	17.66	10
***ase*1Δ *klp*2Δ**	**1.80**	**1.90**	**6.4**	**21**	**0.19**	**0.12**	**62.23**	**13.1**	**16**

[1] (Hoog *et al.* 2007); SD, standard deviation; MAX, maximum MT length found. Data relative to this section in bold.

Furthermore, MT overlap regions showed a decrease in the inter-MT spacing, with the centroid of the peak distribution at 12.6 nm, similar to *ase*1Δ cells (Figure 2.9A). The same was also observed when we only analyzed MT overlap regions where we could determine the MT orientations (n=2; Figure 2.9B). In *ase*1Δ *klp*2Δ, all the MT overlap regions where we could determine the MT orientations were composed of parallel MTs. The average angle of the electron-dense bridges observed in the dual axis tomograms calculated for the double mutant (Figure 2.9C) was also similar to the value observed in *ase*1Δ cells (Table 2.5). Finally, the MT pairing length for *ase*1Δ *klp*2Δ cells showed a significant decrease compared with *wild type*, as did the IMA MT overlap region lengths (Table 2.4 at page 61).

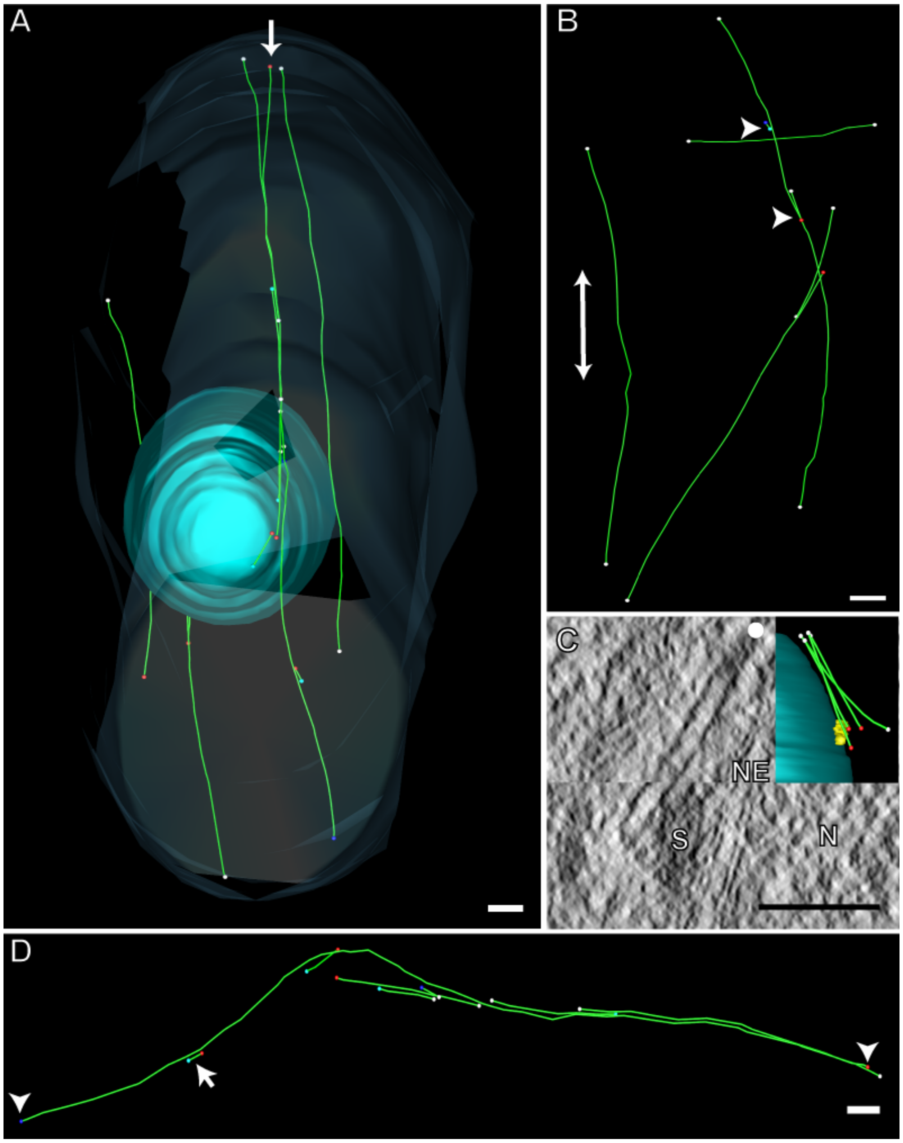

Figure 2.8. The *ase*1Δ *klp*2Δ mutant has MT overlap regions.

(A) Reconstruction of a quasi full cell volume showing a capped end structure close to the plasma membrane (arrow) belonging to a MT that crosses the whole cell length.
(B) All the non SPB-associated IMAs in a partially reconstructed cell volume were MTs spreading apart from another MT lattice are visible; long cell axis indicated by two heads arrow). This cell did not have a SPB-associated IMA.
(C) Tomographic slice of the only case of a SPB-associated IMA found in the reconstructed volumes of ase1Δ klp2Δ cells. Both MTs show their capped end in close proximity to the SPB as can be seen in the model image in the upper right corner.
(D) Longest non SPB-associated IMA from (A) which shows a MT spanning the distance between the two cell tips (arrowheads) and a small MT spreading apart from a MT lattice (arrow). Five other MTs form a MT overlap region surprisingly organized.
MT ends structures are represented by colored spheres: red (capped structure), blue (blunt structure), cyan (flared structure) and white (undetermined structure). Nucleus (N), nuclear envelope (NE), SPB (S). White bars: 250 nm. Black bars: 100 nm.

Concerning SPB-associated IMAs, only one could be identified (Figure 2.8C). However, this IMA was uncharacteristic, as it had two MTs that seemed to emanate from the SPB with the capped end as the closest point to the SPB in both cases. The fact that *ase*1Δ *klp*2Δ mutant mostly lacked SPB attached MTs led us to consider whether Ase1p together with Klp2p could mediate the connection between the MTs and the SPB. To investigate this hypothesis, we decided to measure the minimal distance from the SPB to the closest MT in all mutants. In *wild type*, the closest point of a MT to the SPB is normally a MT lattice that lies in directed contact with the SPB density (Hoog *et al.* 2007). We therefore assumed a distance of zero between the SPB and the MT lattice in *wild type* cells.

We discovered that in general, for *ase*1Δ, *klp*2Δ and *ase*1Δ *klp*2Δ, the closest points of MTs to the SPB were MT ends (Figures 2.1F, 2.3E, 2.8C) while the closest MT wall was 21 nm away from the SPB (excluding one SPB-associated bundle in *ase*1Δ volumes; Figure 2.1E). Furthermore we performed an *in vivo* analysis by live-imaging of cells expressing the SPB marker Cut11-mCherry and the MT marker GFP-atb2 (see Material and Methods). Indeed, we observed a small increase (~4%) in the number of *ase*1Δ cells in which no connection between the SPB and the MTs was visible and a significant increase (~24%) in *ase*1Δ *klp*2Δ cells (Figure 2.10A and 2.10B).

We believed that this analysis confirms our results since the values obtained for SPB - MT mis-localization are highly underestimated, due to low resolution in the *XY* plane (~ 200 nm limited by the technique) and loss of *Z* axis resolution in the analysis.

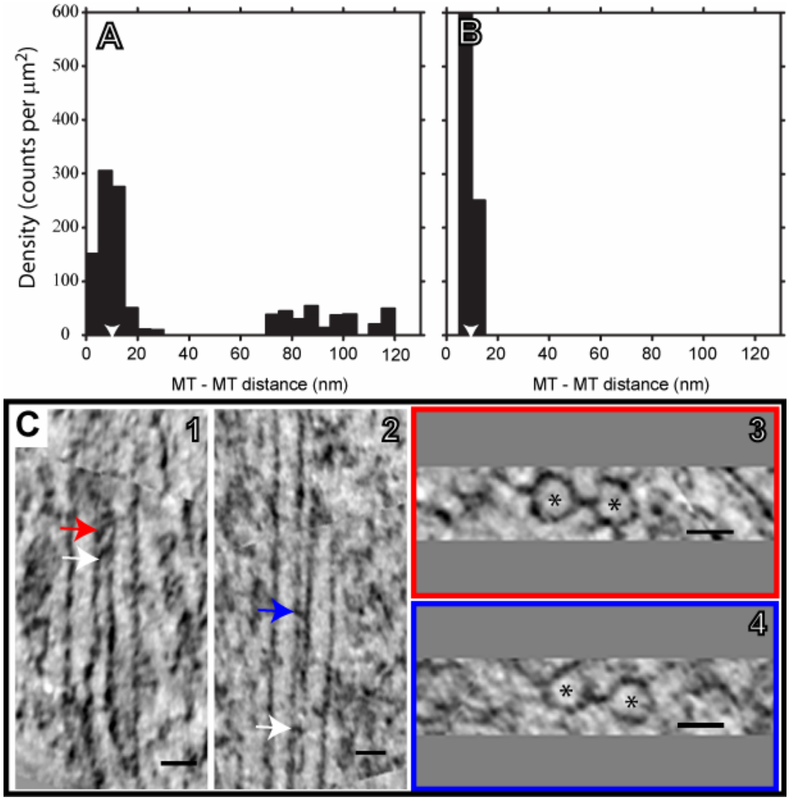

Figure 2.9. Neighbor density analysis showing MT – MT distances and a gallery of electron-dense bridges in *ase*1Δ *klp*2Δ cells.

(A and B) Global inter-MT distances and distances of parallel MTs, respectively, in IMAs for *ase*1Δ *klp*2Δ cells. Triangles points to the centroid of each major density peak.
(C1 and C2) *ase*1Δ *klp*2Δ selected longitudinal tomographic slices of two adjacent MTs showing electron-dense bridges (arrows). Volumes were rotated into the MT lattice plane. (C3 and C4) Cross slice of 1 and 2, respectively, in the plane of red and blue arrows.
Bars: 25 nm.

Our results clearly show the existence of MT overlap regions in cells lacking both Ase1p and Klp2p. Most of the MTs were not bundled, as previously observed in *ase*1Δ mutants. Interestingly, the double mutant showed features visualized in both single mutants. These included IMAs with only two MTs similar to the ones visualized in *klp*2Δ cells, perpendicular MTs to the long cell axis and MTs spreading apart from another MT lattice. Furthermore, we also observed a decrease in the preferred global inter-MT spacing, the average angle of electron-dense bridges, MT pairing length and IMA MT overlap region length.

SPB-associated IMAs were underrepresented compared to single mutant cells this being a unique characteristic of the double deletion mutant.

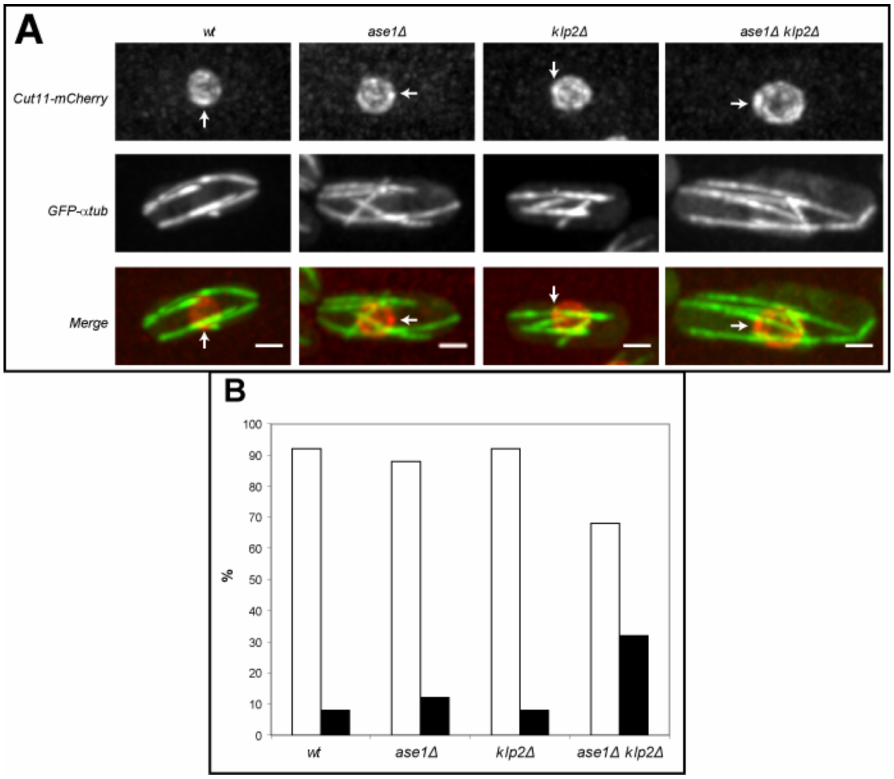
A
wt
ase1Δ
klp2Δ
ase1Δ klp2Δ
Cut11-mCherry
GFP-αtub
Merge
B
100
90
80
70
60
50
40
30
20
10
0
%
wt
ase1Δ
klp2Δ
ase1Δ klp2Δ

Figure 2.10. *ase*1Δ *klp*2Δ mutants have lost the connection between SPB and MTs.

(A) Maximum projection images of strains co-expressing Cut11-mCherry (arrows point to the brighter spot which indicates the SPB) and GFP-atb2. The merged images show the localization of the SPB with respect to the IMAs. Bars: 2 µm

(B) Graph showing the percentage of SPB fluorescent dots that colocalize (white bars) or not (black bars) with IMAs.

2.6 *mto*1Δ *klp*2Δ cells are similar to *mto*1Δ cells

Having observed that similar to *klp*2Δ cells, most IMAs in *mto*1Δ cells are also composed of two MTs, we further analyzed the double deletion mutant lacking both genes.

In the reconstructed volumes the observed phenotypes were very similar to those seen in *mto*1Δ cells. In the 5 partial reconstructed volumes we found 1 to 3 IMAs (1.6 ± 0.89 average, n = 8; see Annex IV for a comparison of bundles per cell in *wt* and all the analysed mutants) and 1 to 3 single MTs (1.5 ± 1.29 average, n = 6; Figure 2.11A and B). The average length of MTs was close to double of the *wild type*, while the relative amount of polymerized tubulin was ~ 40 % less than in *wild type* (Table 2.6).

Table 2.6. MT lengths, polymerized tubulin and electron-dense bridges angles of *wild type*, *ase*1Δ, *klp*2Δ, *mto*1Δ, *ase*1Δ *klp*2Δ and *mto*1Δ *klp*2Δ cells.

	MT lengths (µm)				Relative Polymerized tubulin(µM µm^{-1})		Electron-dense bridges (degrees)		
	Average	SD	MAX	n	Average	SD	Average	SD	n
wt	1.64[1]	1.43[1]	6.0[1]	70[1]	0.22	0.15	73.94	8.08	11
*ase*1Δ	1.62	1.61	6.8	35	0.16	0.13	62.53	9.95	22
*klp*2Δ	1.30	1.43	3.4	44	0.12	0.04	75.1	9.5	14
*mto*1Δ	2.29	1.83	6.9	12	0.07	0.02	62.53	17.66	10
*ase*1Δ *klp*2Δ	1.80	1.90	6.4	21	0.19	0.12	62.23	13.1	16
***mto*1Δ *klp*2Δ**	**2.26**	**1.50**	**5.5**	**27**	**0.13**	**0.04**	**57.39**	**19.85**	**14**

[1](Hoog *et al.* 2007); SD, standard deviation; MAX, maximum MT length found. Data relative to this section in bold.

The inter-MT distance in the IMAs observed showed one peak between 5 nm and 40 nm with a centroid at 16 nm (Figure 2.17E). This distribution was very similar to *wild type* cells (Hoog *et al.* 2007). As for the other mutants, we found electron-dense bridges between MT pairs (Figure 2.17F). These had the smallest average angle of all the mutants analyzed, but also the highest standard deviation (Table 2.6). Similar to *mto*1Δ cells, most of the MTs had open structures at both ends (Figure 2.11A and 2.11D). For this reason, we were not able to determine the orientation of most MTs. Nonetheless, we found one MT that was spreading apart from the lattice of another adjacent MT (Figure 2.11C). This MT had a capped end as the closest point to the adjacent MT. Finally, in one instance we observed that the MTs seemed to congregate/derive all from a single region in the cell tip (Figure 2.11B).

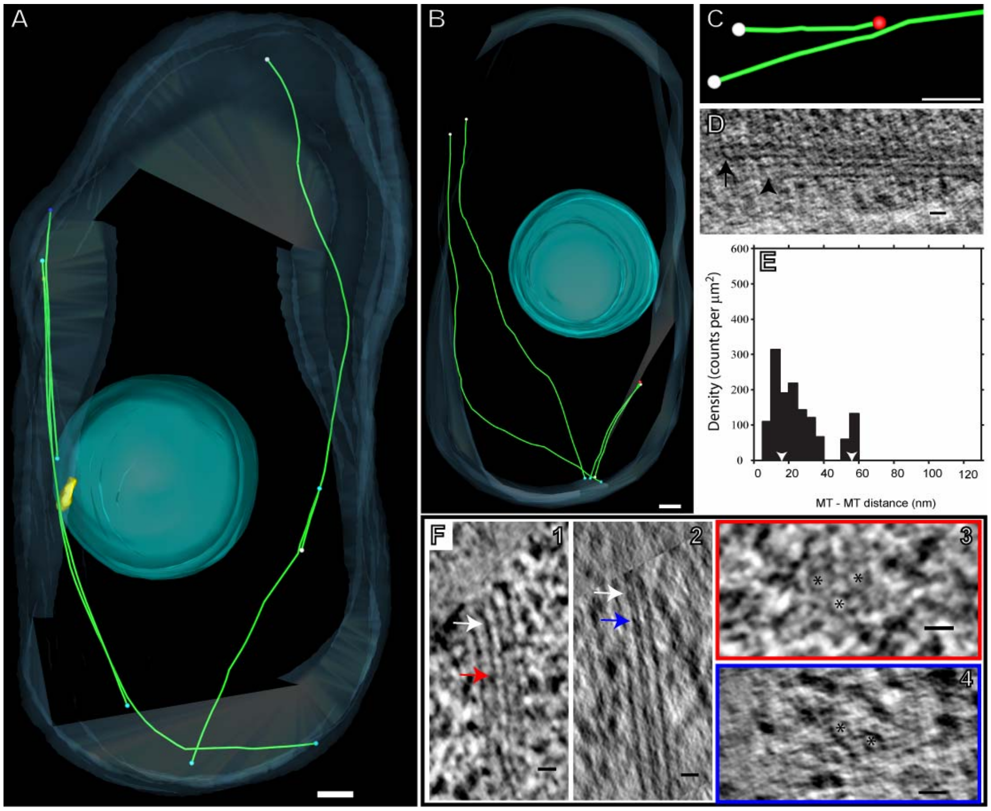

Figure 2.11. *mto*1Δ *klp*2Δ cells show different IMA organizations.

(A) Reconstruction of a partial volume of an *mto*1Δ *klp*2Δ cell showing two IMAs. The right IMA has a long MT overlap region with a MT lattice laying on the SPB surface. Note that one of the MTs of this IMA curls at the cell tip. The left IMA has a short MT overlap region and it reaches both cell tips.

(B) Partial volume where all the IMAs and single MTs seem to originate/congregate to one single locus in the cell.

(C) Even though most of the MTs had open end structures, some capped ends were visible. In this example the MT was spreading apart from the lattice of the adjacent MT with the capped end as the closest point to the lattice of that MT.

(D) Two pairing MTs with different end structures. The above MT has a capped end structure (arrow) while the lower MT has a flared end structure (arrowhead).

(E) Global inter-MT distances in IMAs for *mto*1Δ klp2Δ cells. Triangles points to the centroid of each major density peak.

(F1 and F2) *mto*1Δ *klp*2Δ selected longitudinal tomographic slices of two adjacent MTs showing electron-dense bridges (arrows). Volumes were rotated into the MT lattice plane. (F3 and F4) Cross slice of 1 and 2, respectively, in the plane of red and blue arrows.

MT ends structures are represented by colored spheres: red (capped structure), blue (blunt structure), cyan (flared structure) and white (undetermined structure). White bars, 250 nm. Black bars: 25 nm.

When we measured the MT pairing lengths and the length of the IMA MT overlap region, we discovered that the value for MT pairing was higher than the MT overlap region. We were puzzled and wonderer why this was the case. We realized that such a result was due to the organization of the

IMAs with three MTs. These presented what we called a triangle formation; the MTs were packed together in a triangle shape (Figure 2.11F-3). Thus, any MT was closer to both of the others by less than 35 nm. This led to MT pairing lengths higher than the MT lengths themselves (Table 2.4 at page 61).

The only SPB-associated IMA visualized had one of its three MTs, laterally associated with the SPB surface similar to *wild type* (Hoog *et al.* 2007). The shape of the SPB was abnormal, seeming bigger and slightly projecting out from the nuclear surface.

We show here that the phenotypes seen in *mto*1Δ cells are also prevalent in cells lacking both Mto1p and Klp2p. The differences observed were in the relative amount of polymerized tubulin and MT pairing length (Table 2.4 at page 61). In both cases *mto*1Δ *klp*2Δ cells had slightly higher values than *mto*1Δ cells.

2.7 *mto*1Δ *ase*1Δ cells form a hyper IMA

The observation that cells lacking *ase*1Δ have less MT overlap, together with the observation that *mto*1Δ cells have only one to two IMAs per cell and single MTs, made us wonder whether *mto*1Δ *ase*1Δ cells (gift of P. Tran) would be totally devoid of IMAs.

In fact, we found not only IMAs but what we term hyper-IMA. In the volumes acquired from this mutant that had cytoplasmic MTs, only one had a single MT, while the two others had an IMA with three MTs that extended from cell tip to cell tip (Figure 2.12A). None of the IMAs contacted the nuclear envelope or the SPB (Figure 2.12A). We estimated the relative amount of polymerized tubulin and observed a drastic reduction of the polymerized tubulin, ~ 64 % compared to *wild type* (Table 2.7).

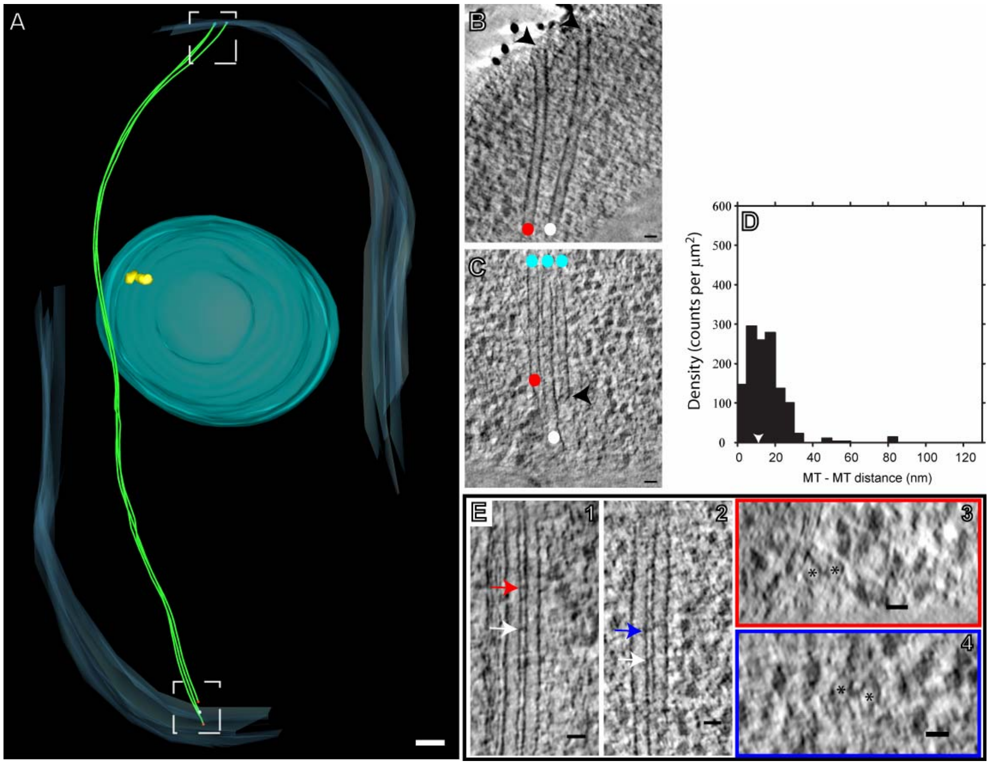

Figure 2.12. *mto*1Δ *ase*1Δ cells show hyper-IMAs.

(A) Model of a partial volume reconstruction of an *mto*1Δ *ase*1Δ cell with a cytoplasmic hyper IMA composed of three MTs that reach both cell ends. Note that the IMA is very compact during its whole length. Also visible is the SPB (yellow) with no MT in close proximity.

(B) Tomographic slice showing the area in the top frame in (A). Both MTs contact the plasma membrane with flared end structures (arrowheads). The colored circles indicate the MT end structure not visible in the image.

(C) Tomographic slice of the area in the bottom frame in (A). All three MTs align in the same plane to each other. A capped end is visible with an electron-dense bridge that connects it to the lattice of the adjacent MT (arrowhead).

(E) Global inter-MT distances in IMAs for *mto*1Δ *ase*1Δ cells. Triangles point the centroid of each major density peak.

(E1 and E2) *mto*1Δ *ase*1Δ selected longitudinal tomographic slices of two adjacent MTs showing electron-dense bridges (arrows). Volumes were rotated into the MT lattice plane. (E3 and E4) Cross slice of 1 and 2, respectively, in the plane of red and blue arrows.

MT ends structures are represented by colored spheres: red (capped structure), blue (blunt structure), cyan (flared structure) and white (undetermined structure).

We measured the global inter-MT distance in the two hyper-bundles. Similar to the previously analyzed *ase*1Δ mutants, the density distribution had a broad peak (between 0 nm and 35 nm) with a centroid at 11.3 nm (Figure 2.12D).

When we analyzed the MT end structures in both hyper bundles we discovered that most MTs had open structures at both ends (Figure 2.12A and B). Nonetheless, we were able to identify two capped ends in one hyper-bundle (Figure 2.12C) which allowed us to verify that parallel pairing occurs in this mutant. Finally, we found electron-dense bridges (Figure 2.12E) that had and average angle similar to the one observed in *wild type* (Table 2.7). As for the *mto*1Δ *klp*2Δ volumes, the MT pairing length was ~ 1.3 fold higher than the MT overlap region length. This is two fold higher than in *wild type* (Table 2.4 at page 61).

Table 2.7. MT lengths, polymerized tubulin and electron-dense bridges angles of *wild type*, and all the mutants analyzed.

	MT lengths (µm)				Relative Polymerized tubulin(µM µm^{-1})		Electron-dense bridges (degrees)		
	Average	SD	MAX	n	Average	SD	Average	SD	n
wt	1.64[1]	1.43[1]	6.0[1]	70[1]	0.22	0.15	73.94	8.08	11
*ase*1Δ	1.62	1.61	6.8	35	0.16	0.13	62.53	9.95	22
*klp*2Δ	1.30	1.43	3.4	44	0.12	0.04	75.1	9.5	14
*mto*1Δ	2.29	1.83	6.9	12	0.07	0.02	62.53	17.66	10
*ase*1Δ *klp*2Δ	1.80	1.90	6.4	21	0.19	0.12	62.23	13.1	16
*mto*1Δ *klp*2Δ	2.26	1.50	5.5	27	0.13	0.04	57.39	19.85	14
***mto*1Δ *ase*1Δ**	**5.77**	**2.03**	**6.9**	**6**	**0.07**	**0.02**	**72.22**	**11.7**	**19**

[1] (Hoog *et al.* 2007); SD, standard deviation; MAX, maximum MT length found. Data relative to this section in bold.

Our data show that cells lacking both Ase1p and Mto1p can form hyper-IMAs that extend from cell tip to cell tip. These are composed of three MTs that also extend along the whole length of the IMAs. Interestingly both hyper-IMAs had one MT with open structures at both ends. In one case we could verify that MT parallel pairing does occur. The inter-MT distance was similar to *ase*1Δ mutants.

2.8 *mto*1Δ cells and *mto*1Δ *ase*1Δ cells have different intra-nuclear MT assemblies

As we already had the samples, we decided to also investigate how cytoplasmic IMAs originate in *mto*1Δ and *mto*1Δ *ase*1Δ cells.

A previous study (Zimmerman and Chang 2005) has shown that after cold shock, which depolymerizes all MTs, most *mto*1Δ cells nucleate new MTs only inside the nucleus. Occasionally, stable MTs extend, deform the nuclear envelope and are able to pierce through it originating cytoplasmic MTs which will then form the IMAs.

Furthermore, this and other studies (Sawin *et al.* 2004; Zimmerman and Chang 2005), suggested that interphase MTs originate MTs that escape from the spindle midzone to the cytoplasm after the formation of the contractile ring.

One of our *mto*1Δ cells had an intra-nuclear interphase MT like array. This IMA like structure was composed of 5 MTs and extended from cell tip to cell tip (Figure 2.13). It formed two protrusions in the nuclear envelope (Figure 2.13A and D) while in the main body of nucleus it curved around the nuclear envelope, passing at the intra-nuclear region opposite to where the SPB was located.

The SPB was clearly on the outside of the nuclear envelope, since the double membrane layers of the nuclear envelope were visible below the SPB density, with no discontinuities observed (Figure 2.13E). Thus the cells were in interphase (Ding *et al.* 1997). We also observed that the bundle formed an elbow shape, at the site where the MTs would leave the nucleolus and enter the nuclear envelope protrusion. In fact, it seemed to us that the MT was broken at that site (Figure 2.13B). No MTs were observed in the cytoplasm.

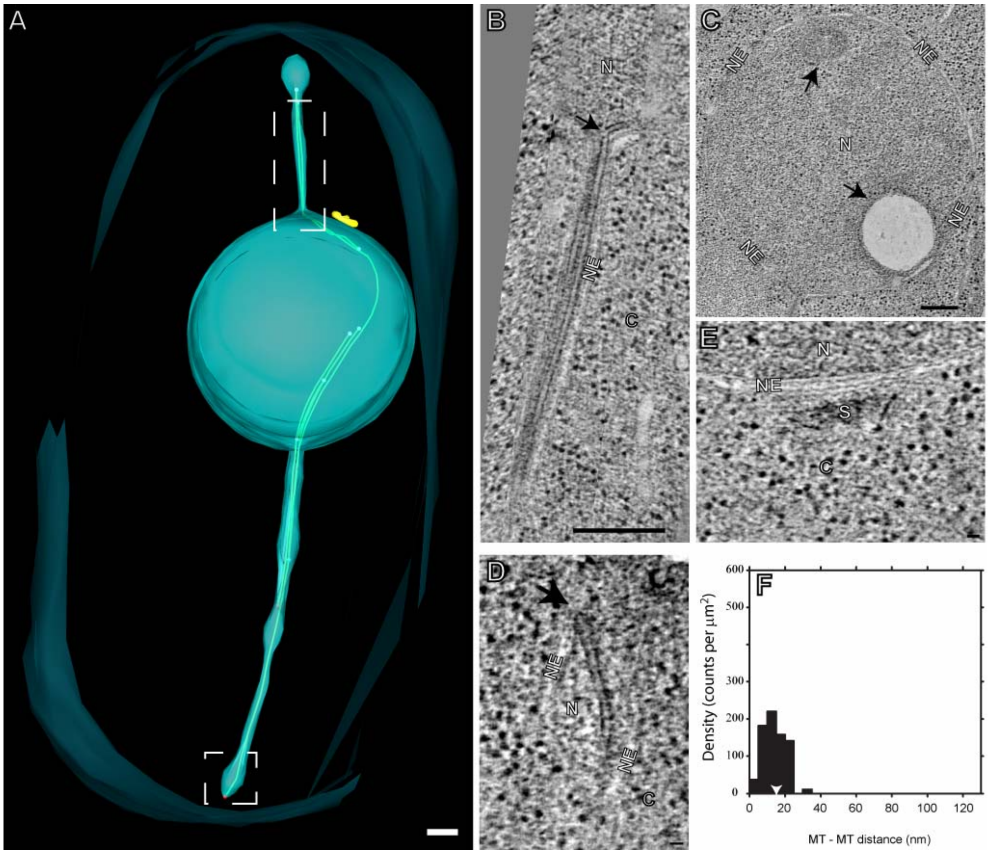

Figure 2.13. *mto*1Δ cells have an intra-nuclear IMA that forms protrusions in the nuclear envelope.

(A) Partial reconstruction of an *mto*1Δ cell with intra-nuclear MTs arranged like an IMA, forming two protrusions in the nuclear envelope. Both protrusions have "balloon" shaped ends.
(B) Tomographic slice of the top framed area in (A). MTs exiting the nucleus (N) and entering the nuclear envelope protrusion are visible. One MT seems to be broken at the transition local between nucleus and protrusion (arrow). This MT has a break on one side of the MT wall, while the other side makes an angle of ~ 90º.
(C) Tomographic slice of the nucleus (N) of the cell in (A) showing the two unknown structures enclosed by the nuclear envelope (arrows).
(D) Tomographic slice of the bottom framed area in (A). The "balloon" shape protrusion end with a MT inside of it is visible. The MT capped end structure is not surrounded by the nuclear envelope (arrow), being in apparent contact with the cytoplasm (C).
(E) Tomographic slice in the area of the SPB (S) of cell (A) showing an intact nuclear envelope separating the SPB from the nucleolus.
(F) Global inter-MT distances in IMAs for mto1Δ ase1Δ cells. Triangles points to the centroid of each major density peak.
MT ends structures are represented by colored spheres: red (capped structure), blue (blunt structure), cyan (flared structure) and white (undetermined structure). Nucleus (N), nuclear envelope (NE), SPB (S), cytoplasm (C). Bars in A to C, 250 nm. Bars in D and E, 25 nm.

We decide to measure the inter-MT distance to see if they are more similar to IMAs or to the inter-MT distances in the *wild type* spindle. The distribution of inter-MT distances presented one peak (Figure 2.13F). It comprised values between 0 nm and 25 nm with a centroid of 16.4 nm. These values were more similar to *wild type* than to *ase*1Δ values.

In one of the protrusions we could see a MT with the capped end at the level of the nuclear envelope and the cytoplasm. In fact, no nuclear envelope membrane was visible separating the MT end and the cytoplasm (Figure 2.13D). Nuclear pore complexes were visible on the nuclear envelope protrusions that wrapped around the bundle. At the tips of the protrusion we could see that the nuclear envelope did not wrap tightly around the MTs (when present) but instead, formed a “balloon” shape around the MT tips (Figure 2.13A and D). In one of the protrusions this “balloon” shape form was devoid of MTs.

When analyzing the volume we noticed that the nucleus possessed two unknown structures inside the nucleus. One was vacuole like and the other a close single membrane bound structure (Figure 2.13C). The vacuole like structure had a non electron dense spherical form, while the membrane like structure had a single membrane layer, was also of a spherical form and presented a darker density in one region.

We further pursued the issue of intra-nuclear MT origin in *mto*1Δ cells by looking at cells lacking both Mto1p and Ase1p. In the cell volumes acquired that had intra-nuclear MTs we did not observe an IMA like structure, such as that seen in the *mto*1Δ volume, but a MT aster-like structure. In one case this structure was more organized, forming a *quasi* bundle that protruded the nuclear envelope (Figure 2.14A). All the asters seemed to loosely focus in the intra-nuclear region in the vicinity of the SPB density (Figure 2.14B). Nonetheless, in all cases we could clearly see the SPB density outside the nuclear envelope (Figure 2.14D). In some cases the capped ends of the MTs were away from the region where the aster was more focused, while in other cases they were in this region (compared Figure 2.14A with B).

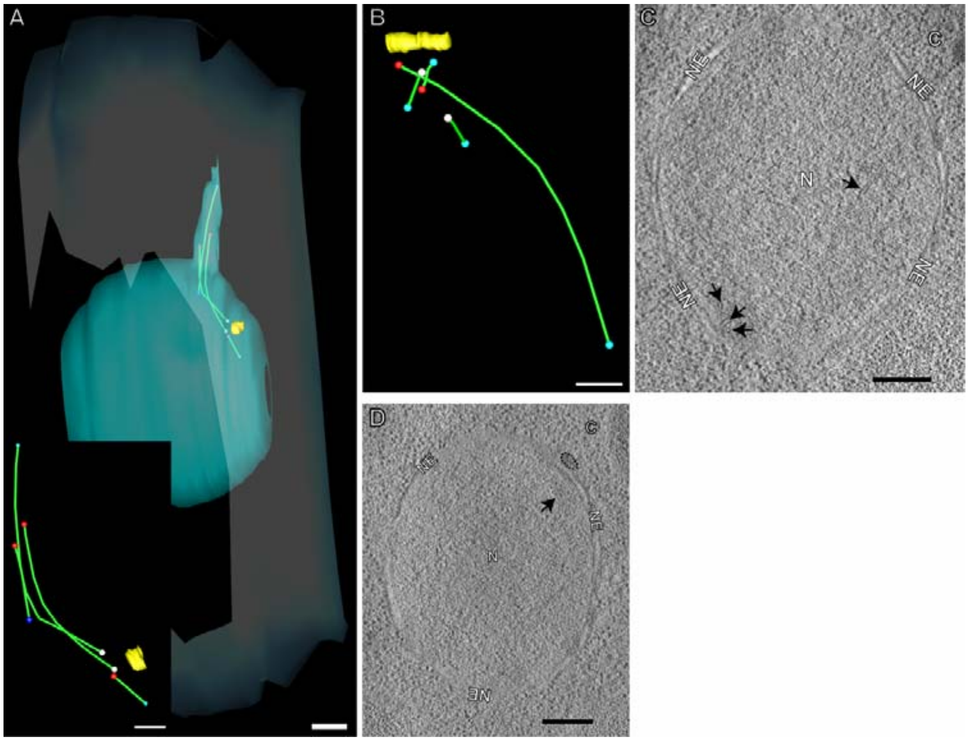

Figure 2.14. Intra-nuclear MTs in *mto*1Δ *ase*1Δ cells do not form an IMA like structure.

(A) Partial volume of an *mto*1Δ *ase*1Δ cell with intra-nuclear MTs that form a quasi bundle that protrudes the nuclear envelope (lower-left corner shows a close up of this bundle). The MTs have capped end structures away from the nucleus region facing the SPB.
(B) Example of another intra-nuclear MT structure. The MTs seem to concentrate in the nucleus region that faces the SPB (which is clearly outside the nuclear envelope).
(C) Tomographic slice of a nucleus with intra-nuclear MTs (arrows; N, nucleus; C, cytoplasm).
(D) Tomographic slice of a nucleus with intra-nuclear MTs (arrow) where the SPB is visible outside the nuclear envelope (dashed line).
MT ends structures are represented by colored spheres: red (capped structure), blue (blunt structure), cyan (flared structure) and white (undetermined structure). Nucleus (N), nuclear envelope (NE), cytoplasm (C). Bars, 250 nm.

Indeed, our results suggest that *mto*1Δ cells are able to form an intra-nuclear IMA-like bundle that is able to form protrusions in the nuclear envelope and pierce it (Figure 2.13), allowing the passage of MTs fragments into the cytoplasm (Zimmerman and Chang 2005). This IMA-like bundle has an inter-MT distance in between *wild type* and *ase*1Δ cells. On the contrary, we found no evidence for an IMA-like structure in *mto*1Δ *ase*1Δ cells (Figure 2.14). Instead we observed a MT aster-like structure that was also able to form protrusions in the nuclear envelope. In all cases the SPB was on the cytoplasmic side of the nuclear envelope and did not appear to be directly nucleating the intra-nuclear MTs. Finally, we observed a vacuole like structure and a membrane compartment inside the nucleus of an *mto*1Δ cell.

2.9 Disorganized IMAs affect the mitochondrial network

The association of MTs with mitochondria has been well documented in previous studies (Yaffe *et al.* 1996; Yaffe *et al.* 2003; Weir and Yaffe 2004), demonstrating how a correct positioning and normal morphology is dependent on MT organization. Indeed, mitochondria seem to elongate by connecting to the growing MT tips, and to retract with depolymerizing MT ends (Yaffe *et al.* 2003). Moreover, Höög *et al* (2007) have shown that a morphological relationship exists between MTs and mitochondria; mitochondria are laterally stretched along IMAs and display extensive branching, fitting the IMAs.

Having reconstructed mutant volumes in which the organization of IMAs was affected we investigated the effect of our mutants on the mitochondria morphology. By considering the published model (Hoog *et al.* 2007) and comparing it with the ones we produced, we found that the mitochondria network in our mutants seemed to be less branched and more compact than in *wild type*. Furthermore, our mutants had a smaller number of separate mitochondrial volumes per similar total volume of mitochondria (Table 2.8).

To quantify these observations, we calculated the ratio of volume to surface in a *wild type* cell *de novo* reconstructed and in our mutant strains, in order to determine if the mitochondria network was indeed less stretched and branched in the mutants. If this were the case, we would expect to see a higher ratio in the mutants compared to *wild type*. This was observed and we found that the ratio of volume to surface significantly increased in all our mutants compared to *wild type* (Table 2.8), with the exception of the *mto*1Δ *klp*2Δ mutant. This mutant had a similar value to *wild type*. The mitochondria network in this volume was mostly aggregated in one region, but several branches extended along the cell, most of them associated with the IMAs of this cell.

Table 2.8. Volume, number and ratio of volume to surface area for mitochondrial network in *wild type* and all analyzed mutants.

	Volume (μm^3)	Discrete mitochondria volumes	Ratio volume/surface	Mitochondria curvature (μm^{-1})	
				Average	SD
wt	*1.23*[1]	*12*[1]	*0.052*	*6.9*	*2.8*
*ase*1Δ	1.23	4	0.074	5.9	2.7
*klp*2Δ	1.32	5	0.08	5.3	1.3
*ase*1Δ *klp*2Δ	1.13	2	0.075	6.0	1.7
*mto*1Δ in*	0.44	-	0.08	5.2	2.7
*mto*1Δ ex*	0.97	1	0.066	6.3	2.7
*mto*1Δ *klp*2Δ	0.81	4	0.054	7.1	2.3
*mto*1Δ *ase*1Δ in*	1.54	4	0.068	6.2	2.2
*mto*1Δ *ase*1Δ ex*	1.37	5	0.071	5.7	2.7

[1](Hoog *et al.* 2007); SD, standard deviation; * in, intra-nucelar MTs, ex, cytoplasmic MTs

Next, we measured the curvature of our mitochondria volumes expecting to confirm the previous result and better understand the structural organization of the mitochondria network (Figure 2.15).

As expected, we showed that higher curvature values were measured in the *wild type* mitochondria than in the analyzed mutants, except for the *mto*1Δ *klp*2Δ mutant (Table 2.8). Moreover, we decided to measure the distance of the MTs to the mitochondria network and marked where the MT was in less than 35 nm from the mitochondria. We found that the MTs seemed to associate with the mitochondria in regions of higher mitochondrial surface curvature (Figure 2.15). Interestingly, no mitochondrial surfaces were ever observed in association with MTs perpendicular to the longitudinal cell axis (Figure 2.15B).

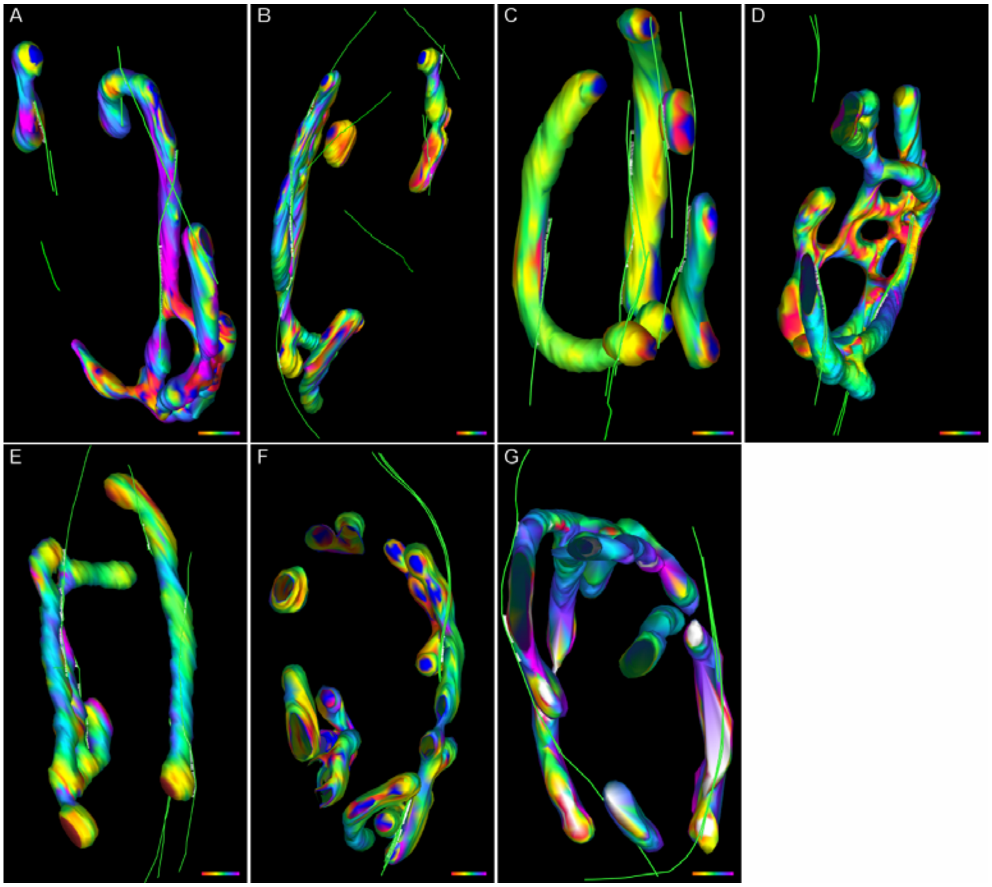

Figure 2.15. Curvature of the mitochondrial network.

Reconstruction of the mitochondria network and MTs for *wild type* (A), *ase*1Δ (B), *klp*2Δ (C), *mto*1Δ (D), *ase*1Δ *klp*2Δ (E), *mto*1Δ *ase*1Δ (F) and *mto*1Δ *klp*2Δ cells (G). The mitochondria network is colored in accordance to the curvature that it possesses. Red corresponds to lower curvature values and magenta to high curvature values (see scale bars for color key, representing a curvature range from 1/µm to 10/µm). White lines connecting MTs to the mitochondria network correspond to 10 nm MT pieces that are at 35 nm or less from the MT. As mention in the text, MTs are laterally associated in higher curvature areas. Bars: 500 nm.

These data clearly show the effect of the disorganization of IMAs on the shape of the mitochondrial network. Indeed, in almost all our mutants, the mitochondrial network was less stretched and branched compared to *wild type*, presenting values of lower curvature. Finally, we showed that the lateral association of MTs seemed to occur in zones of higher curvature in the mitochondria.

3 DISCUSSION

3.1 MT overlap regions remain in *ase*1Δ, *ase*1Δ *klp*2Δ and *ase*1Δ *mto*1Δ cells

In depth analysis of the organization of fission yeast **i**nterphase **m**icrotubule **a**rrays (IMAs) has previously been restricted to the resolution of fluorescence microscopy. A recent study using electron tomography showed that IMAs in *wild type* cells have three to four IMAs composed of two to nine **m**icro**t**ubules (MTs; Hoog *et al.* 2007). Interestingly, previous studies showed that IMAs in *ase*1Δ cells lacked a central region of higher fluorescence intensity, suggesting that these were in fact single MTs (Loiodice *et al.* 2005).

Several questions arose from these studies, namely do *ase*1Δ cells have MT overlap regions? Is the amount of polymerized tubulin identical to *wild type*? If they do have MT overlap regions, how are they organized? We took advantage of the high resolution of electron tomography to answer these questions and provide a clearer image of the organization of MT cytoskeleton in fission yeast.

We show that cells lacking Ase1p have indeed mostly single MTs, but still possess MT overlap regions (Figure 2.1A, B and F). This was an intriguing finding since Ase1p is the only known bundling protein in fission yeast and led us to believe that additional factors contribute to the bundling of MTs. For this reason, we decided to analyze *klp*2Δ and *mto*1Δ cells, since both proteins are known to link MTs to the lattice of an adjacent MT, possibly accounting for the observed MT overlap regions.

Klp2p is involved in generating and stabilizing the MT overlap region of IMAs (Carazo-Salas *et al.* 2005). It attaches to the plus end of MTs by its non-motor domain while the motor domain moves along the lattice of an adjacent MT in a minus end direction (Janson *et al.* 2007). It was suggested that IMAs in *klp*2Δ cells have multiple MT overlap regions (Carazo-Salas *et al.* 2005).

We started by analyzing *klp*2Δ cells and found that these cells have a reduced number of MTs per IMA (Figure 2.3A to D and F; see section 3.4). Nonetheless, we mainly observed IMAs rather than single MTs, an indication that MT bundling was not affected in *klp*2Δ cells. This was expected since Ase1p is present. We therefore analyzed the double deletion *ase*1Δ *klp*2Δ and still found MT overlap regions (Figure 2.8) to a similar extent as observed in *ase*1Δ cells, suggesting the presence of additional bundling proteins in *S. pombe*.

Mto1p forms a complex with Mto2p that associates with the **γ**-**tu**bulin **r**ing **c**omplex (γ-TuRC), targeting it to the MT lattice where the γ-TuRC can nucleate MTs (Sawin *et al.* 2004; Janson *et al.* 2005). This complex attaches two MTs to each other and may allow the formation of IMAs in *ase*1Δ cells. Since *mto*1Δ cells have defective cytoplasmic MT nucleation, and the only source of new cytoplasmic MTs, when at least one is already present, appears to be the events of bend and break, (Sawin *et al.* 2004; Venkatram *et al.* 2004; Zimmerman and Chang 2005) one can assume that MT pairs would be expected only form when two MTs (assuming that only one pierces trough the nuclear envelope at one time) would come close enough to be held together by Ase1p. Consequently, cells without Ase1p and Mto1p would be expected not to form MT pairs or IMAs.

Similar to the IMAs in *klp*2Δ cells, all IMAs in *mto*1Δ cells were composed of two MTs (Figure 2.5; see section 3.4). All analyzed cells showed more than one IMA per cell, indicating that the formation of MT pairs in *mto*1Δ may be easier than we expected. Most intriguing was the visualization in *ase*1Δ *mto*1Δ cells of what we called a hyper-IMA. Indeed, we found that these cells possess IMAs with three equally sized MTs that extend through the whole length of the cell (Figure 2.12A). Remarkably, these MTs were extremely regularly spaced apart from each other (Figure 2.12C and D).

Taken together, these results indicate that additional bundling proteins must exist in *S. pombe* to account for the MT overlap regions observed in cells lacking Ase1p. The observation of MT overlap regions in *ase*1Δ *klp*2Δ and *ase*1Δ *mto*1Δ hints that this protein bundles MTs more effectively when competition for the MT lattice is decrease in the absence of other **m**icrotubule **a**ssociated **p**roteins (MAPs).

3.2 Parallel MT pairs are only observed in *ase*1Δ *klp*2Δ cells

An interesting question in the formation of IMAs, is how the orientation of a newly nucleated MT, relative to the MT lattice on which it is being nucleated, is determined. Recently it was shown that *wild type* IMAs are composed of parallel and antiparallel MTs (Hoog *et al.* 2007). In addition, Janson *et al*. (2007) showed that Ase1p preferentially bundles antiparallel MTs. This led to the proposal that upon nucleation, Ase1p determines the orientation of the newly nucleated MT and subsequently Klp2p can bind to the MT plus end.

If Ase1p is the only protein determining the orientation of a newly nucleated MT and IMAs are composed of parallel and antiparallel paired MTs (Hoog *et al.* 2007), then one would expect that in *ase*1Δ cells the amount of parallel MT pairing would be identical to the antiparallel MT pairing.

In fact this was not what we observed in *ase*1Δ cells. All the MT pairs where we could determine the orientation of both MTs were antiparallel pairs (Figure 2.1A and B), pointing to a more complex system of determining the orientation of the newly nucleated MT. One possibility is that Klp2p has a role in this process by connecting to the MT plus end (Janson *et al.* 2007), and with its minus end directed movement also determines the MT orientation. This would explain the antiparallel orientation of the MT pairs observed in *ase*1Δ cells.

We started by looking at *klp*2Δ reconstructed volumes and as expected, since Ase1p is present, we found that most MT pairs were composed of antiparallel MTs (Figure 2.3A, C and D). In one case we confirmed the existence of a parallel MT pair with higher inter-MT spacing than the antiparallel pairs (Figure 2.3B). We believe this pair not to be bundled by Ase1p. When we analyzed the double deleted *ase*1 *klp*2 cells we confirmed only parallel MT pairs (Figure 2.8C and D). Taken together, these results show that both Ase1p and Klp2p can determine the antiparallel orientation of a newly nucleated MT along the lattice of an adjacent MT.

We believe that only in the absence of both Ase1p and Klp2p, the orientation of MTs in IMAs can be parallel. We support this conclusion with three main observations: (1) antiparallel and parallel MT pairs exist in *wild type* (Hoog *et al.* 2007); (2) we only confirmed antiparallel pairs in *ase*1Δ and *klp*2Δ single mutant cells; and (3) we only confirmed parallel pairs in *ase*1Δ *klp*2Δ cells. In our view, these observations do not reflect an all-or-nothing effect of the mutants in terms of MT pair orientations, but simply an increase of parallel MT pairs due to the absence of Ase1p and Klp2p. This argues in favor of a putative bundling protein that cross-bridges MTs regardless of their orientation. Unfortunately, we were not able to confirm most MT pairs orientations in *mto*1Δ containing mutants, since most MTs had open structures in both ends.

3.3 Nucleation regions in the cell

In several cases, in *ase*1Δ and *ase*1Δ *klp*2Δ cells and in one case in *mto*1Δ *klp*2Δ cells, we observed single MTs spreading apart from the lattice of an adjacent MT (MT obliquely orientated to the MT lattice adjacent to it; Figures 2.1B to D, 2.8B and D, and 2.11C). In most cases the minus end of the MT spreading apart was the closest point to the adjacent MT lattice. Occasionally electron-dense bridges between the capped end and the MT lattice were observed (Figure 2.1D).

Several studies demonstrated that the proteins Mto1 and Mto2 regulate MT nucleation (Sawin *et al.* 2004; Janson *et al.* 2005; Samejima *et al.* 2005;

Zimmerman and Chang 2005) by targeting the γ-TuRC complex to various locations in the fission yeast cell, including the MT lattice where it can nucleate MTs (Janson *et al.* 2005). According to our findings, one can assume that the spreading MTs are most likely attached by the γ-TuRC and the Mto1/Mto2 complex to the adjacent MT lattice.

Surprisingly, despite studies suggesting that cytoplasmic MT nucleation is absent in cells lacking Mto1p (Sawin 2004; Venkatram *et al.* 2004; Zimmerman *et al.* 2004), we observed a few MTs with capped ends in cells lacking Mto1p (Figures 2.11C, and 2.12A to C). One possibility is that MTs that pinch through the nuclear envelope have done so with the γ-TuRC still attached at the minus end, as we seemed to observe in one case (Figure 2.13D). This would then represent an intra-nuclear nucleation event rather than a new cytoplasmic nucleation. However, in one case, we observed a MT spreading apart from the lattice of an adjacent MT, similar to the ones observed in *ase*1Δ and *ase*1Δ *klp*2Δ volumes (Figure 2.11C). Due to these observations, we believed that cytoplasmic MT nucleation still occurs in *mto*1Δ cells but at a very low frequency.

In the *ase*1Δ, *klp*2Δ and *ase*1Δ *klp*2Δ mutants, we often observed single MTs that seemed to emanate from the nuclear surface with their minus ends adjacent to the nuclear envelope (Figures 2.1A, 2.3A and 2.8A). We believe these MTs originated from nucleation seeds localized on the nuclear surface, which is in agreement with the localization of the γ-TuRC and Mto1p/Mto2p complexes to the nuclear envelope surface (Sawin *et al.* 2004). Due to lack of Ase1p and/or Klp2p function, these MTs are not incorporated into an IMA, and their MT minus end position reflects most likely, their nucleation origin.

The localization of MT nucleation to both the MT lattice and the nuclear envelope is of great advantage to the cell. Having MT nucleation around the surface of the nucleus allows for several MTs to quickly come together and form an IMA. This positions the MT overlap region adjacent to the nucleus surface. As most MTs are orientated in an antiparallel fashion, it guarantees that MTs grow outwards to the cell ends, allowing both the correct deposition of polarity factors and centering of the nucleus in cases of misplacement. Additionally, having the MT overlap regions adjacent to the nucleus might be important in the loading of protein cargoes onto the MTs.

Once an IMA is formed, MTs newly nucleated on the nucleus surface are quickly incorporated into the IMAs by the action of Ase1p and Klp2p. Moreover, IMAs ensure their own maintenance due to targeting of MT nucleation seeds to lattices of the MTs from which they are composed (Janson *et al.* 2005). Thus IMAs, once formed, promote a positive feedback loop of localized MT nucleation that ensures their maintenance and MT turnover.

Finally, in *ase*1Δ, *klp*2Δ and *ase*1Δ *klp*2Δ mutants, we observed MTs with their minus end in close proximity to the **s**pindle **p**ole **b**ody (SPB; Figures 2.1E and F, 2.3E, and 2.8C). However, their capped ends were never in direct contact with the SPB density. Our results indicate that MT nucleation events occur at the cytoplasmic surface of the SPB, which is consistent with previous studies showing SPB-associated MT nucleation components (Horio *et al.* 1991; Masuda *et al.* 1992; Fujita *et al.* 2002; Sawin *et al.* 2004). In this context, we believe that newly nucleated MTs are not firmly attached to the SPB during interphase, being at some point released from it and incorporated into the closest IMA.

This local increase in MT nucleation at the cytoplasmic surface of the SPB explains the existence in all *wild type* cells of a SPB-associated IMA and the higher number of MTs observed in SPB-associated versus non SPB-associated IMAs. The SPB-associated IMA has MTs originating from the lattice of other MTs, the nuclear surface and from the SPB surface. All types of newly nucleated MTs are incorporated into the IMA by the action of Ase1p and Klp2p. The formation of an SPB-associated IMA might be essential to ensure a MT lattice laterally connected to the SPB. Without Ase1p and/or Klp2p, the SPB-associated IMA formation is altered or absent and no MT lattice – SPB connection can be established. In addition, the local increase of MT nucleation at the SPB surface, may also explain why upon entry into mitosis, the SPB-associated IMA is the last to fully disassemble (Sagolla *et al.* 2003). If nucleation seeds are attached to the cytoplasmic surface of the SPB, they may be less easily transported into the nucleus than the cytoplasmic nucleation seeds (Sato and Toda 2007).

3.4 ***mto*1Δ cells and *klp*2Δ cells have two to three MTs per IMA**

While looking for small MTs spreading apart from the lattice of an adjacent MT in *mto*1Δ containing mutants, we found that, similar to *klp*2Δ cells, most, if not all their IMAs were composed of two or three MTs (Figures 2.3A to D, and 2.5A and B).

Mto1p is known to severely affect MT nucleation during interphase (Sawin *et al.* 2004; Venkatram *et al.* 2004; Zimmerman and Chang 2005). In fact, Sawin *et al* (2004) did not observe any “de novo” nucleation events in *mto*1Δ cells in over 10 cumulative hours of observations. They found that most of the new MTs appearing derived from bend and break events.

*klp*2Δ cells showed similar IMA organization to the cells lacking Mto1p. Most IMAs were composed of two antiparallel MTs, as previously predicted, but multiple IMA MT overlap regions were not observed (Figure 2.3). One possible explanation for this observation might be the increase in the rate of IMA separation (Carazo-Salas *et al.* 2005). Such a hypothesis explains the higher number of IMAs per cell but does not fully account for the low number of MTs per IMA.

The fact that the IMAs observed in *klp*2Δ, similarly to *mto*1Δ cells, were mostly composed of two MTs, made us consider that Klp2p might have a function in MT dynamics (Troxell *et al.* 2001; Grishchuk *et al.* 2007) or MT nucleation targeting. Regarding MT dynamics, Klp2p might affect the stability of a MT by binding to the growing tip. This effect could be direct or indirect, trough an interaction with other +TIPs. Regarding targeting of MT nucleation, by attaching to the plus end of a MT, Klp2p might aid in the targeting of a newly nucleated MT. Klp2p may grab the plus end of a very small MT composed only by the nucleation seed and a few short protofilaments. If this MT is not yet attached to a MT lattice, Klp2p could also function in its targeting to an adjacent MT lattice. This hypothesis can explain the low number of MTs per IMA and consequently the low MT overlap region length observed in *klp*2Δ cells (Table 2.4 at page 63), as well as the higher number of IMAs per cell (Carazo-Salas *et al.* 2005). In support of this hypothesis, a recent paper showed that Pkl1p, the other Kinesin 14 of *S. pombe*, binds directly to γ-tubulin (Rodriguez *et al.* 2008).

An apparent contradiction between the phenotypes of *klp*2Δ cells and *mto*1Δ cells is the MT pairing length. If both present similar IMA organization, one would expect that they would also present similar MT pairing lengths (Table 2.4 at page 61). We believe that such a disparity is explainable by the fact that MTs in *mto*1Δ cells possess open structures in both ends. Without a nucleation seed at the minus end, a MT can slide along an adjacent MT lattice, when its plus end hits the cell tip and pushes. This would allow adjacent MTs to form long stretches of pairing.

3.5 Less polymerized tubulin is found in all the analyzed mutants

To allow a comparison of the amount of polymerized tubulin among the different strains and reconstructed volumes, we estimated the relative amount of polymerized tubulin for each strain. The data shows that all our mutants had reduced values of polymerized tubulin compared to *wild type* (the percentage of reduction observed range from 14% in *ase*1Δ *klp*2Δ cells to 68% in *mto*1Δ and *mto*1Δ *ase*1Δ cells; Table 2.7 at page 73). In the *mto*1Δ mutants, the observed reduction in the relative amount of polymerized tubulin was expected, since these mutants have an extremely impaired cytoplasmic MT nucleation capability (Sawin *et al.* 2004; Venkatram *et al.* 2004; Zimmerman *et al.* 2004).

Regarding the remaining mutants, in cells lacking Ase1p this result can be attributed to the lack of MT stabilization. Most MTs in *ase*1Δ cells are not part of an IMA and therefore cannot be stabilized by the action of Peg1p/Cls1p. This means that the probability of that MT fully depolymerize is higher. Due to the fact that the velocity of growth is much smaller that the velocity of shrinkage (Drummond and Cross 2000), the net result of reduced MT stabilization is less polymerized tubulin.

Interestingly, this does not fully account for the fact that *mto*1Δ *ase*1Δ cells have a similar value of polymerized tubulin to the *mto*1Δ single mutant. As the nucleation process in *mto*1Δ is already affected, one would expect that losing MT stabilization by the loss of Peg1p/Cls1p function would further impair the formation of IMAs, hence decreasing the relative amount of polymerized tubulin. The question of how there is still MT stabilization in *mto*1Δ *ase*1Δ cells remains to be elucidated (see section 3.8).

In cells lacking Klp2p, the relative low amount of polymerized tubulin can be explained in three ways: first, the lack of MT sliding would allow more molecules of Ase1p (and therefore Peg1/Cls1p) to bind in between two MTs. This would provoke a lack of MT stabilization by Peg1p/Cls1p (due to Ase1p sequestration) on other MTs nucleated along an IMA. Second, if Klp2p does play a role in MT nucleation targeting (see section 3.4), isolated newly nucleated MTs will not be targeted to a MT lattice and form a MT overlap region by Ase1p action. This means that they will also not be stabilized by Peg1p/Cls1p and will have a high probability of fully depolymerizing. Finally, Klp2p might play a role in MT dynamics (Troxell *et al.* 2001; Grishchuk *et al.* 2007); see section 3.4).

3.6 Ase1p is essential for MT spacing

From the onset of this study, an important question was whether MT spacing would change, if MT overlap regions were present in the absence of Ase1p.

Indeed, our data shows that cells lacking Ase1p have a significant decrease in the global inter-MT spacing, compared to *wild type* (Figures 2.2A, 2.9A, 2.12D). Interestingly, this decrease was visible also in antiparallel MT pairs (in *ase*1Δ cells; Figures 2.2B) and parallel MT pairs (in *ase*1Δ *klp*2Δ cells; Figures 2.9B). In *klp*2Δ, *mto*1Δ and *mto*1Δ *klp*2Δ cells we observed a slight decrease in the global inter MT spacing (Figures 2.4A, 2.6A, and 2.11E). The refined analysis for the *klp*2 mutant showed that antiparallel MT pairs had two peaks in the inter-MT spacing distribution while the only parallel MT pair had an inter-MT distance of 35-40 **n**ano**m**eters (nm; Figure 2.4B).

Careful analysis of the published *wild type* data reveals that most of these distances fall within the major distribution peak seen for *wild type* (between ~10 and ~ 50 nm; Hoog *et al.* 2007). Additionally, we know that *wild type* bundles contain both parallel and antiparallel MT pairs (Hoog *et al.* 2007), and that Ase1p preferably bundles antiparallel MTs (Janson *et al.* 2005). One can therefore assume that different classes of inter-MT distances exist in *wild type* cells, and that Ase1p is responsible for a prevalent class, possibly corresponding to middle – higher spacing class (between the values of 20 to 40 nm). Its absence would eliminate such a class, possibly reducing the peak amplitude and shifting its centroid to lower values, as observed in our *ase*1Δ mutants. This hypothesis would also explain the two peaks observed in our refined analysis of *klp*2Δ MT overlap regions (Figure 2.4B), since antiparallel MT pairs may be bundled not only by Ase1p, but also by additional bundling factors as our results suggest.

The altered MT spacing in all our mutants prompted us to look for electron-dense bridges similar to the ones previously observed in *wild type*

(Hoog *et al.* 2007). Even though we cannot determine the protein (or complex) forming such bridges due to the impossibility of labels to penetrate in the thick sections used in tomography, their presence confirms the existence of links in between MTs. Furthermore, we can visualize how these links change in response to altered inter-MT spacing.

Both *wild type* and all the studied mutants showed similar electron-dense bridges (Figures 2.2C and D, 2.4C, 2.6B, 2.9C, 2.11F, and 2.12E). The smaller longitudinal angle of these bridges in relation to the MT walls showed that cells lacking Ase1p or Mto1p had smaller average angles than *wild type* (Table 2.7 at page 73). This is consistent with the idea that the electron-dense bridges observed are affected by the different inter-MT spacing in the mutants. Intriguingly`, the double deletion of *mto*1 *ase*1 seemed to restore these angles to *wild type* values (Table 2.9 at page 73).

3.7 The origin of MTs in *mto*1Δ cells

As previously mention, it was suggested that cells lacking Mto1p do not nucleate MTs *de novo* in the cytoplasm. In fact, it was shown that in *mto*1Δ mutants the mitotic spindle does not fully breakdown after anaphase and septation. Instead MTs continue to grow inside the nucleus, which deform the nuclear envelope and at some point pinch trough it and are released into the cytoplasm (Sawin 2004; Venkatram *et al.* 2004; Zimmerman *et al.* 2004).

Consistent with these previous findings we reconstructed an *mto*1Δ volume that presented intra-nuclear MTs (Figure 2.13). The first question is from where are these MTs being nucleated in the nucleus? We localized capped ends in the intra-nuclear MTs, thus we infer that intra-nuclear γ-TuRC complexes are responsible for MT nucleation. However, another question arises: what is allowing intra-nuclear MT stabilization and bundling?

This *mto*1Δ cell had an IMA like structure in the nucleus, which formed protrusions in the nuclear envelope. In one of those protrusions we visualize what we believe to be a MT capped end in direct contact with the cytosol (Figure 2.13D). We know this cell was not in mitosis as its SPB was fully outside the nuclear envelope (Ding *et al.* 1997). Equally, we also visualized intra-nuclear MTs in *mto*1Δ *ase*1Δ cells (Figure 2.14). In this case we did not observe an IMA like structure but instead asters-like structures, which we attributed to the absence of Ase1p. Once more, all the cells had their SPBs fully outside the nuclear envelope (Figure 2.14C and D). Even do we did not visualize MT bundling in these asters, they were still able to form protrusions in the nuclear envelope.

The visualization of intra-nuclear MT bundling in *mto*1Δ cells and not *mto*1Δ *ase*1Δ cells, suggests that our putative bundling protein is not present in the nucleus of interphase *S. pombe* cells. In these cases, only upon release of MTs from the nucleus were MTs bundled.

Once in the cytoplasm, *mto*1Δ MTs show altered MT dynamics such as treadmilling and a severe defect in MT catastrophe, which leads to MTs bending around the cell tips. At this point, the major source of "new" MTs is believed to be the bend and break events of MTs, were one MT bends until it breaks into two parts (Sawin 2004; Venkatram *et al.* 2004; Zimmerman *et al.* 2004). Again, our results are in agreement with these studies. In fact we found that most MTs in cells lacking Mto1p have open structures at both ends, explaining the treadmilling behavior observed in these cells. Nonetheless, we also found MTs with capped ends associated with other MTs (Figure 2.11C), raising the question, if indeed *mto*1Δ cells are completely devoid of cytoplasmic MT nucleation? We believe that cytoplasmic MT nucleation still occurs at very low levels in these cells, possibly by a residual function of Mto2p.

3.8 A remaining question: how are IMAs formed and maintained in *mto*1Δ *ase*1Δ cells?

A surprising phenotype that we encountered was the existence of IMAs in cells lacking both Mto1p and Ase1p. Indeed, we were puzzle by the existence of IMAs with extremely organized and tightly packed (Figure 2.18), in cells that barely have any cytoplasmic MT nucleation (see section 3.7).

As we previously suggested, this IMA formation must be dependent on an additional bundling protein in *S. pombe*. Several proteins are known to populate the MT overlap regions which could provide a bundling action. Among these proteins are the two *S. pombe* members of the Dis1/XMAP215 family, Alp14p and Dis1p (Nabeshima *et al.* 1995; Garcia *et al.* 2001); Mal3p, member of the EB1 family (Beinhauer *et al.* 1997; Busch and Brunner 2004; Sandblad *et al.* 2006; Bieling *et al.* 2007); and also Peg1p/Cls1p (Grallert *et al.* 2006; Bratman and Chang 2007). However, this latter option is a conundrum, since Peg1p/Cls1p is dependent on Ase1p for MT overlap localization (Bratman and Chang 2007).

In fact all the MAPs that populate the MT lattices could play a role in bundling MTs. For example, a protein that has several MT binding sites could connect to two MTs and transiently link them. Furthermore, even a protein that only has one MT binding site, if it forms homodimers, may also be able to transiently bundle MTs.

Nevertheless, one question prevails: how is a bundle in *mto*1Δ *ase*1Δ maintained?

In this case, Peg1p/Cls1p is a possible candidate to maintain the IMAs. Peg1p/Cls1p localizes to the nucleus in the absence of Ase1p (Bratman and Chang 2007). As MTs in *mto*1Δ cells are at first intra-nuclear, when they pinch out from the nucleus Peg1p/Cls1p may come attached to them. In accordance to this, Bratman and Chang (2007) showed that ~55 % of *mto*1Δ cells loose all their MTs if Peg1p/Cls1p function is affected. We believe that this might also be due to most MTs presenting open structures at both ends, making them extremely dependent on Cls1p stabilization.

3.9 A unified model

Based on our results, and taking into consideration all the available data on the subject, we propose a unified model for the formation, stabilization and maintenance of interphase MT arrays.

We believe that newly nucleated MTs arise from nucleation seeds in several regions of the cell. As we mention previously, nucleation seeds are compose of the γ-TuRC and the Mto1p/Mto2p complex. As previously visualized by fluorescence live imaging (Sawin *et al.* 2004; Venkatram *et al.* 2004; Janson *et al.* 2005; Samejima *et al.* 2005; Venkatram *et al.* 2005; Zimmerman and Chang 2005; Carazo-Salas and Nurse 2006; Daga *et al.* 2006), and now shown by us by analysis of MT ends, interphase MT nucleation seeds are present at the nuclear surface, the cytoplasmic surface of the SPB, in the cytosol and along the lattice of MTs. The targeting of these nucleation seeds is mainly, but no exclusively, performed by Mto1p and Mto2p (Figure 3.1-1; Sawin *et al.* 2004; Venkatram *et al.* 2004; Janson *et al.* 2005; Samejima *et al.* 2005; Venkatram *et al.* 2005; Zimmerman and Chang 2005).

Following MT nucleation, the next step in the formation of an IMA is to bring MTs together to form MT overlap regions. In this step, both Klp2p and Ase1p have an important function. We suggest that in cases were MTs are nucleated in the cytosol or on the nuclear envelope, Klp2p aids the localization of these MTs by binding to the growing ends and with its motor domain brings the newly nucleated MT in close proximity to a MT lattice (Figure 3.1-6). In this case, Klp2p will also help to establish the antiparallel orientation between both MTs. Once both MT lattices are close together, Ase1p will be able to bridge them and form a stable overlap zone (Figure 3.1-7).

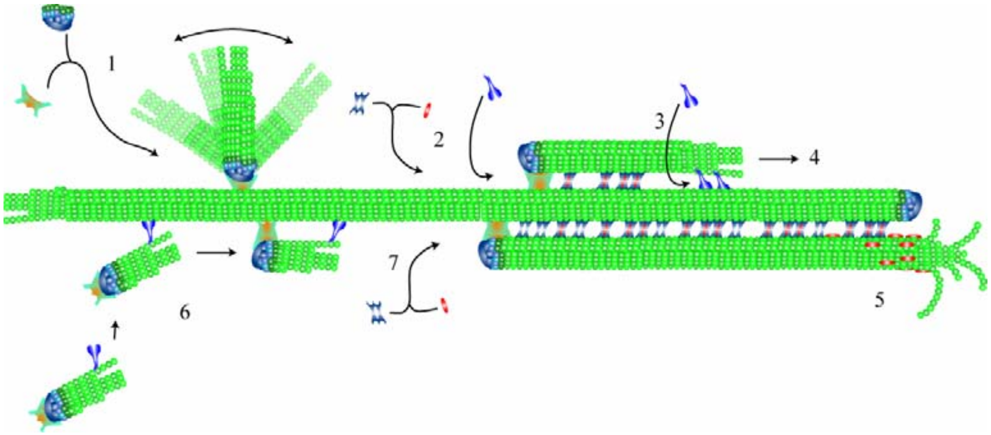

Figure 3.1. A unified model for IMA formation in *S. pombe*.

The formation of an IMA in *S. pombe* and its maintenance involves several steps and numerous proteins. 1 – Targeting of nucleation to the MT lattice. 2 and 7 – Determination of antiparallel orientation between adjacent MTs by MT selective bundling of Ase1p or Klp2p cross-linking. Targeting of stabilizing agent. 3 and 4 – Focusing of MT overlap region by MT sliding. 5 – MT overlaps maintenance by stabilization of depolymerizing MT and subsequent growth rescue. 6 – Newly nucleated MT in the cytosol is targeted by Klp2p to a neighbor MT lattice. See text for more details.

In cases were a MT is nucleated along a MT lattice it is subject to a dual polarity bias to establish the antiparallel orientation (Figure 3.1-2). We believe that both Klp2p and Ase1p can independently establish an antiparallel MT orientation. If Klp2p attaches to the newly nucleated MT before Ase1p, Klp2p can establish the antiparallel orientation between both MTs. Likewise, the preferential binding of antiparallel MTs by Ase1p will determine an antiparallel orientation between a newly nucleated MT and the adjacent MT (Janson *et al.* 2007). After the establishment of antiparallel orientation, Klp2p can focus the MT overlap region by sliding MTs along each other (Janson *et al.* 2007).

In addition to Ase1p, we suggest that a known protein with an unknown function (e.g. kinesins that may also contribute to the formation of

MT pairs and therefore IMAs), or a yet unknown protein also bundles MTs independently of their orientation.

Finally an IMA must be stabilized in order to perform its function. This is accomplished by Peg1p/Cls1p which hinders full MT depolymerization at the MT overlap regions (Bratman and Chang 2007).

3.10 The mitochondria network is affected by altered IMAs

The interaction between the mitochondria network and MTs is well documented, not only in yeast (Yaffe *et al.* 1996; Yaffe *et al.* 2003; Weir and Yaffe 2004) but also in higher organisms (Yaffe 1999). This mechanism of positioning of the mitochondria by the MTs may be necessary to support the essential mitochondrial metabolic functions.

Indeed, we showed that in cells where the IMA organization is deficient the mitochondria network appears less stretched and branched than in *wild type* (Table 2.8 at page 79).

Moreover, MTs seem to preferentially associate with the mitochondria in zones of higher curvature (Figure 2.15). Therefore, we believe that the stretching and branching of the mitochondria network depends on the specific *wild type* IMA organization, which provides a higher number of MTs and more force generation compared with the analyzed mutants. As a result the overall mitochondrial surface area in contact with the cytosol is increased, which might be important for the cell respiratory function.

3.11 Future directions

This work opens several new questions which should be addressed in future studies.

Our observations of the presence of MT overlap regions even in the absence of *ase*1, *ase*1 and *klp*2, and *ase*1 and *mto*1, provide conclusive evidence that Ase1p is not the only bundling protein in *S. pombe*. Further studies are now necessary to identify the protein that together with Ase1p bundles MTs during interphase.

Such an endeavor will require, among other experiments, a genetic screen for mutants that, in an *ase*1Δ genetic background, will aggravate the phenotype visualized in *ase*1Δ cells. In order to avoid losing several candidates due to synthetical lethality, such an approach might have to be correlated with an overexpression genetic screen, once more in an *ase*1Δ genetic background, for rescue of the *ase*1Δ phenotype.

Another interesting question arising from this study is why are *klp*2Δ cell IMAs only formed by two MTs?

We proposed that this might be due to a defect on MT nucleation targeting. To assess this hypothesis, MT nucleation events and their localization in the cell, will have to be assessed by fluorescent live imaging in both *wild type* and *klp*2Δ deletion mutants. Furthermore, quantification of MT dynamics both *in vivo* and *in vitro* would be valuable in order to properly understand the *klp*2Δ phenotype.

Finally, in our *mto*1Δ mutants we visualized MT capped ends, which is an evidence for the existence of interphase MT nucleation even in the absence of Mto1p. Detailed studies on the exact appearance of interphase MTs in these mutants are lacking and would provide a better insight into the regulation of MT nucleation in interphase.

4

MATERIALS AND METHODS

4.1 *S. pombe* cell culture techniques.

Standard methods were used for maintenance of fission yeast strains (Table 4.1; Moreno *et al.* 1991). Cells were either grown in rich **y**east **e**xtract **m**edium (YE5'S) or **E**dinburgh **M**inimal **M**edium **2** (EMM2) containing the appropriate amino acid supplements (Forsburg and Rhind 2006). Briefly, yeast cells were stored in glycerol-containing medium and then woken on YE5'S or EMM2 agar plates and incubated at 25°C or 30°C for 1-3 days until colonies formed. Liquid pre-cultures (10ml) of the appropriate medium were inoculated and grown for 8-16 hours with constant agitation and then used to inoculate a larger culture volume. These cultures were grown for 16-20 hours to an optical density OD_{595} of 0.4 to 0.7 to ensure cells were in exponential growth phase and subsequently used for strain construction or imaging experiments. All medium and solutions used for cell culture were autoclaved or filter sterilized before use.

Table 4.1. List of strains and plasmids used in this study.

Strain	Genotype	Source
DB 707	*h- klp2-D25::ura4+, ade6-M210, his3-D1, leu1-32, ura4-D18*	(Troxell *et al.* 2001)
DB 1165	*h-, mto1Δ::kanMX6, ade6-M210, leu1-32, ura4-D18*	(Sawin *et al.* 2004)
DB 1197	*h-, lys1+::nmt1-GFP- α2tub*	(Sagolla *et al.* 2003)
DB 1487	*h+, ase1Δ::KanMX6, leu1.32, ura4.D18*	(Loiodice *et al.* 2005)
DB 1539	*h-, ase1Δ::kanMX6, klp2Δ:ura4+, leu1.32*	(Janson *et al.* 2007)
DB 1540	*h-, ase1Δ::kanMX6, mto1Δ::ura4+, leu1.32*	This study
DB 1574	*h-, Cut11-mCherry::KanMX6*	This study
DB 2074	*h+, ase1Δ ::KanMX6, lys1+::nmt1-GFP- α2tub, Cut11-mCherry::KanMX6*	This study
DB 2075	*h+, mto1Δ::kanMX6, klp2-D25::ura4+, ura4-D18*	This study
DB 2080	*h-, Cut11-mCherry::KanMX6, lys1+::nmt1-GFP-α2tub*	This study
DB 2082	*h?, klp2-D25::ura4+, lys1+::nmt1-GFP- α2tub, Cut11-mCherry::KanMX6*	This study
DB 2094	*h+, ase1Δ ::KanMX6, klp2-D25::ura4+, lys1+::nmt1-GFP- α2tub, Cut11-mCherry::KanMX6*	This study

Plasmid	Genotype	Source
DL 332	*pFA6a-mCherry-kanMX6*	(Snaith *et al.* 2005)

4.1.1 Strains under control of the *nmt*1 promoter

When strains containing **g**reen **f**luorescence **p**rotein (GFP)-atb2 under the control of the *nmt*1 promoter were used the strains were grown and imaged in the presence of 15µM thiamine to repress over-expression from this promoter.

4.1.2 Construction of strains by crossing

Strains were crossed by mixing a toothpick of equal amounts of each parent strain of opposite mating type together on **m**alt **e**xtract **a**gar (MEA; (Forsburg and Rhind 2006) or **m**inimal **g**lutamate (EMMG; EMM2 containing 1g/L sodium glutamate instead of Na4Cl) with 20 µl water. Plates were incubated at 25ºC. After 48 hours the presence of spores was checked by microscopy and tetrads were dissected using a micro-manipulator on appropriate non-selective medium. Plates were incubated at 25ºC or 30ºC until colonies were formed. Plates were replica-plated onto selective medium to assign markers and/or checked by colony **p**olymerase **c**hain **r**eaction (PCR) where no appropriate selection markers could be used to determine genotypes.

4.1.3 Construction of strains by homologous recombination

4.1.3.1 Generation of PCR fragments for transformation

Strains were constructed using the homologous recombination-based transformation method described by (Bahler *et al.* 1998). Briefly, ~100bp PCR primers (Thermo Fisher Scientific, Ulm, Germany) containing 80 **b**ase **p**airs (bp) gene-specific sequence followed by 20 to 24 bp sequence, corresponding to the plasmid template (Table 4.1) were used to amplify a transformation cassette containing a selection marker (Uracil, Kanamycin resistance; (Bahler *et al.* 1998) and an additional tag sequence for 3' modification of the target gene. See Table 4.2 for a list of primer sequences and plasmid templates. This PCR fragment was extracted using phenol/chloroform (AppliChem GmbH, Darmstadt, Germany) and resuspended in 10mM **Tris**-(hydroxymethyl)-aminomethane (Tris)-HCL at 1µg/µl. 50ml exponentially-growing cells (OD_{595} ~ 0.5) cultured in rich medium were transformed.

All the PCR reactions were run (Byozim Diagnostics GmbH, Pstfach, Germany) with the following steps: one initial step at 95ºC for 10 min, followed by 30 repeats of 1 min at 94ºC, 1 min at 48ºC and 2 min at 72ºC. The final step was of 10 min at 72ºC. Following this step the temperature was dropped to 4ºC until running the PCR reactions in a 1% agarose (Sigma-Aldrich, Hamburg, Germany) for 20 min at 120 volts.

Each PCR reaction contained the final concetraction of the following reagents: 1x Buffer with magnesium; 2.5 **m**ili**m**olar (mM) of dNTPs; 2.5 mM of magnesium sulfate; 1 **m**icro**m**olar (µM) of each primer; and 2.5 units of TAQ polymerase (all PCR products from Sigma-Aldrich Biochemie GmbH, Hamburg, Germany).

4.1.3.2 Transformation protocol for *S. pombe* cells

Cells were washed twice with an 50ml water, and the cell pellet was resuspended in 1 ml of 0.1M LiAc/TE (pH 7.5) and transferred to an Eppendorf tube, and resuspended in LiAc/TE at 2x109 cells/ml. 100 µl of the concentrated cells were mixed with 2µl sheared herring testes DNA (10 mg/ml) and 10 µl of the transforming DNA. After 10 min incubation at room temperature, 260µl of 40% PEG/0.1M LiAc/TE was added. The cell suspension was mixed gently and incubated for 1 hour at 30ºC (or 25ºC for temperature sensitive strains). 43 µl of **d**i**m**ethyl**s**ulph**o**xide (DMSO) was added, and the cells were heat shocked for 5 min at 42ºC. Cells were then washed once with 1 ml of water, resuspended in 0·5 ml of water, and plated onto two rich medium non-selective plates. These plates were incubated for 1 day at 25ºC or 30ºC, resulting in a lawn of cells. The cells were then replica plated onto selective plates. Cells transformed with fragments carrying the kanMX6 marker were plated onto YE5'S containing 100 mg/l Geneticin. Cells transformed with fragments carrying the ura4+ marker were plated onto EMM2 plates without uracil. The replica plates were incubated for 2–3 days at 25ºC or 30ºC, and large colonies were re-streaked onto fresh selective plates.

4.1.4 Screening transformants by colony PCR

Single colonies were checked for stable integration of the DNA fragment by homologous recombination. A toothpick of cells was resuspended in the 50 µl of the PCR reaction. The PCR reaction targeted a 2 to 3 kb region of DNA including the site of integration. One primer corresponded to a sequence within the transforming fragment. For modules containing kanMX6 we used primer:

5'-GCTAGGATACAGTTCTCACATCACATCCG-3'.

For modules containing ura4+ we used primer:

5'-CCAAGCCGATACCAGGGACATAG-3'.

The other fragment corresponded to a region of the targeted gene outside the sequences covered by the transforming fragment and is listed in Table 4.2. A PCR product was obtained only for strains in which the transformation fragment was stably integrated. As a negative control of non integration of the modules, a PCR reaction with primers targeting a ~ 1 Kb region of module target region was used (Table 4.2).

Table 4.2. Primers used in this study

Name	*Primer sequence (5' → 3')*
Ase1del_rev	*GCG TCT AAA CGA GCC GTA TC*
DPE 690	TAG GTC CAT TCT ATG TTT GTG G
Klp2_rev	TTC AAG ATT GGC AGT GGA AA
Ase1gene_for	TTT GAA TCG TTT GTC AAT GG
Ase1gene_rev	AAC AGA GAA TCC CAA AGC TG
Klp2gene_for	GTC TGC CGA AGA ACA CTT TT
Klp2gene_rev	TTC AGG GGA AAA TAC ACG AT
Mto1gene_for	GGT TTC AGA GCC AAG AGC AG
Mto1gene_rev	CTT TTC TCA AAG CCG CAA AC
DPE 589	CTC AAC TTA ACT TAT CTC CAA GGA TAG AGC GTC GCT GCT GGG TAT TGT TTC GAG AAT ACA AAA GCA ACT CCC GGA TCC CCG GGT TAA TTA A
DPE 590	GGA TGC GTG TAT ATC GTT GGA CTA ACG AAC ATT TTT CAC AAA ATA GCA AGT GAA CAA ATC CCC TCT CTT CGA ATT CGA GCT CGT TTA AAC

All the primers in this table were generated using the application Primer3 (http://fokker.wi.mit.edu/primer3/input.htm) with default parameters.
All primers in this study were ordered from Thermo Fisher Scientific GmbH (Ulm, Germany).

4.2 Live cell imaging

4.2.1 Cell preparation

Cells were grown from overnight pre-cultures to exponential phase (**o**ptical **d**ensity (OD) **a**bsorvance $(A)_{595}$ ~ 0.5) in 20 ml EMM2 containing the necessary amino acid supplements. Cells were transferred to glass bottom microwell dishes (MatTek, Ashland, MA, USA) coated with 1μl 2mg/ml lectin BS-1 (Sigma-Aldrich, Hamburg, Germany) in H_2O. Dishes were spun at 300 rpm for 1 min in a bench-top centrifuge to attach the cells to the bottom of the MatTek dish. Unattached cells were washed away and 2ml fresh medium was added.

4.2.2 Microscopes used for imaging

A 488nm Argon Krypton dual laser line for GFP signals and dsRed/mCherry signals was used. A Perkin Elmer UltraView ERS dual spinning disc system (Waltham, MA, USA) coupled to a Carl Zeiss Axiovert 200 M microscope (München, Germany) with a 100X oil immersion objective (Plan Fluor, numerical aperture 1.3) was used to acquire images. Images were acquired with a Hamamatsu C9199-02 EMCCD camera (Hamamatsu , Japan) with a pixel size of 8 µm. Z-stacks were taken with 13-20 planes per stack, with a distance of 0.5µm between planes.

4.2.3 Image analysis

Images from the confocal spinning disc microscope systems were acquired using the Perkin Elmer software (Waltham, MA, USA). Data was analyzed using ImageJ (NIH, USA). Data acquired with the Perkin Elmer systems was imported into ImageJ using a plugin written by A. Seitz (EMBL, Heidelberg, Germany) and Z-stacks were maximum-projected using a custom routine written by T. Zimmerman (EMBL, Heidelberg, Germany). Quantification of MT/**s**pindle **p**ole **b**ody (SPB) colocalization was done by visual inspection. Plotting of numerical data was done with Sigma Plot 11.0 (SYSTAT, CA, USA).

4.3 Electron microscopy

4.3.1 High pressure freezing

At the time of freezing, 10 ml of cell culture at OD_{595} ~0.5 was filtered using a Millipore 15 ml filtration set-up with a polycarbonate filter (0.4 **m**icro**m**eters [µm] pore size; Millipore, MA, USA). Cell paste was loaded into a membrane carrier (Leica Mycrosystems GmbH, Wetzlar, Germany) and frozen in an EM PACTII high pressure freezer (Leica Mycrosystems GmbH, Wetzlar, Germany).

4.3.2 Fixation and freeze substitution

Fixation occurred during freeze substitution using anhydrous acetone containing 0.1% dehydrated glutaraldehyde (Electron Microscopy Sciences, Hatfield, PA, USA), 0.25% uranyl acetate (UA; SERVA Electrophoresis GmbH, Heidelberg, Germany), and 0.01% osmium tetroxide (OsO_4; SERVA Electrophoresis GmbH, Heidelberg, Germany). Substitution took place over 56 hours at -90ºC; the temperature was then increased 5ºC per hour to -45ºC. Plastic infiltration was carried out in steps (3:1 acetone:lowicryl [HM20; Polysciences Inc, PA, USA] ratio and then 1:1, 1:3, and finally two times Lowicryl, each step lasting 1–3 hr) at this temperature followed by UV polymerization in an EM AFS (Leica Mycrosystems GmbH, Wetzlar, Germany). Polymerization continued for 45 hr at this temperature and then increased to room temperature at 10ºC per hour. Once room temperature had been reached then samples were then illuminated for a further 12 hours.

4.3.3 Serial sectioning

Serial semi-thick sections (210 to 300 **n**ano**m**eters [nm]) were cut with a Leica Ultracut UCT microtome (Leica Mycrosystems GmbH, Wetzlar, Germany). Sections were collected on Formvar-coated, palladium-copper slot grids (Agar Scientific GmbH, Wetzlar, Germany) and post-stained by putting the grid on a drop of 2% UA in 70% methanol (MERCK, Darmstadt, Germany) followed by touching a drop 50% methanol and passing to a drop of water for 2 min. Next, the grid was blotted to remove the water excess and was passed to a drop Reyonolds lead citrate (Electron Microscopy Sciences, Hatfield, Pa, USA) solution for 1 min. After being in a water drop for 2 mins, it was blotted and stored. Cationic gold particles (15 nm; Brittish Biocell, Cardiff, UK) were applied to both sides of the grid to be used as fiducial markers.

4.3.4 Tomogram acquisition and calculation

For tomography, the grids were placed in either high-tilt holder (Model 2020; Fischione Instruments, Corporate Circle, PA) or high-tilt rotate holder (Model 650; Gatan, Pleasanton, CA). Cells were selected by low magnification visual inspection of the grids. Serial tilt series were acquired for the selected cells which spanned several serial sections. Montage tomographic datasets were collected using a FEI Tecnai TF20 or a FEI Tecnai TF30 (FEI Company, Oregon, USA) at a magnification of ~14,500x or ~15,500x, respectively using the tilt-series acquisition software, SerialEM (Mastronarde 2005). Images were acquired every 1º over a ± 65º range using a Gatan 4K x 4K CCD camera. Image processing was performed on a Sun Opteron workstation (Sun Microsystems GmbH, Kirchheim, Germany). Images were aligned using the fiducial marker positions and tomograms computed using the R-weighted back-projection algorithm (Gilbert 1972) and joined using eTomo graphical interface (Mastronarde 1997). Sections shrinkness due to beam interaction was calculated according to the formula: (number of sections * thickness of section) / (number of slices * pixel size of slice).

4.3.5 Tomogram modeling and analysis

The IMOD software package (Kremer *et al.* 1996) was used to display, model, and analyze tomograms and models. Relevant structures were modeled as reported in Höög et al. (2007). MTs were tracked and ends morphology analyzed using the “slicer” tool. MT ends were marked in different colors to allow distinction (O'Toole *et al.* 2003b; Hoog *et al.* 2007). Membrane structures (nucleus and mitochondria) were modeled every tenth slice using closed contours. The cell wall was modeled every fiftieth section using also closed contours. MT lengths and organelle volumes were extracted from models using Imodinfo program. The Nda program was use to calculate the distance between MTs and the centroid of the major distribution peaks, after converting the model to resemble a model from serial cross-sections, using the Resamplemod program (McDonald *et al.* 1992). A serial section like model was also used to calculate MT pairing lengths using the Mtpairing program (Annex V), and MT overlap regions lengths with the program Mtoverlap (Annex V). The program Mtk was used to calculate the 3D distances between structures (Marsh *et al.* 2001). MT volumes were extracted and rotated in the MT lattice plane using the Mtrotlong program. The Imodcurvature program was used to calculate the mitochondria curvature angles by finding the cylinder that best fits the points around each location (Annex V).

The number of moles of polymerized tubulin was estimated by calculating the number of polymerized tubulin subunits present in each volume and dividing this number by the Avogradro's constant. The acquired cell volume was obtained with the program Imodinfo from a model of the edges of each final joined tomogram. The final polymerized tubulin concentration was calculated by dividing the number of moles by the acquired volume of each joined tomogram. Finally the relative concentration was obtained by dividing the concentration by the volume for each joined tomogram.

5 ANNEXES

Annex I. γ-tubulin complexes in various species.

Drosophila melanogaster γ-TuSC (9.8 S) γ -TuRC (36 S)	*Xenopus* γ -TuRC (>25 S)	Human γ -TuRC (32 S)	*Arabidopsis thaliana* γ -TuC	*Saccharomices cerevisiae* Tub4p complex (6-11S) (22S)	*Schizosaccharomices pombe* γ -TuC (22S)	*Aspergillus nidulans* γ -TuC (8-20S)	*Dyctiostelium discoideum* γ -TuSC (ND)	*Caenorhabditis elegans*[*]
γ-tubulin 23C γ-tubulin 37CD	γ-tubulin	γ-tubulin (two genes)	γ-tubulin (two genes)	Tub4p[$]	Tubg1/Gtb1[$]	mipA	γ-tubulin	*tbg-1*
Dgrip84 (3 splicing variants)	Xgrip110	hGCP2	AtSpc97p	Spc97p[$]	Alp4p[$]	AnGCP2	DdSpc97p	Ce-Grip-1
Dgrip91	Xgrip109	hGCP3	AtSpc98p	Spc98p[$]	Alp6p[$]	AnGCP3	DdSpc98p	?
Dgrip75	Xgrip76	hGCP4	AtGCP4	-	Gfh1p	AnGCP4	-	
Dgrip128	Xgrip133	hGCP5	AtGCP5 (five isoforms)	-	?	AnGCP5	-	
Dgrip163	Xgrip210	hGCP6	AtGCP6	-	Alp6p	AnGCP6	-	
Dgp71WD	X-Nedd1	GCP-WD/NEDD1	At-Nedd1	-	?	?	-	

ND, not determined; [*], γ-tubulin complex not yet characterized; -, Orthologs not present; [$], essential gene.
Adapted from (Wiese and Zheng 2006).

Annex II. Extensive table of +TIPs families and their characteristics.

+TIP family	Homologues	Structural domains	Interaction partners among +TIPs	Main functions*
NON-MOTOR PROTEINS				
EB family EB1, EB2, EB3	Mal3 (Sp) Bim1 (Sc)	CH, coiled coil, EBH, EEY/F	Most known +TIPs (CAPGly domains, basic/serine rich stretches)	Promotion of MT growth and dynamicity Anti-catastrophe activity Targeting of other +TIPs to MT ends
CAP-Gly family CLIP170 CLIP115	Tip1 (Sp) Bik1 (Sc) D-CLIP-190 (Dm)	CAP-Gly, coiled coil, basic/serine rich	EB proteins CLASPs CLIP170 p150Glued Stu2 Kar9 Tea1 Tea2 (Kip2) LIS1 (Pac1) XKCM1	MT rescue and stabilization Targeting of dynein to MT ends MT interaction with the cell cortex, kinetochores and vesicles
p150glued(dynactin subunit)	Ssm4 (Sp) Nip100(Sc) NudM (An)	Zinc finger, EEY/F (only in CLIP170)	Cytoplasmic dynein CLIP170	Binding dynein to cargo Regulation of dynein processivity
CLASPs CLASP1/2	Orbit/MAST(Dm) Peg1(Sp) Stu1(Sc) Cls-2 (Ce)	TOG-like, basic/serine rich	EB proteins CLIP170 CLIP115	MT rescue and stabilization MT interaction with kinetochores, cell cortex and the Golgi
APC	dAPC1/ 2 (Dm)	Armadillo, SAMP repeats, coiled coil, basic/serine rich	EB proteins XKCM1	MT stabilization, anti-catastrophe activity. Interactions with the cell cortex and kinetochores MT-unrelated functions in Wnt signaling, etc
XMAP215/Dis1 family ChTOG	XMAP215(Xl), Dis1, Alp14 (Sp) Stu2(Sc) Msps (Dm) DdCP224 (Dd) ZYG-9 (Ce)	TOG	EB proteins Bik1 Kar9 XKCM1	MT stabilization, promotion of MT growth MT-cortex interactions
Spectraplakins MACF2 (ACF7)	Shot/Kakapo (Dm)	CH, plakin, coiled coil, spectrin, EF hand, GAS2,basic/serine rich	EB proteins	MT stabilization, linking MTs to actin and the cell cortex
LIS1	Pac1(Sc) NudA (An)	LisH, WD40, coiled coil	CLIP170 (Bik1) Dynein Dynactin	Dynein activation, interaction with the cell cortex
Melanophilin		coiled coil basic/serine rich	EB1	Melanosome tansport
Neuron Navigator	Unc-53 (Ce)	AAA-ATPase, coiled coil, basic/serine rich		Regulation of neuronal migration

Navigator-1,2,3				
Rho GEF2 (Dm)	Many related Rho-GEFs, but no direct +TIP homologue	PDZ, PKC conserved region1, RhoGEF, PH, basic/serine rich	EB1	Regulation of Rho activity
Tea1 (Sp)		Kelch repeat, coiled coil	Tip1	Control of actin polymerization and cell growth at the cell ends through interaction with formin
Kar9 (Sc)		unique Kar9 domain (helical), basic/serine rich	Bim1 Stu2 Bik1	MT capture and transport along actin filaments by myosin V homologue Myo2
STIM1		EF hand, SAM, transmembrane, ERM, basic/serine rich	EB1	Calcium sensing and activation of calcium channels in store-operated calcium entry; Extension of ER tubules driven by microtubule growth.
MICROTUBULE MOTOR PROTEINS				
Cytoplasmic dynein Dynein heavy chain	Dyn1 (Sc) Dhc1(Sp)	AAA-ATPase, coiled coil	Dynactin (p150Glued) LIS1	MT minus-end-directed transport of macromolecular complexes and organelles Pulling at MTs at the cortex, transport of MTs
Kinesin-13 MCAK (KIF2C)	Klp10A (Dm) XKCM1 (Xl)	Kinesin motor, coiled coil, basic/serine rich	EB proteins XMAP215 CLIP170 APC	MT depolymerization, induction of catastrophes
Kinesin-14 Ncd (Dm)	Klp2 (Sp) ATK5 (At) Kar3 (in complex with Cik1) (Sc)	Kinesin motor, coiled coil, basic/serine rich	EB proteins	MT minus-end-directed transport Antiparallel MT sliding MT depolymerization
Tea2 (Sp)	Kip2 (Sc)	Kinesin motor, coiled coil, basic/serine rich	Mal3 Tip1 (Bik1)	MT stabilization and creation of cortical asymmetry by transporting other +TIPs to MT plus ends

Annex III. Graphic representation of each partial volume acquired for all the mutants analyzed.

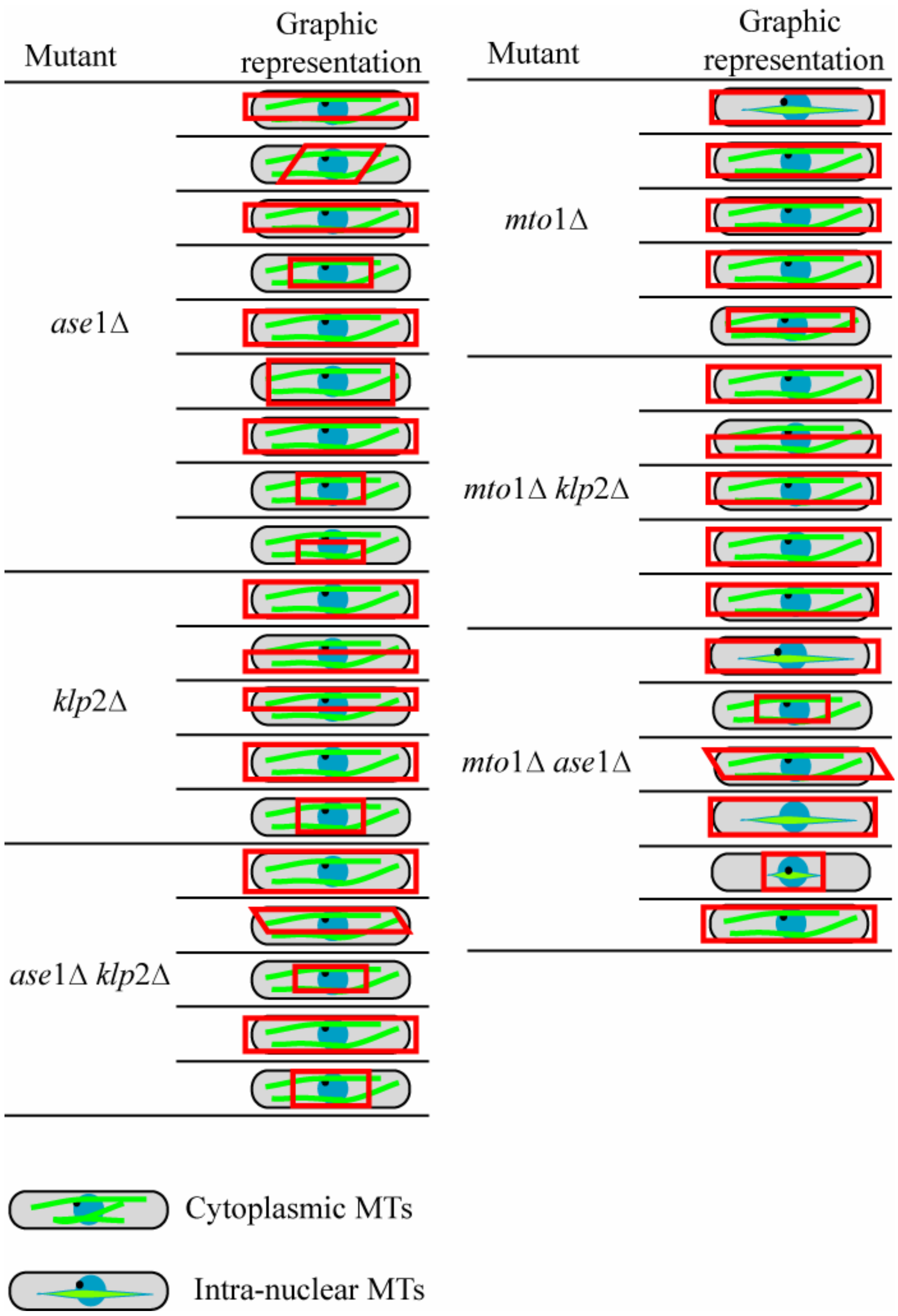
Mutant
Graphic representation
Mutant
Graphic representation
*ase*1Δ
*klp*2Δ
*ase*1Δ *klp*2Δ
*mto*1Δ
*mto*1Δ *klp*2Δ
*mto*1Δ *ase*1Δ
Cytoplasmic MTs
Intra-nuclear MTs

*Red frame represents acquired volume.

Annex IV. Percentage of isolated MTs (x = 1) and number of MTs per IMA (x = 2 to 8) in association with the SPB (A) or not (B) for *wild type* and all the analysed mutants.

A

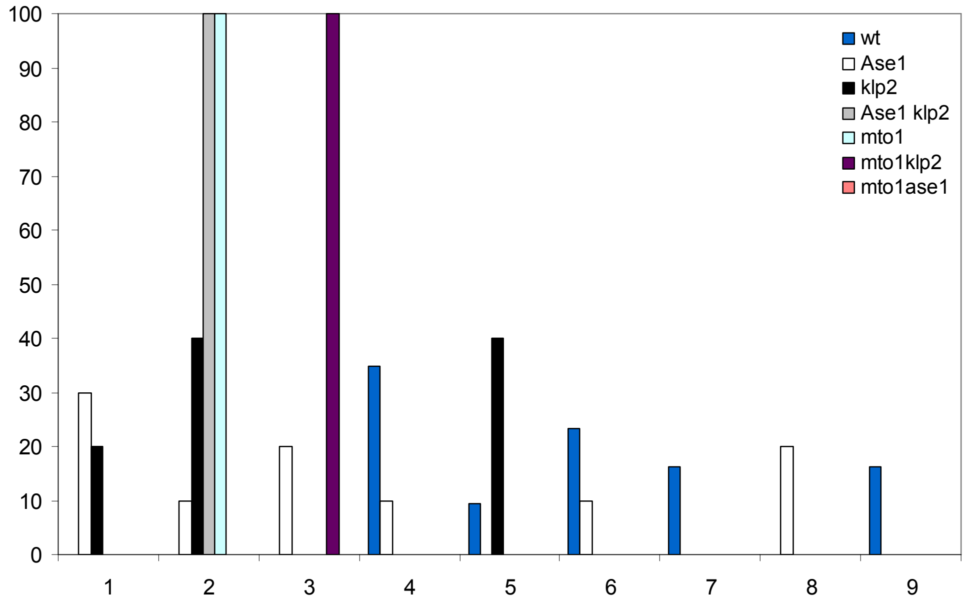

B

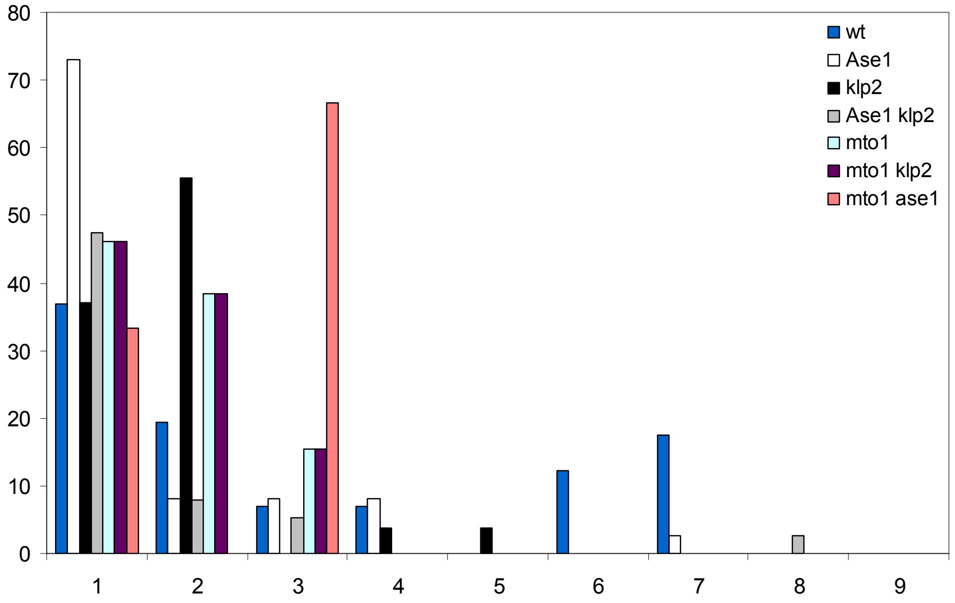

Wild type data from Hoog *et al*. (2007).

Annex V. Examples of program scripts used in this study

MT PAIRING

Input file example:

```
{
: 1
: [serial model name]
:
: 0            0 for all objects in model, or enter number of limiting regions
: 1            listing of bundles to calculate pairing for
: 1969,3186 lower and upper sections to calculate pairing
: 4            number of sections shared
: 1            number of kinds of pairs to compute pairing for
: 0,0           two types for each pair in turn, 0,0 to refer to all types
: 1             simple pairing calculation
: .045          distance X/Y below pairing quantity equals 1
: 0            minimal length to store pair
: 1            plot per MT data
: 1,2          columns x=MT length, y=absol. summed fractional pairing length
: 1            symbol type
: 0            0 for graphics plot, 1 to plot on terminal
: -1           output to file graphic
: [output name file]
: 0            no plot
}
```

MT OVERLAP

Input file example:

```
{
:              no mapping of one type into another
: 1            number of bundles to read from model file
: [name of input model]
:              no tilt file information
: 0            take all of the objects in the model
: 1            default format of types
: 1            bundles to work with
: 2            single Z center value for all bundles
: 1   3D       overlap factor
: 1            compute sum of overlap factors for each MT
: .215         distance in X/Y plane below which overlap will equal 1
: 1            plot all bundles in same graph
: 14           plot the graph to a postscript file
}
```

IMODCURVATURE

Shell command line:

```
$ imodcurvature –ob [object number] –zr 400 –wl 400 –rc 10,1000 –st –ka [input model] [output model]
```

6 REFERENCES

Akhmanova, A., C. C. Hoogenraad, K. Drabek, T. Stepanova, B. Dortland, T. Verkerk, W. Vermeulen, B. M. Burgering, C. I. De Zeeuw, F. Grosveld and N. Galjart (2001). "Clasps are CLIP-115 and -170 associating proteins involved in the regional regulation of microtubule dynamics in motile fibroblasts." Cell **104**(6): 923-35.

Akhmanova, A. and M. O. Steinmetz (2008). "Tracking the ends: a dynamic protein network controls the fate of microtubule tips." Nat Rev Mol Cell Biol **9**(4): 309-22.

Amos, L. A. and D. Schlieper (2005). "Microtubules and maps." Adv Protein Chem **71**: 257-98.

Andersen, S. S. (1999). "Balanced regulation of microtubule dynamics during the cell cycle: a contemporary view." Bioessays **21**(1): 53-60.

Arai, R. and I. Mabuchi (2002). "F-actin ring formation and the role of F-actin cables in the fission yeast Schizosaccharomyces pombe." J Cell Sci **115**(Pt 5): 887-98.

Arai, R., K. Nakano and I. Mabuchi (1998). "Subcellular localization and possible function of actin, tropomyosin and actin-related protein 3 (Arp3) in the fission yeast Schizosaccharomyces pombe." Eur J Cell Biol **76**(4): 288-95.

Ausmees, N., J. R. Kuhn and C. Jacobs-Wagner (2003). "The bacterial cytoskeleton: an intermediate filament-like function in cell shape." Cell **115**(6): 705-13.

Bahler, J. and M. Peter (2000). Cell polarity in yeast. Frontiers in Molecular Biology: Cell Polarity. D. Drubin, Oxford University Press.

Bahler, J., J. Q. Wu, M. S. Longtine, N. G. Shah, A. McKenzie, 3rd, A. B. Steever, A. Wach, P. Philippsen and J. R. Pringle (1998). "Heterologous modules for efficient and versatile PCR-based gene targeting in Schizosaccharomyces pombe." Yeast **14**(10): 943-51.

Bartolini, F. and G. G. Gundersen (2006). "Generation of noncentrosomal microtubule arrays." J Cell Sci **119**(Pt 20): 4155-63.

Baumeister, W., R. Grimm and J. Walz (1999). "Electron tomography of molecules and cells." Trends Cell Biol **9**(2): 81-5.

Beinhauer, J. D., I. M. Hagan, J. H. Hegemann and U. Fleig (1997). "Mal3, the fission yeast homologue of the human APC-interacting protein EB-1 is required for microtubule integrity and the maintenance of cell form." J Cell Biol **139**(3): 717-28.

Belmont, A. S., J. W. Sedat and D. A. Agard (1987). "A three-dimensional approach to mitotic chromosome structure: evidence for a complex hierarchical organization." J Cell Biol **105**(1): 77-92.

Belmont, L. D. and T. J. Mitchison (1996). "Identification of a protein that interacts with tubulin dimers and increases the catastrophe rate of microtubules." Cell **84**(4): 623-31.

Bettencourt-Dias, M. and D. M. Glover (2007). "Centrosome biogenesis and function: centrosomics brings new understanding." Nat Rev Mol Cell Biol **8**(6): 451-63.

Bieling, P., L. Laan, H. Schek, E. L. Munteanu, L. Sandblad, M. Dogterom, D. Brunner and T. Surrey (2007). "Reconstitution of a microtubule plus-end tracking system in vitro." Nature **450**(7172): 1100-5.

Bloom, K. (2001). "Nuclear migration: cortical anchors for cytoplasmic dynein." Curr Biol **11**(8): R326-9.

Bork, P., C. Sander and A. Valencia (1992). "An ATPase domain common to prokaryotic cell cycle proteins, sugar kinases, actin, and hsp70 heat shock proteins." Proc Natl Acad Sci U S A **89**(16): 7290-4.

Bratman, S. V. and F. Chang (2007). "Stabilization of overlapping microtubules by fission yeast CLASP." Dev Cell **13**(6): 812-27.

Bretscher, A. (2005). "Microtubule tips redirect actin assembly." Dev Cell **8**(4): 458-9.

Browning, H., J. Hayles, J. Mata, L. Aveline, P. Nurse and J. R. McIntosh (2000). "Tea2p is a kinesin-like protein required to generate polarized growth in fission yeast." J Cell Biol **151**(1): 15-28.

Brunner, D. and P. Nurse (2000). "CLIP170-like tip1p spatially organizes microtubular dynamics in fission yeast." Cell **102**(5): 695-704.

Busch, K. E. and D. Brunner (2004). "The microtubule plus end-tracking proteins mal3p and tip1p cooperate for cell-end targeting of interphase microtubules." Curr Biol **14**(7): 548-59.

Busch, K. E., J. Hayles, P. Nurse and D. Brunner (2004). "Tea2p kinesin is involved in spatial microtubule organization by transporting tip1p on microtubules." Dev Cell **6**(6): 831-43.

Carazo-Salas, R. E., C. Antony and P. Nurse (2005). "The kinesin Klp2 mediates polarization of interphase microtubules in fission yeast." Science **309**(5732): 297-300.

Carazo-Salas, R. E. and P. Nurse (2006). "Self-organization of interphase microtubule arrays in fission yeast." Nat Cell Biol **8**(10): 1102-7.

Carlier, M. F., D. Didry, R. Melki, M. Chabre and D. Pantaloni (1988). "Stabilization of microtubules by inorganic phosphate and its structural analogues, the fluoride complexes of aluminum and beryllium." Biochemistry **27**(10): 3555-9.

Chan, J., C. G. Jensen, L. C. Jensen, M. Bush and C. W. Lloyd (1999). "The 65-kDa carrot microtubule-associated protein forms regularly arranged filamentous cross-bridges between microtubules." Proc Natl Acad Sci U S A **96**(26): 14931-6.

Chan, J., T. Rutten and C. Lloyd (1996). "Isolation of microtubule-associated proteins from carrot cytoskeletons: a 120 kDa map decorates all four microtubule arrays and the nucleus." Plant J **10**(2): 251-9.

Chang-Jie, J. and S. Sonobe (1993). "Identification and preliminary characterization of a 65 kDa higher-plant microtubule-associated protein." J Cell Sci **105 (Pt 4)**: 891-901.

Chang, F., B. Feierbach and S. Martin (2005). "Regulation of actin assembly by microtubules in fission yeast cell polarity." Novartis Found Symp **269**: 59-66; discussion 66-72, 223-30.

Chang, P. and T. Stearns (2000). "Delta-tubulin and epsilon-tubulin: two new human centrosomal tubulins reveal new aspects of centrosome structure and function." Nat Cell Biol **2**(1): 30-5.

Chapin, S. J., J. C. Bulinski and G. G. Gundersen (1991). "Microtubule bundling in cells." Nature **349**(6304): 24.

Chiron, S., A. Bobkova, H. Zhou and M. P. Yaffe (2008). "CLASP regulates mitochondrial distribution in Schizosaccharomyces pombe." J Cell Biol **182**(1): 41-9.

Courtheoux, T., G. Gay, C. Reyes, S. Goldstone, Y. Gachet and S. Tournier (2007). "Dynein participates in chromosome segregation in fission yeast." Biol Cell **99**(11): 627-37.

Daga, R. R., K. G. Lee, S. Bratman, S. Salas-Pino and F. Chang (2006). "Self-organization of microtubule bundles in anucleate fission yeast cells." Nat Cell Biol **8**(10): 1108-13.

Davis, B. K. (2002). "Molecular evolution before the origin of species." Prog Biophys Mol Biol **79**(1-3): 77-133.

de Boer, P., R. Crossley and L. Rothfield (1992). "The essential bacterial cell-division protein FtsZ is a GTPase." Nature **359**(6392): 254-6.

des Georges, A., M. Katsuki, D. R. Drummond, M. Osei, R. A. Cross and L. A. Amos (2008). "Mal3, the Schizosaccharomyces pombe homolog of EB1, changes the microtubule lattice." Nat Struct Mol Biol.

Desai, A. and T. J. Mitchison (1997). "Microtubule polymerization dynamics." Annu Rev Cell Dev Biol **13**: 83-117.

Diamantopoulos, G. S., F. Perez, H. V. Goodson, G. Batelier, R. Melki, T. E. Kreis and J. E. Rickard (1999). "Dynamic localization of CLIP-170 to microtubule plus ends is coupled to microtubule assembly." J Cell Biol **144**(1): 99-112.

Dictenberg, J. B., W. Zimmerman, C. A. Sparks, A. Young, C. Vidair, Y. Zheng, W. Carrington, F. S. Fay and S. J. Doxsey (1998). "Pericentrin and gamma-tubulin form a protein complex and are organized into a novel lattice at the centrosome." J Cell Biol **141**(1): 163-74.

Ding, D. Q., Y. Chikashige, T. Haraguchi and Y. Hiraoka (1998). "Oscillatory nuclear movement in fission yeast meiotic prophase is driven by astral microtubules, as revealed by continuous observation of chromosomes and microtubules in living cells." J Cell Sci **111 (Pt 6)**: 701-12.

Ding, R., K. L. McDonald and J. R. McIntosh (1993). "Three-dimensional reconstruction and analysis of mitotic spindles from the yeast, Schizosaccharomyces pombe." J Cell Biol **120**(1): 141-51.

Ding, R., R. R. West, D. M. Morphew, B. R. Oakley and J. R. McIntosh (1997). "The spindle pole body of Schizosaccharomyces pombe enters and leaves the nuclear envelope as the cell cycle proceeds." Mol Biol Cell **8**(8): 1461-79.

Doolittle, R. F. (1995). "The origins and evolution of eukaryotic proteins." Philos Trans R Soc Lond B Biol Sci **349**(1329): 235-40.

Doolittle, R. F. and A. L. York (2002). "Bacterial actins? An evolutionary perspective." Bioessays **24**(4): 293-6.

Drummond, D. R. and R. A. Cross (2000). "Dynamics of interphase microtubules in Schizosaccharomyces pombe." Curr Biol **10**(13): 766-75.

Dutcher, S. K. (2003). "Long-lost relatives reappear: identification of new members of the tubulin superfamily." Curr Opin Microbiol **6**(6): 634-40.

Dutcher, S. K. and E. C. Trabuco (1998). "The UNI3 gene is required for assembly of basal bodies of Chlamydomonas and encodes delta-tubulin, a new member of the tubulin superfamily." Mol Biol Cell **9**(6): 1293-308.

Dye, N. A. and L. Shapiro (2007). "The push and pull of the bacterial cytoskeleton." Trends Cell Biol **17**(5): 239-45.

Efimov, A., A. Kharitonov, N. Efimova, J. Loncarek, P. M. Miller, N. Andreyeva, P. Gleeson, N. Galjart, A. R. Maia, I. X. McLeod, J. R. Yates, 3rd, H. Maiato, A. Khodjakov, A. Akhmanova and I. Kaverina (2007). "Asymmetric CLASP-dependent nucleation of noncentrosomal microtubules at the trans-Golgi network." Dev Cell **12**(6): 917-30.

Endow, S. A., S. J. Kang, L. L. Satterwhite, M. D. Rose, V. P. Skeen and E. D. Salmon (1994). "Yeast Kar3 is a minus-end microtubule motor protein that destabilizes microtubules preferentially at the minus ends." Embo J **13**(11): 2708-13.

Erickson, H. P. (1998). "Atomic structures of tubulin and FtsZ." Trends Cell Biol **8**(4): 133-7.

Erickson, H. P. (2007). "Evolution of the cytoskeleton." Bioessays **29**(7): 668-77.

Feierbach, B. and F. Chang (2001). "Roles of the fission yeast formin for3p in cell polarity, actin cable formation and symmetric cell division." Curr Biol **11**(21): 1656-65.

Flory, M. R., M. Morphew, J. D. Joseph, A. R. Means and T. N. Davis (2002). "Pcp1p, an Spc110p-related calmodulin target at the centrosome of the fission yeast Schizosaccharomyces pombe." Cell Growth Differ **13**(2): 47-58.

Forsburg, S. L. and N. Rhind (2006). "Basic methods for fission yeast." Yeast **23**(3): 173-83.

Fujita, A., L. Vardy, M. A. Garcia and T. Toda (2002). "A fourth component of the fission yeast gamma-tubulin complex, Alp16, is required for cytoplasmic microtubule integrity and becomes indispensable when gamma-tubulin function is compromised." Mol Biol Cell **13**(7): 2360-73.

Furuta, K. and Y. Y. Toyoshima (2008). "Minus-End-Directed Motor Ncd Exhibits Processive Movement that Is Enhanced by Microtubule Bundling In Vitro." Curr Biol **18**(2): 152-7.

Garcia, M. A., L. Vardy, N. Koonrugsa and T. Toda (2001). "Fission yeast ch-TOG/XMAP215 homologue Alp14 connects mitotic spindles with the kinetochore and is a component of the Mad2-dependent spindle checkpoint." Embo J **20**(13): 3389-401.

Gard, D. L. and M. W. Kirschner (1987). "A microtubule-associated protein from Xenopus eggs that specifically promotes assembly at the plus-end." J Cell Biol **105**(5): 2203-15.

Gardner, M. K., D. J. Odde and K. Bloom (2008). "Kinesin-8 molecular motors: putting the brakes on chromosome oscillations." Trends Cell Biol **18**(7): 307-10.

Giddings, T. H., Jr., E. T. O'Toole, M. Morphew, D. N. Mastronarde, J. R. McIntosh and M. Winey (2001). "Using rapid freeze and freeze-substitution for the preparation of yeast cells for electron microscopy and three-dimensional analysis." Methods Cell Biol **67**: 27-42.

Giganti, A. and E. Friederich (2003). "The actin cytoskeleton as a therapeutic target: state of the art and future directions." Prog Cell Cycle Res **5**: 511-25.

Gilbert, P. F. (1972). "The reconstruction of a three-dimensional structure from projections and its application to electron microscopy. II. Direct methods." Proc R Soc Lond B Biol Sci **182**(66): 89-102.

Gimona, M., K. Djinovic-Carugo, W. J. Kranewitter and S. J. Winder (2002). "Functional plasticity of CH domains." FEBS Lett **513**(1): 98-106.

Glick, B. S. (1996). "Cell biology: alternatives to baker's yeast." Curr Biol **6**(12): 1570-2.

Godsel, L. M., R. P. Hobbs and K. J. Green (2008). "Intermediate filament assembly: dynamics to disease." Trends Cell Biol **18**(1): 28-37.

Goldman, R. D., B. Grin, M. G. Mendez and E. R. Kuczmarski (2008). "Intermediate filaments: versatile building blocks of cell structure." Curr Opin Cell Biol **20**(1): 28-34.

Goodson, H. V., S. J. Kang and S. A. Endow (1994). "Molecular phylogeny of the kinesin family of microtubule motor proteins." J Cell Sci **107 (Pt 7)**: 1875-84.

Grallert, A., C. Beuter, R. A. Craven, S. Bagley, D. Wilks, U. Fleig and I. M. Hagan (2006). "S. pombe CLASP needs dynein, not EB1 or CLIP170, to induce microtubule instability and slows polymerization rates at cell tips in a dynein-dependent manner." Genes Dev **20**(17): 2421-36.

Grishchuk, E. L., I. S. Spiridonov and J. R. McIntosh (2007). "Mitotic chromosome biorientation in fission yeast is enhanced by dynein and a minus-end-directed, kinesin-like protein." Mol Biol Cell **18**(6): 2216-25.

Groden, J., A. Thliveris, W. Samowitz, M. Carlson, L. Gelbert, H. Albertsen, G. Joslyn, J. Stevens, L. Spirio, M. Robertson and et al. (1991). "Identification and characterization of the familial adenomatous polyposis coli gene." Cell **66**(3): 589-600.

Gunawardane, R. N., S. B. Lizarraga, C. Wiese, A. Wilde and Y. Zheng (2000). "gamma-Tubulin complexes and their role in microtubule nucleation." Curr Top Dev Biol **49**: 55-73.

Gundersen, G. G. and J. C. Bulinski (1986). "Microtubule arrays in differentiated cells contain elevated levels of a post-translationally modified form of tubulin." Eur J Cell Biol **42**(2): 288-94.

Gundersen, G. G., S. Khawaja and J. C. Bulinski (1989). "Generation of a stable, posttranslationally modified microtubule array is an early event in myogenic differentiation." J Cell Biol **109**(5): 2275-88.

Hagan, I. and M. Yanagida (1992). "Kinesin-related cut7 protein associates with mitotic and meiotic spindles in fission yeast." Nature **356**(6364): 74-6.

Hagan, I. M. (1998). "The fission yeast microtubule cytoskeleton." J Cell Sci **111 (Pt 12)**: 1603-12.

Hagan, I. M. and J. Petersen (2000). "The microtubule organizing centers of Schizosaccharomyces pombe." Curr Top Dev Biol **49**: 133-59.

Harris, S. D. (2006). "Cell polarity in filamentous fungi: shaping the mold." Int Rev Cytol **251**: 41-77.

Hayashi, I. and M. Ikura (2003). "Crystal structure of the amino-terminal microtubule-binding domain of end-binding protein 1 (EB1)." J Biol Chem **278**(38): 36430-4.

Hayles, J. and P. Nurse (2001). "A journey into space." Nat Rev Mol Cell Biol **2**(9): 647-56.

Helfand, B. T., L. Chang and R. D. Goldman (2004). "Intermediate filaments are dynamic and motile elements of cellular architecture." J Cell Sci **117**(Pt 2): 133-41.

Hisaoka, M., S. Okamoto, S. Koyama, T. Ishida, T. Imamura, H. Kanda, T. Kameya, J. M. Meis-Kindblom, L. G. Kindblom and H. Hashimoto (2003). "Microtubule-associated protein-2 and class III beta-tubulin are expressed in extraskeletal myxoid chondrosarcoma." Mod Pathol **16**(5): 453-9.

Hoog, J. L. and C. Antony (2007). "Whole-cell investigation of microtubule cytoskeleton architecture by electron tomography." Methods Cell Biol **79**: 145-67.

Hoog, J. L., C. Schwartz, A. T. Noon, E. T. O'Toole, D. N. Mastronarde, J. R. McIntosh and C. Antony (2007). "Organization of interphase microtubules in fission yeast analyzed by electron tomography." Dev Cell **12**(3): 349-61.

Horio, T., S. Uzawa, M. K. Jung, B. R. Oakley, K. Tanaka and M. Yanagida (1991). "The fission yeast gamma-tubulin is essential for mitosis and is localized at microtubule organizing centers." J Cell Sci **99 (Pt 4)**: 693-700.

Howell, B., H. Deacon and L. Cassimeris (1999a). "Decreasing oncoprotein 18/stathmin levels reduces microtubule catastrophes and increases microtubule polymer in vivo." J Cell Sci **112 (Pt 21)**: 3713-22.

Howell, B., N. Larsson, M. Gullberg and L. Cassimeris (1999b). "Dissociation of the tubulin-sequestering and microtubule catastrophe-promoting activities of oncoprotein 18/stathmin." Mol Biol Cell **10**(1): 105-18.

Hyman, A. and E. Karsenti (1998). "The role of nucleation in patterning microtubule networks." J Cell Sci **111 (Pt 15)**: 2077-83.

Ishikawa, H., R. Bischoff and H. Holtzer (1968). "Mitosis and intermediate-sized filaments in developing skeletal muscle." J Cell Biol **38**(3): 538-55.

Janson, M. E., R. Loughlin, I. Loiodice, C. Fu, D. Brunner, F. J. Nedelec and P. T. Tran (2007). "Crosslinkers and motors organize dynamic microtubules to form stable bipolar arrays in fission yeast." Cell **128**(2): 357-68.

Janson, M. E., T. G. Setty, A. Paoletti and P. T. Tran (2005). "Efficient formation of bipolar microtubule bundles requires microtubule-bound gamma-tubulin complexes." J Cell Biol **169**(2): 297-308.

Jeong, J. W., D. K. Rhee, S. Y. Cho, K. L. Hae, D. U. Kim, M. Won and H. B. Kim (2002). "Cloning and characterization of the kinesin-related protein, Krp1p, in Schizosaccharomyces pombe." Mol Cells **13**(3): 389-98.

Jiang, W., G. Jimenez, N. J. Wells, T. J. Hope, G. M. Wahl, T. Hunter and R. Fukunaga (1998). "PRC1: a human mitotic spindle-associated CDK substrate protein required for cytokinesis." Mol Cell **2**(6): 877-85.

Jones, L. J., R. Carballido-Lopez and J. Errington (2001). "Control of cell shape in bacteria: helical, actin-like filaments in Bacillus subtilis." Cell **104**(6): 913-22.

Juang, Y. L., J. Huang, J. M. Peters, M. E. McLaughlin, C. Y. Tai and D. Pellman (1997). "APC-mediated proteolysis of Ase1 and the morphogenesis of the mitotic spindle." Science **275**(5304): 1311-4.

Kabsch, W. and J. Vandekerckhove (1992). "Structure and function of actin." Annu Rev Biophys Biomol Struct **21**: 49-76.

Kamasaki, T., R. Arai, M. Osumi and I. Mabuchi (2005). "Directionality of F-actin cables changes during the fission yeast cell cycle." Nat Cell Biol **7**(9): 916-7.

King, M. C., T. G. Drivas and G. Blobel (2008). "A network of nuclear envelope membrane proteins linking centromeres to microtubules." Cell **134**(3): 427-38.

Knop, M. and E. Schiebel (1998). "Receptors determine the cellular localization of a gamma-tubulin complex and thereby the site of microtubule formation." Embo J **17**(14): 3952-67.

Koster, A. J., H. Chen, J. W. Sedat and D. A. Agard (1992). "Automated microscopy for electron tomography." Ultramicroscopy **46**(1-4): 207-27.

Kremer, J. R., D. N. Mastronarde and J. R. McIntosh (1996). "Computer visualization of three-dimensional image data using IMOD." J Struct Biol **116**(1): 71-6.

Kruse, T., B. Blagoev, A. Lobner-Olesen, M. Wachi, K. Sasaki, N. Iwai, M. Mann and K. Gerdes (2006). "Actin homolog MreB and RNA polymerase interact and are both required for chromosome segregation in Escherichia coli." Genes Dev **20**(1): 113-24.

La Carbona, S., C. Allix, M. Philippe and X. Le Goff (2004). "The protein kinase kin1 is required for cellular symmetry in fission yeast." Biol Cell **96**(2): 169-79.

Laing, N. G. and K. J. Nowak (2005). "When contractile proteins go bad: the sarcomere and skeletal muscle disease." Bioessays **27**(8): 809-22.

Lee, H., U. Engel, J. Rusch, S. Scherrer, K. Sheard and D. Van Vactor (2004). "The microtubule plus end tracking protein Orbit/MAST/CLASP acts downstream of the tyrosine kinase Abl in mediating axon guidance." Neuron **42**(6): 913-26.

Leupold, U. (1950). "Die Verebung von homothallie und heterothallie bei Schizosaccharomyces pombe." Compt. Rend. Lab. Carlsberg **24**: 381-475.

Loiodice, I., J. Staub, T. G. Setty, N. P. Nguyen, A. Paoletti and P. T. Tran (2005). "Ase1p organizes antiparallel microtubule arrays during interphase and mitosis in fission yeast." Mol Biol Cell **16**(4): 1756-68.

Lucic, V., F. Forster and W. Baumeister (2005). "Structural studies by electron tomography: from cells to molecules." Annu Rev Biochem **74**: 833-65.

Maddox, P. S., J. K. Stemple, L. Satterwhite, E. D. Salmon and K. Bloom (2003). "The minus end-directed motor Kar3 is required for coupling dynamic microtubule plus ends to the cortical shmoo tip in budding yeast." Curr Biol **13**(16): 1423-8.

Mao, T., L. Jin, H. Li, B. Liu and M. Yuan (2005). "Two microtubule-associated proteins of the Arabidopsis MAP65 family function differently on microtubules." Plant Physiol **138**(2): 654-62.

Margolis, R. L. and L. Wilson (1978). "Opposite end assembly and disassembly of microtubules at steady state in vitro." Cell **13**(1): 1-8.

Margolis, R. L. and L. Wilson (1998). "Microtubule treadmilling: what goes around comes around." Bioessays **20**(10): 830-6.

Marks, J., I. M. Hagan and J. S. Hyams (1986). "Growth polarity and cytokinesis in fission yeast: the role of the cytoskeleton." J Cell Sci Suppl **5**: 229-41.

Marsh, B. J., D. N. Mastronarde, J. R. McIntosh and K. E. Howell (2001). "Structural evidence for multiple transport mechanisms through the Golgi in the pancreatic beta-cell line, HIT-T15." Biochem Soc Trans **29**(Pt 4): 461-7.

Marx, A., J. Muller, E. M. Mandelkow, G. Woehlke, C. Bouchet-Marquis, A. Hoenger and E. Mandelkow (2008). "X-ray structure and microtubule interaction of the motor domain of Neurospora crassa NcKin3, a kinesin with unusual processivity." Biochemistry **47**(7): 1848-61.

Mastronarde, D. N. (1997). "Dual-axis tomography: an approach with alignment methods that preserve resolution." J Struct Biol **120**(3): 343-52.

Mastronarde, D. N. (2005). "Automated electron microscope tomography using robust prediction of specimen movements." J Struct Biol **152**(1): 36-51.

Masuda, H., M. Sevik and W. Z. Cande (1992). "In vitro microtubule-nucleating activity of spindle pole bodies in fission yeast Schizosaccharomyces pombe: cell cycle-dependent activation in xenopus cell-free extracts." J Cell Biol **117**(5): 1055-66.

Mata, J. and P. Nurse (1997). "tea1 and the microtubular cytoskeleton are important for generating global spatial order within the fission yeast cell." Cell **89**(6): 939-49.

Mathe, E., Y. H. Inoue, W. Palframan, G. Brown and D. M. Glover (2003). "Orbit/Mast, the CLASP orthologue of Drosophila, is required for asymmetric stem cell and cystocyte divisions and development of the polarised microtubule network that interconnects oocyte and nurse cells during oogenesis." Development **130**(5): 901-15.

McDonald, K. L., E. T. O'Toole, D. N. Mastronarde and J. R. McIntosh (1992). "Kinetochore microtubules in PTK cells." J Cell Biol **118**(2): 369-83.

McEwen, B. F., M. Radermacher, C. L. Rieder and J. Frank (1986). "Tomographic three-dimensional reconstruction of cilia ultrastructure from thick sections." Proc Natl Acad Sci U S A **83**(23): 9040-4.

McIntosh, J. R. (2001). "Electron microscopy of cells: a new beginning for a new century." J Cell Biol **153**(6): F25-32.

McIntosh, R., D. Nicastro and D. Mastronarde (2005). "New views of cells in 3D: an introduction to electron tomography." Trends Cell Biol **15**(1): 43-51.

Megraw, T. L., K. Li, L. R. Kao and T. C. Kaufman (1999). "The centrosomin protein is required for centrosome assembly and function during cleavage in Drosophila." Development **126**(13): 2829-39.

Miki, F., A. Kurabayashi, Y. Tange, K. Okazaki, M. Shimanuki and O. Niwa (2004). "Two-hybrid search for proteins that interact with Sad1 and Kms1, two membrane-bound components of the spindle pole body in fission yeast." Mol Genet Genomics **270**(6): 449-61.

Miller, R. K. and M. D. Rose (1998). "Kar9p is a novel cortical protein required for cytoplasmic microtubule orientation in yeast." J Cell Biol **140**(2): 377-90.

Mitchison, J. M. and P. Nurse (1985). "Growth in cell length in the fission yeast Schizosaccharomyces pombe." J Cell Sci **75**: 357-76.

Mitchison, T. and M. Kirschner (1984). "Dynamic instability of microtubule growth." Nature **312**(5991): 237-42.

Mollinari, C., J. P. Kleman, W. Jiang, G. Schoehn, T. Hunter and R. L. Margolis (2002). "PRC1 is a microtubule binding and bundling protein essential to maintain the mitotic spindle midzone." J Cell Biol **157**(7): 1175-86.

Moores, C. A., J. Cooper, M. Wagenbach, Y. Ovechkina, L. Wordeman and R. A. Milligan (2006). "The role of the kinesin-13 neck in microtubule depolymerization." Cell Cycle **5**(16): 1812-5.

Moores, C. A. and R. A. Milligan (2006). "Lucky 13-microtubule depolymerisation by kinesin-13 motors." J Cell Sci **119**(Pt 19): 3905-13.

Moores, C. A. and R. A. Milligan (2008). "Visualisation of a kinesin-13 motor on microtubule end mimics." J Mol Biol **377**(3): 647-54.

Moreno, S., A. Klar and P. Nurse (1991). "Molecular genetic analysis of fission yeast Schizosaccharomyces pombe." Methods Enzymol **194**: 795-823.

Moritz, M., M. B. Braunfeld, V. Guenebaut, J. Heuser and D. A. Agard (2000). "Structure of the gamma-tubulin ring complex: a template for microtubule nucleation." Nat Cell Biol **2**(6): 365-70.

Moser, B. A. and P. Russell (2000). "Cell cycle regulation in Schizosaccharomyces pombe." Curr Opin Microbiol **3**(6): 631-6.

Mukherjee, A., K. Dai and J. Lutkenhaus (1993). "Escherichia coli cell division protein FtsZ is a guanine nucleotide binding protein." Proc Natl Acad Sci U S A **90**(3): 1053-7.

Muller-Reichert, T., D. Chretien, F. Severin and A. A. Hyman (1998). "Structural changes at microtubule ends accompanying GTP hydrolysis: information from a slowly hydrolyzable analogue of GTP, guanylyl (alpha,beta)methylenediphosphonate." Proc Natl Acad Sci U S A **95**(7): 3661-6.

Muller, S., A. Smertenko, V. Wagner, M. Heinrich, P. J. Hussey and M. T. Hauser (2004). "The plant microtubule-associated protein AtMAP65-3/PLE is essential for cytokinetic phragmoplast function." Curr Biol **14**(5): 412-7.

Nabeshima, K., H. Kurooka, M. Takeuchi, K. Kinoshita, Y. Nakaseko and M. Yanagida (1995). "p93dis1, which is required for sister chromatid separation, is a novel microtubule and spindle pole body-associating protein phosphorylated at the Cdc2 target sites." Genes Dev **9**(13): 1572-85.

Nelson, W. J. (2003). "Adaptation of core mechanisms to generate cell polarity." Nature **422**(6933): 766-74.

Nogales, E., K. H. Downing, L. A. Amos and J. Lowe (1998). "Tubulin and FtsZ form a distinct family of GTPases." Nat Struct Biol **5**(6): 451-8.

Nogales, E., M. Whittaker, R. A. Milligan and K. H. Downing (1999). "High-resolution model of the microtubule." Cell **96**(1): 79-88.

Nurse, P. (2000). "A long twentieth century of the cell cycle and beyond." Cell **100**(1): 71-8.

O'Toole, E. T., T. H. Giddings, J. R. McIntosh and S. K. Dutcher (2003a). "Three-dimensional organization of basal bodies from wild-type and delta-tubulin deletion strains of Chlamydomonas reinhardtii." Mol Biol Cell **14**(7): 2999-3012.

O'Toole, E. T., K. L. McDonald, J. Mantler, J. R. McIntosh, A. A. Hyman and T. Muller-Reichert (2003b). "Morphologically distinct microtubule ends in the mitotic centrosome of Caenorhabditis elegans." J Cell Biol **163**(3): 451-6.

O'Toole, E. T., M. Winey and J. R. McIntosh (1999). "High-voltage electron tomography of spindle pole bodies and early mitotic spindles in the yeast Saccharomyces cerevisiae." Mol Biol Cell **10**(6): 2017-31.

O'Toole, E. T., M. Winey, J. R. McIntosh and D. N. Mastronarde (2002). "Electron tomography of yeast cells." Methods Enzymol **351**: 81-95.

Oakley, C. E. and B. R. Oakley (1989). "Identification of gamma-tubulin, a new member of the tubulin superfamily encoded by mipA gene of Aspergillus nidulans." Nature **338**(6217): 662-4.

Parnaik, V. K. (2008). "Role of nuclear lamins in nuclear organization, cellular signaling, and inherited diseases." Int Rev Cell Mol Biol **266**: 157-206.

Parry, D. A., S. V. Strelkov, P. Burkhard, U. Aebi and H. Herrmann (2007). "Towards a molecular description of intermediate filament structure and assembly." Exp Cell Res **313**(10): 2204-16.

Pelham, R. J., Jr. and F. Chang (2001). "Role of actin polymerization and actin cables in actin-patch movement in Schizosaccharomyces pombe." Nat Cell Biol **3**(3): 235-44.

Pellman, D., M. Bagget, Y. H. Tu, G. R. Fink and H. Tu (1995). "Two microtubule-associated proteins required for anaphase spindle movement in Saccharomyces cerevisiae." J Cell Biol **130**(6): 1373-85.

Perez, F., G. S. Diamantopoulos, R. Stalder and T. E. Kreis (1999). "CLIP-170 highlights growing microtubule ends in vivo." Cell **96**(4): 517-27.

Pidoux, A. L., M. LeDizet and W. Z. Cande (1996). "Fission yeast pkl1 is a kinesin-related protein involved in mitotic spindle function." Mol Biol Cell **7**(10): 1639-55.

Pierre, P., R. Pepperkok and T. E. Kreis (1994). "Molecular characterization of two functional domains of CLIP-170 in vivo." J Cell Sci **107 (Pt 7)**: 1909-20.

Pierre, P., J. Scheel, J. E. Rickard and T. E. Kreis (1992). "CLIP-170 links endocytic vesicles to microtubules." Cell **70**(6): 887-900.

Pollard, T. D. and G. G. Borisy (2003). "Cellular motility driven by assembly and disassembly of actin filaments." Cell **112**(4): 453-65.

RayChaudhuri, D. and J. T. Park (1992). "Escherichia coli cell-division gene ftsZ encodes a novel GTP-binding protein." Nature **359**(6392): 251-4.

Robert, M. and P. S. Mathuranath (2007). "Tau and tauopathies." Neurol India **55**(1): 11-6.

Rodriguez, A. S., J. Batac, A. N. Killilea, J. Filopei, D. R. Simeonov, I. Lin and J. L. Paluh (2008). "Protein complexes at the microtubule organizing center regulate bipolar spindle assembly." Cell Cycle **7**(9): 1246-53.

Ruiz, F., N. Garreau de Loubresse and J. Beisson (1987). "A mutation affecting basal body duplication and cell shape in Paramecium." J Cell Biol **104**(3): 417-30.

Ruiz, F., A. Krzywicka, C. Klotz, A. Keller, J. Cohen, F. Koll, G. Balavoine and J. Beisson (2000). "The SM19 gene, required for duplication of basal bodies in Paramecium, encodes a novel tubulin, eta-tubulin." Curr Biol **10**(22): 1451-4.

Sagolla, M. J., S. Uzawa and W. Z. Cande (2003). "Individual microtubule dynamics contribute to the function of mitotic and cytoplasmic arrays in fission yeast." J Cell Sci **116**(Pt 24): 4891-903.

Salinas, S., R. E. Carazo-Salas, C. Proukakis, J. M. Cooper, A. E. Weston, G. Schiavo and T. T. Warner (2005). "Human spastin has multiple microtubule-related functions." J Neurochem **95**(5): 1411-20.

Salinas, S., R. E. Carazo-Salas, C. Proukakis, G. Schiavo and T. T. Warner (2007). "Spastin and microtubules: Functions in health and disease." J Neurosci Res **85**(12): 2778-82.

Samejima, I., P. C. Lourenco, H. A. Snaith and K. E. Sawin (2005). "Fission yeast mto2p regulates microtubule nucleation by the centrosomin-related protein mto1p." Mol Biol Cell **16**(6): 3040-51.

Sanchez-Perez, I., S. J. Renwick, K. Crawley, I. Karig, V. Buck, J. C. Meadows, A. Franco-Sanchez, U. Fleig, T. Toda and J. B. Millar (2005). "The DASH complex and Klp5/Klp6 kinesin coordinate bipolar chromosome attachment in fission yeast." Embo J **24**(16): 2931-43.

Sandblad, L., K. E. Busch, P. Tittmann, H. Gross, D. Brunner and A. Hoenger (2006). "The Schizosaccharomyces pombe EB1 homolog Mal3p binds and stabilizes the microtubule lattice seam." Cell **127**(7): 1415-24.

Sasabe, M. and Y. Machida (2006). "MAP65: a bridge linking a MAP kinase to microtubule turnover." Curr Opin Plant Biol **9**(6): 563-70.

Sasabe, M., T. Soyano, Y. Takahashi, S. Sonobe, H. Igarashi, T. J. Itoh, M. Hidaka and Y. Machida (2006). "Phosphorylation of NtMAP65-1 by a MAP kinase down-regulates its activity of microtubule bundling and stimulates progression of cytokinesis of tobacco cells." Genes Dev **20**(8): 1004-14.

Sato, M. and T. Toda (2007). "Alp7/TACC is a crucial target in Ran-GTPase-dependent spindle formation in fission yeast." Nature **447**(7142): 334-7.

Sawin, K. E. (2004). "Microtubule dynamics: faint speckle, hidden dragon." Curr Biol **14**(17): R702-4.

Sawin, K. E., P. C. Lourenco and H. A. Snaith (2004). "Microtubule nucleation at non-spindle pole body microtubule-organizing centers requires fission yeast centrosomin-related protein mod20p." Curr Biol **14**(9): 763-75.

Schiebel, E. (2000). "gamma-tubulin complexes: binding to the centrosome, regulation and microtubule nucleation." Curr Opin Cell Biol **12**(1): 113-8.

Schuyler, S. C., J. Y. Liu and D. Pellman (2003). "The molecular function of Ase1p: evidence for a MAP-dependent midzone-specific spindle matrix. Microtubule-associated proteins." J Cell Biol **160**(4): 517-28.

Segbert, C., R. Barkus, J. Powers, S. Strome, W. M. Saxton and O. Bossinger (2003). "KLP-18, a Klp2 kinesin, is required for assembly of acentrosomal meiotic spindles in Caenorhabditis elegans." Mol Biol Cell **14**(11): 4458-69.

Sharp, D. J., K. R. Yu, J. C. Sisson, W. Sullivan and J. M. Scholey (1999). "Antagonistic microtubule-sliding motors position mitotic centrosomes in Drosophila early embryos." Nat Cell Biol **1**(1): 51-4.

Slep, K. C., S. L. Rogers, S. L. Elliott, H. Ohkura, P. A. Kolodziej and R. D. Vale (2005). "Structural determinants for EB1-mediated recruitment of APC and spectraplakins to the microtubule plus end." J Cell Biol **168**(4): 587-98.

Slep, K. C. and R. D. Vale (2007). "Structural basis of microtubule plus end tracking by XMAP215, CLIP-170, and EB1." Mol Cell **27**(6): 976-91.

Smertenko, A., N. Saleh, H. Igarashi, H. Mori, I. Hauser-Hahn, C. J. Jiang, S. Sonobe, C. W. Lloyd and P. J. Hussey (2000). "A new class of microtubule-associated proteins in plants." Nat Cell Biol **2**(10): 750-3.

Smertenko, A. P., H. Y. Chang, V. Wagner, D. Kaloriti, S. Fenyk, S. Sonobe, C. Lloyd, M. T. Hauser and P. J. Hussey (2004). "The Arabidopsis microtubule-associated protein AtMAP65-1: molecular analysis of its microtubule bundling activity." Plant Cell **16**(8): 2035-47.

Snaith, H. A., I. Samejima and K. E. Sawin (2005). "Multistep and multimode cortical anchoring of tea1p at cell tips in fission yeast." Embo J **24**(21): 3690-9.

Snell, V. and P. Nurse (1994). "Genetic analysis of cell morphogenesis in fission yeast--a role for casein kinase II in the establishment of polarized growth." Embo J **13**(9): 2066-74.

Song, Y. H., A. Marx, J. Muller, G. Woehlke, M. Schliwa, A. Krebs, A. Hoenger and E. Mandelkow (2001). "Structure of a fast kinesin: implications for ATPase mechanism and interactions with microtubules." Embo J **20**(22): 6213-25.

Squire, J. M. (1997). "Architecture and function in the muscle sarcomere." Curr Opin Struct Biol **7**(2): 247-57.

Steinmetz, M. O., K. N. Goldie and U. Aebi (1997a). "A correlative analysis of actin filament assembly, structure, and dynamics." J Cell Biol **138**(3): 559-74.

Steinmetz, M. O., D. Stoffler, A. Hoenger, A. Bremer and U. Aebi (1997b). "Actin: from cell biology to atomic detail." J Struct Biol **119**(3): 295-320.

Steven, A. C. and U. Aebi (2003). "The next ice age: cryo-electron tomography of intact cells." Trends Cell Biol **13**(3): 107-10.

Terada, Y., Y. Uetake and R. Kuriyama (2003). "Interaction of Aurora-A and centrosomin at the microtubule-nucleating site in Drosophila and mammalian cells." J Cell Biol **162**(5): 757-63.

Toya, M., M. Sato, U. Haselmann, K. Asakawa, D. Brunner, C. Antony and T. Toda (2007). "Gamma-tubulin complex-mediated anchoring of spindle microtubules to spindle-pole bodies requires Msd1 in fission yeast." Nat Cell Biol **9**(6): 646-53.

Tran, P. T., P. Maddox, F. Chang and S. Inoue (1999). "Dynamic confocal imaging of interphase and mitotic microtubules in the fission yeast, S. pombe." Biol Bull **197**(2): 262-3.

Tran, P. T., L. Marsh, V. Doye, S. Inoue and F. Chang (2001). "A mechanism for nuclear positioning in fission yeast based on microtubule pushing." J Cell Biol **153**(2): 397-411.

Troxell, C. L., M. A. Sweezy, R. R. West, K. D. Reed, B. D. Carson, A. L. Pidoux, W. Z. Cande and J. R. McIntosh (2001). "pkl1(+)and klp2(+): Two kinesins of the Kar3 subfamily in fission yeast perform different functions in both mitosis and meiosis." Mol Biol Cell **12**(11): 3476-88.

Ubersax, J. A., E. L. Woodbury, P. N. Quang, M. Paraz, J. D. Blethrow, K. Shah, K. M. Shokat and D. O. Morgan (2003). "Targets of the cyclin-dependent kinase Cdk1." Nature **425**(6960): 859-64.

Vaizel-Ohayon, D. and E. D. Schejter (1999). "Mutations in centrosomin reveal requirements for centrosomal function during early Drosophila embryogenesis." Curr Biol **9**(16): 889-98.

Vale, R. D. (2003). "The molecular motor toolbox for intracellular transport." Cell **112**(4): 467-80.

Valiron, O., N. Caudron and D. Job (2001). "Microtubule dynamics." Cell Mol Life Sci **58**(14): 2069-84.

Van Damme, D., F. Y. Bouget, K. Van Poucke, D. Inze and D. Geelen (2004a). "Molecular dissection of plant cytokinesis and phragmoplast structure: a survey of GFP-tagged proteins." Plant J **40**(3): 386-98.

Van Damme, D., K. Van Poucke, E. Boutant, C. Ritzenthaler, D. Inze and D. Geelen (2004b). "In vivo dynamics and differential microtubule-binding activities of MAP65 proteins." Plant Physiol **136**(4): 3956-67.

van den Ent, F., L. A. Amos and J. Lowe (2001). "Prokaryotic origin of the actin cytoskeleton." Nature **413**(6851): 39-44.

Vanoosthuyse, V., R. Valsdottir, J. P. Javerzat and K. G. Hardwick (2004). "Kinetochore targeting of fission yeast Mad and Bub proteins is essential for spindle checkpoint function but not for all chromosome segregation roles of Bub1p." Mol Cell Biol **24**(22): 9786-801.

Vaughan, S., T. Attwood, M. Navarro, V. Scott, P. McKean and K. Gull (2000). "New tubulins in protozoal parasites." Curr Biol **10**(7): R258-9.

Venkatram, S., J. L. Jennings, A. Link and K. L. Gould (2005). "Mto2p, a novel fission yeast protein required for cytoplasmic microtubule organization and anchoring of the cytokinetic actin ring." Mol Biol Cell **16**(6): 3052-63.

Venkatram, S., J. J. Tasto, A. Feoktistova, J. L. Jennings, A. J. Link and K. L. Gould (2004). "Identification and characterization of two novel proteins affecting fission yeast gamma-tubulin complex function." Mol Biol Cell **15**(5): 2287-301.

Verbrugghe, K. J. and J. G. White (2004). "SPD-1 is required for the formation of the spindle midzone but is not essential for the completion of cytokinesis in C. elegans embryos." Curr Biol **14**(19): 1755-60.

Verde, F., J. Mata and P. Nurse (1995). "Fission yeast cell morphogenesis: identification of new genes and analysis of their role during the cell cycle." J Cell Biol **131**(6 Pt 1): 1529-38.

Verni, F., M. P. Somma, K. C. Gunsalus, S. Bonaccorsi, G. Belloni, M. L. Goldberg and M. Gatti (2004). "Feo, the Drosophila homolog of PRC1, is required for central-spindle formation and cytokinesis." Curr Biol **14**(17): 1569-75.

Vinh, D. B., J. W. Kern, W. O. Hancock, J. Howard and T. N. Davis (2002). "Reconstitution and characterization of budding yeast gamma-tubulin complex." Mol Biol Cell **13**(4): 1144-57.

Wade, R. H. (2007). "Microtubules: an overview." Methods Mol Med **137**: 1-16.

Walker, R. A., E. T. O'Brien, N. K. Pryer, M. F. Soboeiro, W. A. Voter, H. P. Erickson and E. D. Salmon (1988). "Dynamic instability of individual microtubules analyzed by video light microscopy: rate constants and transition frequencies." J Cell Biol **107**(4): 1437-48.

Weir, B. A. and M. P. Yaffe (2004). "Mmd1p, a novel, conserved protein essential for normal mitochondrial morphology and distribution in the fission yeast Schizosaccharomyces pombe." Mol Biol Cell **15**(4): 1656-65.

Wicker-Planquart, C., V. Stoppin-Mellet, L. Blanchoin and M. Vantard (2004). "Interactions of tobacco microtubule-associated protein MAP65-1b with microtubules." Plant J **39**(1): 126-34.

Wiese, C. and Y. Zheng (2006). "Microtubule nucleation: gamma-tubulin and beyond." J Cell Sci **119**(Pt 20): 4143-53.

Wixon, J. (2002). "Featured Organism: Schizosaccharomyces pombe, The Fission Yeast." Comp Funct Genomics **3**(2): 194-204.

Wolpert, L. (1996). "One hundred years of positional information." Trends Genet **12**(9): 359-64.

Wood, V., R. Gwilliam, M. A. Rajandream, M. Lyne, R. Lyne, A. Stewart, J. Sgouros, N. Peat, J. Hayles, S. Baker, D. Basham, S. Bowman, K. Brooks, D. Brown, S. Brown, T. Chillingworth, C. Churcher, M. Collins, R. Connor, A. Cronin, P. Davis, T. Feltwell, A. Fraser, S. Gentles, A. Goble, N. Hamlin, D. Harris, J. Hidalgo, G. Hodgson, S. Holroyd, T. Hornsby, S. Howarth, E. J. Huckle, S. Hunt,

K. Jagels, K. James, L. Jones, M. Jones, S. Leather, S. McDonald, J. McLean, P. Mooney, S. Moule, K. Mungall, L. Murphy, D. Niblett, C. Odell, K. Oliver, S. O'Neil, D. Pearson, M. A. Quail, E. Rabbinowitsch, K. Rutherford, S. Rutter, D. Saunders, K. Seeger, S. Sharp, J. Skelton, M. Simmonds, R. Squares, S. Squares, K. Stevens, K. Taylor, R. G. Taylor, A. Tivey, S. Walsh, T. Warren, S. Whitehead, J. Woodward, G. Volckaert, R. Aert, J. Robben, B. Grymonprez, I. Weltjens, E. Vanstreels, M. Rieger, M. Schafer, S. Muller-Auer, C. Gabel, M. Fuchs, A. Dusterhoft, C. Fritzc, E. Holzer, D. Moestl, H. Hilbert, K. Borzym, I. Langer, A. Beck, H. Lehrach, R. Reinhardt, T. M. Pohl, P. Eger, W. Zimmermann, H. Wedler, R. Wambutt, B. Purnelle, A. Goffeau, E. Cadieu, S. Dreano, S. Gloux, V. Lelaure, S. Mottier, F. Galibert, S. J. Aves, Z. Xiang, C. Hunt, K. Moore, S. M. Hurst, M. Lucas, M. Rochet, C. Gaillardin, V. A. Tallada, A. Garzon, G. Thode, R. R. Daga, L. Cruzado, J. Jimenez, M. Sanchez, F. del Rey, J. Benito, A. Dominguez, J. L. Revuelta, S. Moreno, J. Armstrong, S. L. Forsburg, L. Cerutti, T. Lowe, W. R. McCombie, I. Paulsen, J. Potashkin, G. V. Shpakovski, D. Ussery, B. G. Barrell and P. Nurse (2002). "The genome sequence of Schizosaccharomyces pombe." Nature **415**(6874): 871-80.

Yaffe, M. P. (1999). "The machinery of mitochondrial inheritance and behavior." Science **283**(5407): 1493-7.

Yaffe, M. P., D. Harata, F. Verde, M. Eddison, T. Toda and P. Nurse (1996). "Microtubules mediate mitochondrial distribution in fission yeast." Proc Natl Acad Sci U S A **93**(21): 11664-8.

Yaffe, M. P., N. Stuurman and R. D. Vale (2003). "Mitochondrial positioning in fission yeast is driven by association with dynamic microtubules and mitotic spindle poles." Proc Natl Acad Sci U S A **100**(20): 11424-8.

Yamashita, A., M. Sato, A. Fujita, M. Yamamoto and T. Toda (2005). "The roles of fission yeast ase1 in mitotic cell division, meiotic nuclear oscillation, and cytokinesis checkpoint signaling." Mol Biol Cell **16**(3): 1378-95.

Yamashita, A., Y. Watanabe and M. Yamamoto (1997). "Microtubule-associated coiled-coil protein Ssm4 is involved in the meiotic development in fission yeast." Genes Cells **2**(2): 155-66.

Yildiz, A. and P. R. Selvin (2005). "Kinesin: walking, crawling or sliding along?" Trends Cell Biol **15**(2): 112-20.

Zelnak, A. B. (2007). "Clinical pharmacology and use of microtubule-targeting agents in cancer therapy." Methods Mol Med **137**: 209-34.

Zheng, L., C. Schwartz, L. Wee and S. Oliferenko (2006). "The fission yeast transforming acidic coiled coil-related protein Mia1p/Alp7p is required for formation and maintenance of persistent microtubule-organizing centers at the nuclear envelope." Mol Biol Cell **17**(5): 2212-22.

Zheng, Y., M. L. Wong, B. Alberts and T. Mitchison (1995). "Nucleation of microtubule assembly by a gamma-tubulin-containing ring complex." Nature **378**(6557): 578-83.

Zhu, C. and W. Jiang (2005). "Cell cycle-dependent translocation of PRC1 on the spindle by Kif4 is essential for midzone formation and cytokinesis." Proc Natl Acad Sci U S A **102**(2): 343-8.

Zhu, C., E. Lau, R. Schwarzenbacher, E. Bossy-Wetzel and W. Jiang (2006). "Spatiotemporal control of spindle midzone formation by PRC1 in human cells." Proc Natl Acad Sci U S A **103**(16): 6196-201.

Zimmerman, S. and F. Chang (2005). "Effects of {gamma}-tubulin complex proteins on microtubule nucleation and catastrophe in fission yeast." Mol Biol Cell **16**(6): 2719-33.

Zimmerman, S., R. R. Daga and F. Chang (2004). "Intra-nuclear microtubules and a mitotic spindle orientation checkpoint." Nat Cell Biol **6**(12): 1245-6.